TECHNICAL REPORT STANDARD TITLE PAGE

1. Report No.	2. Government Accession No.	3. Receipient's Calalog No.
FL/DOT/ RMC/0383-2062		

4. Title and Subtitle	5. Report Date
Static and Fatigue Behavior of Longitudinal Joints in Multi-Box Beam Prestressed Concrete Bridges	November 1989 / March 1992
	6. Performing Organization Code
7. Authors	8.Performing Organization Report No.
M. Arockiasamy and D. V. Reddy	
9. Performing Organization Name and Address	10. Work Unit No.
Florida Atlantic University Department of Ocean Engineering Boca Raton, Florida 33431	
	11. Contract or Grant No.
	HPR 86-21
12. Sponsoring Agency Name and Address	13. Type of Report and Period Covered
Florida Department of Transportation 605 Suwannee Street Tallahassee, Florida 32399-0466	Final Report Sept. 1987 - Nov. 1989
	14. Sponsoring Agency Code
	99700-7370-119, C-2062

15. Supplementary Notes

Prepared in cooperation with the Federal Highway Administration

16. Abstract

The report presents the analytical and experimental studies on the acrylic and precast prestressed concrete multi-box model bridge systems subjected to static and fatigue loading. The concept feasibility is demonstrated based on the improved structural serviceability in terms of the reduced deflections. The grouted in-situ joints at the bottom and cast in-situ slab at the top, which are prestressed by the transverse post-tensioning contribute significantly to efficient lateral load distribution characteristics.

The analytical displacements based on the grillage analysis compare reasonably well with the experimental value. The longitudinal grouted joints with an initial prestress of 150 psi in the transverse direction exhibit adequate structural integrity even upto 6 million cycles of repeated loading. The ratio of the ultimate moment to cracking moment is greater than 1.2 which ensures the adequacy of the total amount of prestressed steel as suggested by AASHTO. The agreement of the predicted first crack and ultimate collapse loads with the measured values is excellent.

17. Key Words	18. Distribution Statement
Fatigue behavior; longitudinal joints; acrylic and prestressed concrete bridge models; multi-box beam bridge	No restrictions. This document is available to the public through the National Technical Information Service, Springfield, Virginia 22161

19. Security Classif. (of this report)	20. Security Classif. (of this page)	21. No. of Pages	22. Price
Unclassified	Unclassified	145	

Form DOT F 1700.7 (8-89)

DISCLAIMER

The opinions, findings and conclusions expressed in this publication are those of the authors who are responsible for the facts and accuracy of the data presented herein. The contents do not necessarily reflect the views or policies of the Florida Department of Transportation or the U.S. Department of Transportation. This report does not constitute a standard, specification or regulation.

The report is prepared in cooperation with the State of Florida Department of Transportation and the U.S. Department of Transportation.

ACKNOWLEDGEMENT

The authors would like express sincere thanks to Dr. Mohsen El Shahawy, Chief Structural Analyst, and Dr. Moussa A. Issa, Structural Analyst of Florida Department of Transportation for their helpful suggestions, discussions, and constructive criticisms. Acknowledgements are due to Mr. Paul Csagoly and Mr. William N. Nickas, former thief Structural Analyst and Structural Analyst respectively of the Structural Research Center, Tallahassee. They wish to express their appreciation to Dr. S.E. Dunn, Chairman of Ocean Engineering, and Acting Dean, College of Engineering, Florida Atlantic University for his continued interest and encouragement. Appreciation is expressed to Mr. Chundi Reddy, President, Tecton Engineering Corporation, Florida, and Stresscon, Hialeah, Florida, for assistance in the fabrication and erection of the prestressed concrete multi-box bridge model system.

The authors are grateful to Dr. P. Arumugasaamy, Visiting Assistant Research Professor, Florida Atlantic University, for his active participation in the fabrication and testing of the acrylic model and the design of the prestressed concrete model bridge system.

The support of the following individuals is gratefully acknowledged:

Mr. T.V. Ramachandran and Mr. K.P. Ramkumar Graduate

Students, Florida Atlantic University for their contribution in the design and testing of the acrylic and concrete models respectively.

Mr. G. Murugesh and Mr. V.Sinha, Graduate Students, Florida Atlantic University for their assistance in fatigue and ultimate load tests and preparation of the figures and illustrations in the report.

Finally, Ms. Barbara Steinberg is acknowledged for her, excellent and patient typing.

SUMMARY

The study presents the results of the analytical and experimental studies on the acrylic and precast prestressed concrete multi-box beam model systems subjected to static and fatigue loads. The feasibility concept of the multi-box beam bridge system is demonstrated based on the improved structural serviceability and reduced deflections. The use of voided beams with bottom flange reduces considerably the dead load and also provides higher torsional strength. The grouted in-situ joints at the bottom and cast-in-situ slab at the top, which are prestressed by the lateral post-tensioning, contribute significantly to efficient lateral load distribution characteristics. The analytical displacements based on the grillage analysis compare reasonably well with the experimental values. The predicted strains in concrete across the depth of the beam under serviceability conditions agree reasonably well with the measured concrete strains. However, the increase in concrete strains with the increase in the number of cycles of fatigue loading is negligible indicating little softening characteristics with fatigue loading. Longitudinal grouted joints with an initial prestress of 50 psi in the transverse direction exhibit adequate structural integrity even up to 6 million cycles of repeated loading. The measured deflections indicate no loss of post tension stress even after six million cycles of loading. The

cracking moment, computed using the elastic theory, is a fraction of the ultimate flexural strength. The ratio of the ultimate to cracking moments is greater than 1.2, which satisfies the minimum steel requirements to develop the ultimate load in flexure as suggested by AASHTO. The agreement of the computed first crack and ultimate collapse loads with the measured values was excellent.

CONTENTS

LIST OF TABLES

Conversion factors - U.S. customary units to S.I. units

Current practices in the concrete industry use U.S. customary units. Hence, U.S. customary units have been used in this thesis as well. However, to facilitate readers familiar with the SI units, a conversion table is given below.

To convert from	To	Multiply by
in	m	0.025 400
ft	m	0.304 800
in^2	mm^2	645.160 000
ft^2	m^2	0.092 903
in^3	mm^3	$16.387\ 064 \times 10^{-6}$
ft^3	m^3	$28.316\ 847 \times 10^{-3}$
quart (U.S. liquid)	liter (1000 mm^3)	0.946 353
gallon (U.S. liquid)	m^3	$3.785\ 412 \times 10^{-3}$
in^4	cm^4	41.623 143
cm^4	m^4	$1.000\ 000 \times 10^{-8}$
ft^4	m^4	$8.630\ 975 \times 10^{-3}$
gram	dyne	980.665 000
kg (force or mass)	N	9.806 650
lb (mass)	kg (mass)	0.453 592
kips (1000 lbs)	kN	4.448 222
kip/ft	kN/m	14.593 898
lb/ft	kg/m	1.488 164
kg/m^2	N/m^2 (pascal)	9.806 650
kg/cm^2	kN/m^2 (kPa)	98.066 500
kip/ft^2	kN/m^2	47.880 260
lb/in^2 (psi)	kN/m^2	6.894 757
lb · in (torque)	N · m	0.112 985
lb · ft	N · m	1.355 818
kip · ft	kN · m	1.355 818
lb · ft (energy of work)	joule	1.355 818
cal · g (International value)	joule	4.186 800
lb/ft^3	kg/m^3	16.018 460
kip/ft^3	kN/m^3	157.087 477
g/cm^3	lb/ft^3	62.427 900
g/cm^3	kN/m^3	9.806 650

CHAPTER 1

INTRODUCTION

1.1. Background

Precast prestressed concrete is widely being used for highway and railway bridge construction in view of the savings in weight and cost, and offers the advantage of better quality control in the precast structural components. Construction time is reduced considerably due to ease in handling and erection of precast members. Different forms of precast members are used depending upon span, geometry, and aesthetics of the environment. The shapes frequently used are symmetrical and unsymmetrical I sections, T sections and box sections. Voided slabs and segmental shapes are also frequently used in construction. Composite members are generally designed using the standard sections.

A concrete bridge is subjected to dynamic effects of moving loads which cause fatigue. There is increasing awareness of the effects of repeated loading on a member, even if repeated loading does not cause a fatigue failure. The fatigue and ultimate strength behavior of joints have received considerable attention due to increasing concern with larger load requirements, coupled with more slender structural members and higher working stresses. Different methods have been used for joining the precast

beams together for an efficient lateral load distribution. These include i) shear keys filled with grout, ii) bonding beams together with an epoxy resin and sand mixture, iii) welding of steel angles or plates installed in the top of the beams, iv) bolting the webs of adjacent beams, v) lateral post tensioning through ducts in the flanges of the beams, and vi) use of tierods in the case of standard box slabs with diaphragms.

1.2 Objective and Scope

Box girders are increasingly used for bridge construction due to their higher torsional stiffness, better load distribution properties, greater efficiency with respect to longitudinal bending and improved aesthetic appearance. A conceptual multibox beam bridge system is developed by Florida Department of Transportation (D.O.T) to study the load distribution, crack growth and longitudinal joint behavior under fatigue loads (Fig. 1.1). The circular voids in the precast beams together with the rectangular void between the flanges and cast-in-situ slab achieve a 42 percent reduction in structural weight as compared to a rectangular cross section.

The objectives of the present study are the following:

i) Study of the behavior of the deck system for a given loading at critical locations simulating the HS 20-44 AASHTO truck loading

ii) Determination of the lateral load distribution factors

based on 1:20 scale acrylic model of the deck

iii) Study of the behavior of the 1:2.5 scale concrete model under static and fatigue loading with emphasis on longitudinal joint behavior and flexural stiffness of the longitudinally pretensioned and transversely posttensioned box bridge system

iv) Evaluation of the cracking behavior and ultimate load capacity of the model bridge system.

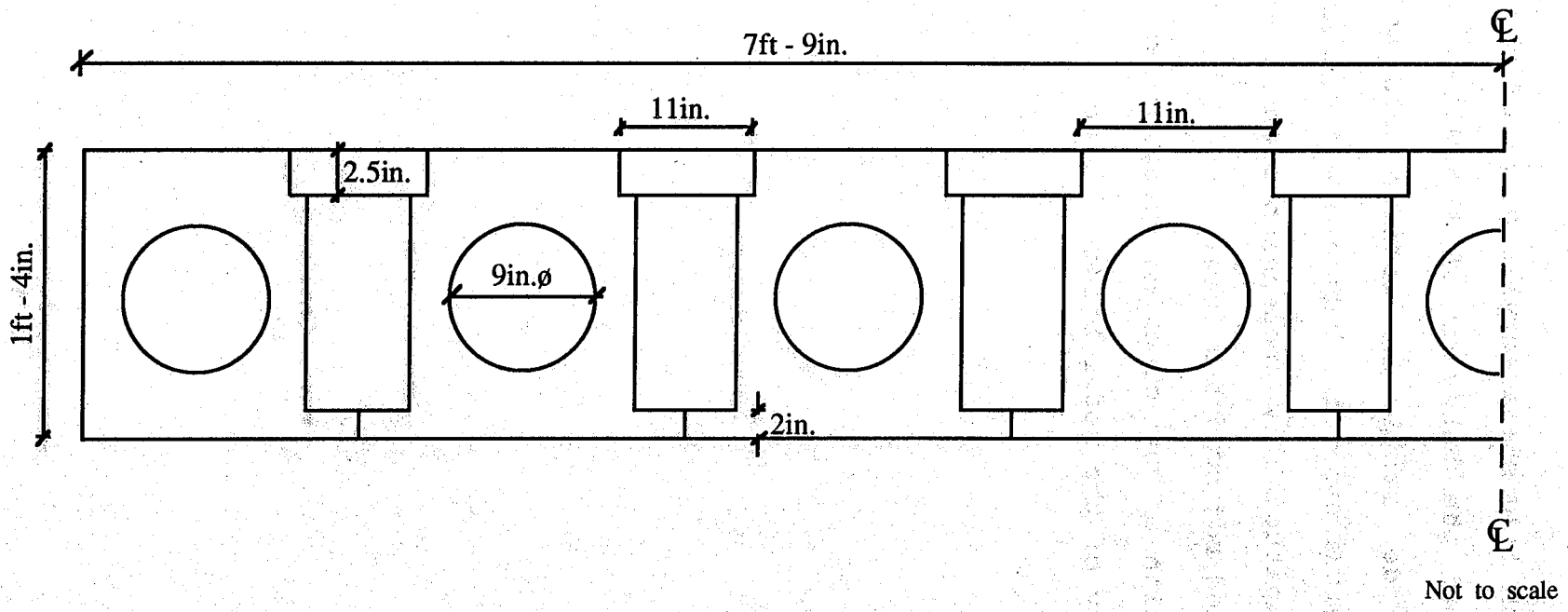

Fig. 1.1 Typical cross section of the multi-box bridge model

CHAPTER 2

LITERATURE REVIEW

2.1 Introduction

The need for replacement of a number of highway bridges in the United States has caused renewed interest in an intensive search for more economical bridge systems. Box beam construction for bridges is very common due to a variety of reasons. Box sections are preferred where heavy shear and torsional stresses are to be resisted. They have high torsional rigidity and direct shear is shared between the webs of the boxes. In box beams resistance is developed by flanges and webs working together in combined torsion, shear and bending. The torsional resistance of the box beam is proportional to the area enclosed by the median line of the box and this is affected by the width as well as the depth. This chapter briefly summarizes the available literature on analysis and design of box beam bridges, wheel load distribution and behavior of precast prestressed beams under fatigue loads.

2.2 Joint Behavior

The description of precast bridge deck design systems, details of joints, and joint material used on a number of highway and railway bridge systems has been presented by Biswas [1]. The performance of the joints was critical to the integrity of the

structural system. The geometric configuration of a joint together with the choice of an appropriate interface material contributes to the proper short-term and long-term service. A comprehensive review by Guckenberger, Daschner, and Kupfer [2] on precast prestressed segmental box bridges focused on how the joints between the segments affect the behavior and strength. Koseki and Breen [3] reported a detailed review of shear strength of joints for precast bridges. The behavior of joints of precast segmental concrete bridges has been described by Wium and Buyukozturk [4]. The structural strength of epoxy-glued joints for a segmental precast bridge deck was determined by Moreton [5] based on tests. They showed that no particular restrictions are necessary for allowable stresses in post-tensioned glued segmental concrete sections compared to normal, monolithic concrete. A precast prestressed concrete double-tee bridge system was evaluated by Reddy and Arockiasamy [6,7] in terms of the structural integrity, monitored by crack widths of the longitudinal and transverse joints with increasing cycles of fatigue loading.

2.3 Transverse Post-tensioning

Cracks in concrete due to dynamic vehicular loads lead to water, oxygen and chloride intrusion resulting in corrosion of reinforcement and spalling. The main benefit of prestressing is to eliminate or control cracking so as to restrict chloride and oxygen penetration. The study of prestressing as a method of

improving durability of bridge decks by Poston, Carrasquillo and Bren [8] showed that prestressing reduces the ingress of chlorides at crack, locations, but not below the generally accepted chloride corrosion threshold levels even for surface crack widths as small as 0.002 in. The main benefit of prestressing is to eliminate or control cracking so as to restrict chloride and oxygen penetration. The test results showed that in cracked concrete, concrete quality and cover had little effect on chloride penetration during the short time period of the accelerated testing.

Poston et al. [9] conducted a comprehensive study to develop design criteria for transverse prestressing of bridge decks. Important design areas such as effective distribution of edge prestressing force across a bridge slab as influenced by the diaphragm and girder restraint, behavior under typical wheel loads, effect of post-tensioning strand spacing on the distribution of horizontal slab stresses were studied using a series of interrelated physical tests and finite element analysis. The conclusions may be summarized as follows:

i) If diaphragms are omitted from a bridge at the time of transverse post tensioning, the transverse stress distribution is essentially uniform and the slab stresses equal the applied edge stress less normal friction and time losses. Diaphragms significantly affect the transverse stress distribution, but lateral stiffness of girders has little effect on it.

ii) Jacking sequence of deck transverse post tensioning does not have a significant influence on the final transverse stress distribution.

iii) No significant vertical camber or deflection, should arise from transverse prestressing of a bridge deck to compressive stress levels which are necessary to ensure a crack free design.

iv) Losses in prestressing can result in substantially less effective compression to resist cracking.

v) Both two and three-dimensional elastic finite element analyses predict reasonably the transverse prestressing :effects in slab girder bridge decks.

2.4 Analysis

The review of a number of methods developed for analyzing box beam and cellular structures has been presented by Bakht, Jaeger, Cheung and mufti [10]. The fundamental concepts and the techniques are presented in the following sections:

2.4.1 Load distribution theory

This approach replaces the actual bridge structure by an equivalent orthotropic plate which is then treated according to classical plate theory. This concept was first developed for grillages of negligible torsional stiffness and isotropic slabs. It was further modified to include the effects of' torsion. The tabulated comprehensive results of distribution coefficients was converted to a set of design curves by Morrice, Little and Rowe

for ready use in design offices [11].

Stanton and Mattock [12] studied load distribution and connection design for precast stemmed multibeam bridge superstructures. Their research indicated that the ratio of bridge span to bridge width and the ratio of flexural to torsional stiffness of the members have significant influence over the load fraction, and that two bridges having the same values for these ratios will have the same load fraction regardless of the shape of the cross section. Warping effects exert little influence on common member sizes and standard truck wheel spacingsv hence the results of this study should be approximately applicable to bridges made from any cross section, within the limits of the stiffnesses studied. The results on the study of the joints showed that the primary loads to be carried are shear forces perpendicular to the deck. Loads imposed before grouting by leveling of any differential cambers must be carried by the connectors alone. Those caused by wheel loads are transferred almost entirely through the grout joint, because it is much stiffer than the steel connectors.

2.4.2 Sandwich plate method

The plate is idealized as being composed of two flange plates which sustain all the bending and twisting effects and a core medium which takes all the shear forces. Arendts and Sanders [13] developed a method of analysis of concrete boxgirder bridges based on the concept of modeling of the actual

structure by an: equivalent plate. In the longitudinal direction, the webs contribute most of the shearing rigidity which may be assumed large; hence longitudinal shearing deformations are small. However, shearing deformations in the transverse; direction would not be small since shearing deformation would be produced by bending and relative horizontal slip between the top and bottom flanges. Based on the shearing behavior of the actual structure, the equivalent plate possesses infinite shearing, rigidity in the longitudinal direction and finite shearing rigidity in the transverse direction. The equivalent plate in the form of a sandwich plate has the following structural properties:

i) isotropic flexural and torsional rigidities,

ii) infinite shearing rigidity in the longitudinal direction and

iii) finite shearing rigidity in the transverse direction.

The complete description for the behavior of the equivalent plate method can be specified by the flexural rigidity, aspect ratio of the structure, ratio of the flexural rigidity to the shearing rigidity, and the equivalent width.

2.4.3 Grillage method

Grillage idealization incorporating orthogonally connected beam and slab elements to analyze cellular structures has been verified and confirmed by Bakht et al. [10]. The structure is assumed to be built of slender members connected at their ends to

form joints. The method of solution is based on the fundamental assumptions of linear structural behavior. Hendry and Jaeger [14] used the grid framework to analyze the deck slabs in which the load is represented by a harmonic series and the coefficients evaluated by Fourier analysis. The grillage analogy method is well documented by the published literature by Lightfoot [15], Yettram and Husain [16], Sawki [17], myth and Srinivasan [18], and Hambly and Pennells [19].

2.4.4 Finite element methods

This method is used with varying degrees of refinement to suit the ;particular geometry. A comprehensive discussion of the theory and application of the method is given by Zienkiewicz [20]. Davies, Somerville, and Zienkiewicz [21] have focused their study on the type of idealization necessary for the solution and choice of elements to economically analyze various types of bridges with sufficient engineering accuracy. Scordelis [22] developed a general purpose computer program based on FEM and direct stiffness harmonic analysis methods for box girder applications. The method is the most general one available to treat arbitrary loadings, boundary conditions varying material and dimensional properties and cutouts. But it requires a refined mesh size and large computer time to achieve accurate results.

2.4.5 Finite strip method

The development and application of finite strip analysis for bridge structures have been illustrated by Cusens and Loo [2.3]. This method, like the finite element analysis utilizes minimum potential energy theorem to develop the relationship between unknown nodal displacement parameters and the applied loading. The difference stems from the displacement patterns; the finite strip method assumes a combination of one-way polynomial function in the transvese direction, and a harmonic function in the spanwise direction in contradistinction to the finite element method which assumes two way polynomial functions.

2.4.6 Fatigue life

The fatigue life of prestressed and partially prestressed concrete, beams has been studied over the last two decades. Reports on the various experimental studies indicate the acceptable stress range, cycles of loading and the effect of bond on the fatigue life. Analytical models are now being developed to correlate these results.

Abeles, Brown, and Hu [24] reported results regarding static and fatigue tests on fifty two beams including three beam sizes and six different strand arrangements. Detailed studies were made on the influence of strand stress, steel ratio, group strand action, bond and non-prestressed strand on fatigue life. The minimum load considered was the bridge dead load (DL) which was assumed to be 30% of the static failure load. The live load (LL)

was assumed to be 22% of the static failure load. The maximum load level in the fatigue tests ranged from bridge design load, DL + LL (=52% of static failure load) to DL + 2.7 LL (=90 static failure load). The results indicated that the fatigue resistance of the tested beams can be comparable to that of the strands in air. The fatigue resistance of beams was better than that of the strands in air in cases where bond was excellent, but with poor bond 'the beam fatigue resistance was greatly reduced. Abeles, Brown and Hu [25] presented the effect of bond on fatigue life of the specimens.

Naaman [26] has analyzed the fatigue behavior of prestressed, partially prestressed, and reinforced concrete beams. The relative magnitude of the stress change under load is the most important variable that influences the fatigue life. This is more critical in partially prestressed beams as compared to reinforced or fully prestressed concrete. It is generally noted that concrete in direct compression or tension can sustain about 10 million cycles of fluctuating stress between 0 and 50% of its static strength. The fatigue strength of the prestressing steel depends on the type of prestressing steel (wire, strand, bars), steel treatment, anchor types and degree of bond. Stress relieving increases their fatigue limits significantly. High stress concentrations at the grips lower the fatigue life. In the case of strand twisting-untwisting during fatigue and fretting between a failed wire and adjacent wires or the center wire precipitate failure of these wires and the strand

itself. Fatigue data of prestressing strands suggest a fatigue life of about 2 million cycles at a stress range, in the steel corresponding to 10% of the ultimate strength with a minimum stress not exceeding 60% of the ultimate. Their fatigue life at other stress ranges for common design variables can be predicted from the relation:

$$fps/fp_u = -0.123 \log N + 0.87$$

Abeles, Barton and Brown [27] studied the fatigue resistance of precast prestressed concrete highway, bridge elements subjected to realistic type of fatigue loads. The tests showed that failure does not occur even after millions of repetitions of loading in the 650 - 1000 psi concrete stress, range even when cracks open and close at the tensile face millions of times. Fatigue failure occurred after about 300,000 cycles of loading extending over a large range of stress with a mean of 2500 psi in the nominal tensile stress range of 500 psi - 2980 psi. This, corresponded to a loading between approximately 30 % and 70 % of the static failure load.

Balaguru [28] proposed a theoretical model to predict the fatigue life, increase in deflection, and crack widths of prestressed concrete beams, using the fatigue properties of constituent materials namely concrete; prestressed, and nonprestressing steel.

A general analysis procedure for prestressed and partially prestressed concrete composite beams under instantaneous loading was presented by Al-Zaid and Naaman [29]. The method satisfies the equilibrium, strain compatibility and linear elastic stress

strain relations it applies to reinforced, prestressed, and partially prestressed concrete sections. The study established the feasibility and structural adequacy of the precast prestressed concrete double-tee concepts for short and medium span highway bridges in Florida and elsewhere.

2.4.7 Non-linear modeling of the behavior of prestressed concrete bridges

Safe and cost effective designs require realistic information on load-displacement response, strength and failure model of structural elements. The complex behavior of prestressed concrete under monotonic and fatigue loads arises from i) the nonlinear stress-strain behavior of concrete in multiaxial stress state, ii) progressive cracking of concrete induced by the tensile stress field and the consequent crack interface behavior, iii) difficulties in the formulation of stress and / or strain dependent failure criterion for concrete, iv) complex steel-concrete interface behavior such as bond slip, dowel action and progressive destruction of bond in local areas, and v) the time dependent creep, shrinkage and temperature effects. The restraining effect of the reinforcement is one of the main sources of shrinkage warping and creep deformations. The interaction effect of nonprestressed reinforcement on the prestress losses and the concrete precompression needs to be considered for the safe design of concrete bridges.

In the case of prestressed concrete bridges subjected to both

sustained and cyclic loading, the stresses in concrete, reinforcing and prestressing steels Vary continually with time due to the effects of shrinkage, static and cyclic creep of concrete and relaxation of prestressing steel. Published literature indicates [30, 31, 32, 33, 34] that i) time-dependent strength and deformation of' concrete are related, ii) microcracking is propagated as concrete continues to creep, and iii) microcracking leads to failure under high sustained stresses.

CHAPTER 3

ANALYSIS AND DESIGN OF ACRYLIC AND CONCRETE MODELS

3.1 Introduction

This chapter summarizes the analysis and design of the acrylic and concrete model multi-box bridge systems. The prototype bridge system is intended for three lane medium span bridges. The geometric parameters for both the models, the analyses using the grillage analogy method and the designs are presented based on a single AASHTO HS20-44 truck live load,

3.2. Acrylic Model

3.2.1 Mechanical and section properties (35)

The 1:20 acrylic scale model was based on the medium span mul i-box beam prestressed concrete bridge with the following dimensions:

Width = 40 ft.

Span = 60 ft.

Barrier height = 32 in.

Deck depth = 32 in.

Perspex was chosen for the construction of the acrylic model due to its low modulus of elasticity, extensive linear ranges, good machinability, and relatively low cost. However, the use of thermoplastic material (perspex) induces material property distortion, since the Poisson's ratio of the model material (= 0.35) is not the same as that of the prototype material, concrete (= 0.15 - 0.2). If the structural behavior were to be analyzed by plane stress, a discrepancy in the Poisson's ratio could cause distortions in the model strains, but not the model stresses, reactions and bending moments. The mechanical properties of the perspex were determined based on four-point flexural tests on two beam types: monolithic beam and transversely joined beam with three segments. The flexural behavior is found to be linearly elastic under loading and unloading conditions. However, it was observed that the beams exhibit creep deformation, characteristic of the inherent material behavior. The typical values of Young's modulus and Poisson's ratio as determined from the tests are the following:

Young's modulus, E = 520,034 psi

Poisson's ratio = 0.35

Density = 0.0434 lb/ in^3

The section properties of the acrylic model beams are shown in Table 3.1 below:

Table 3.1 Section properties of the acrylic model

Beam type/ slab element	Area A_c (in^2)	Moment of inertia, I_c (in^4)	y_b in.	z_b in^3	$r = \frac{I_c}{A_c}$ in.	$K_t = \frac{r^2}{y_b}$ in.	Torsional moment of inertia in^4
Edge beam (including parapet)	3.127	4.2569	1.3025	3.268	1.167	1.045	0.5879
Intermediate beam	2.3769	0.8658	0.8243	1.05	0.6032	0.4414	0.8008
Edge slab elements	1.045	0.45073	0.89545	-	-	-	0.02607
Intermediate slab elements	2.09	0.90146	0.89545	-	-	-	0.05502

3.2.2 Discretization of acrylic model

The discretization of the model is shown in Fig. 3.1. There were 199 members and 110 nodes in the grid used for the analysis. The longitudinal elements were beam elements and the transverse elements were the slabs spanning in the top and bottom in the transverse direction.

The analysis was performed for the load locations shown in Figs. 3,2, 3.3 and, 3.4; the AASHTO HS 20-44 load values were scaled down to 180 lb, 100 lb and 300 lb. The loads on each beam were then determined by considering the four-point loading and used in the input data for the grillage analysis program.

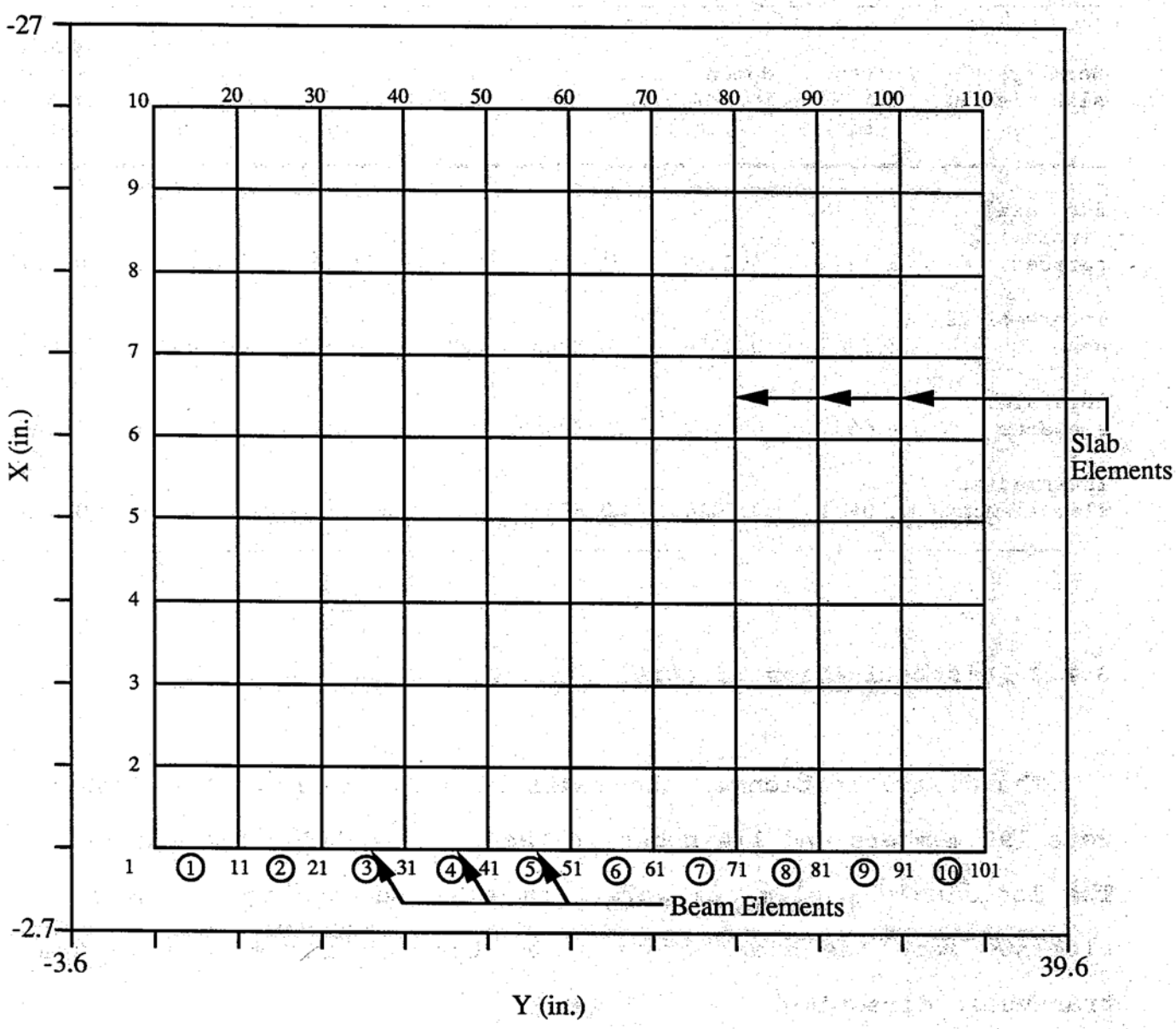

Fig. 3.1 Equivalent plane grid of the acrylic model

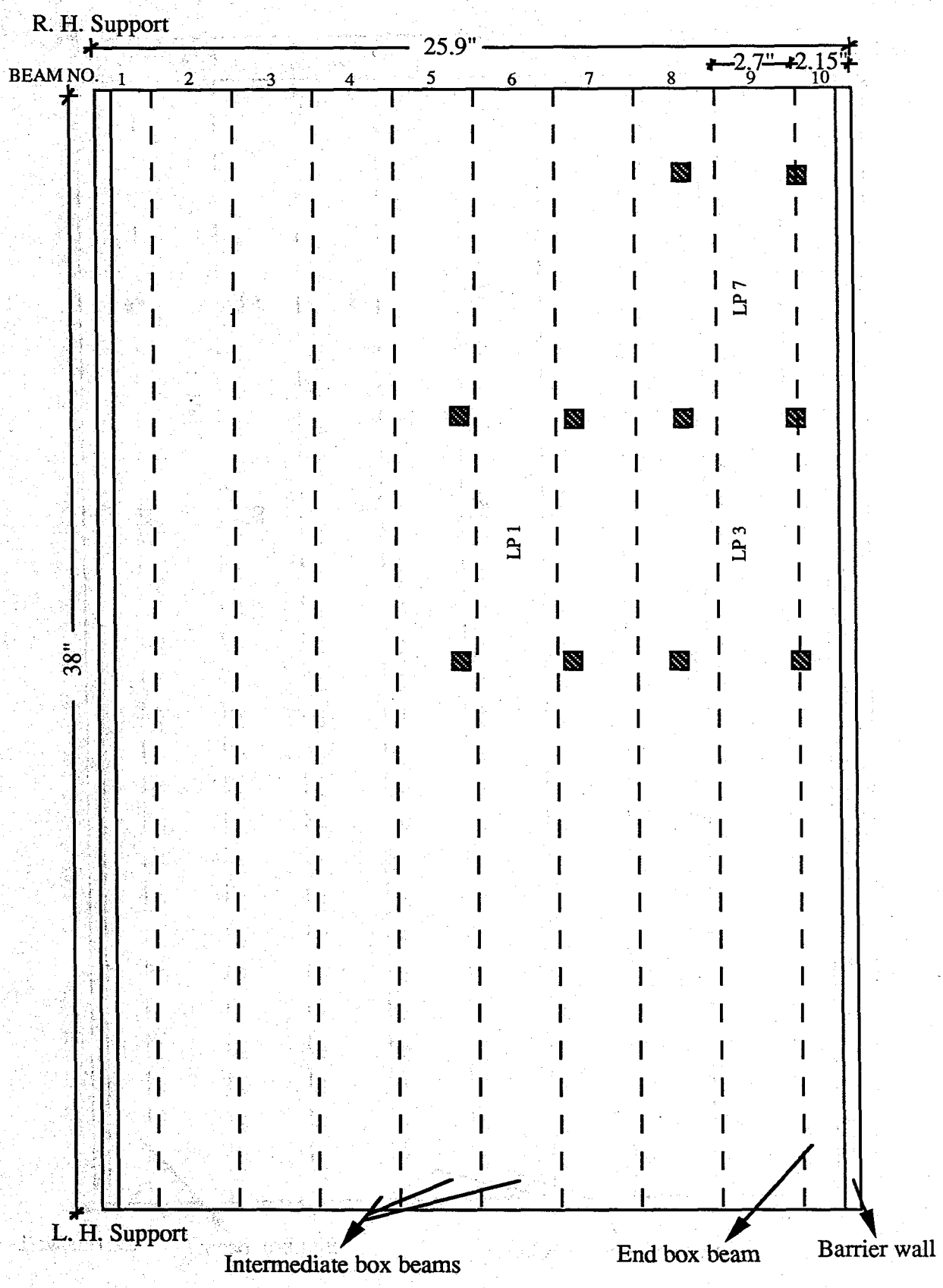

Fig. 3.2 Location of the loading device for the acrylic model test -load positions 1 , 3 , & 7

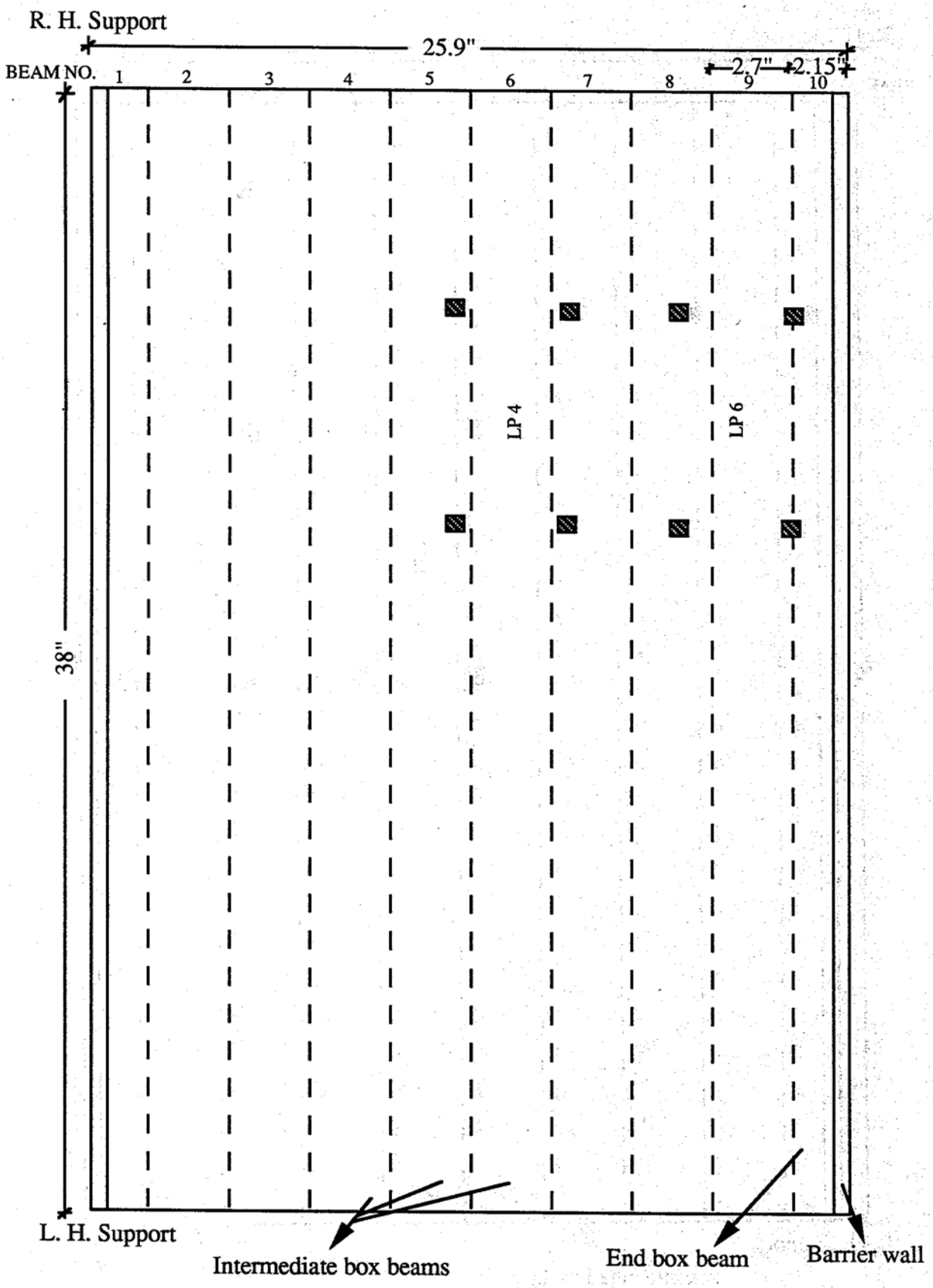

Fig. 3.3 Location of the loading device for the acrylic model test -load positions 4 & 6

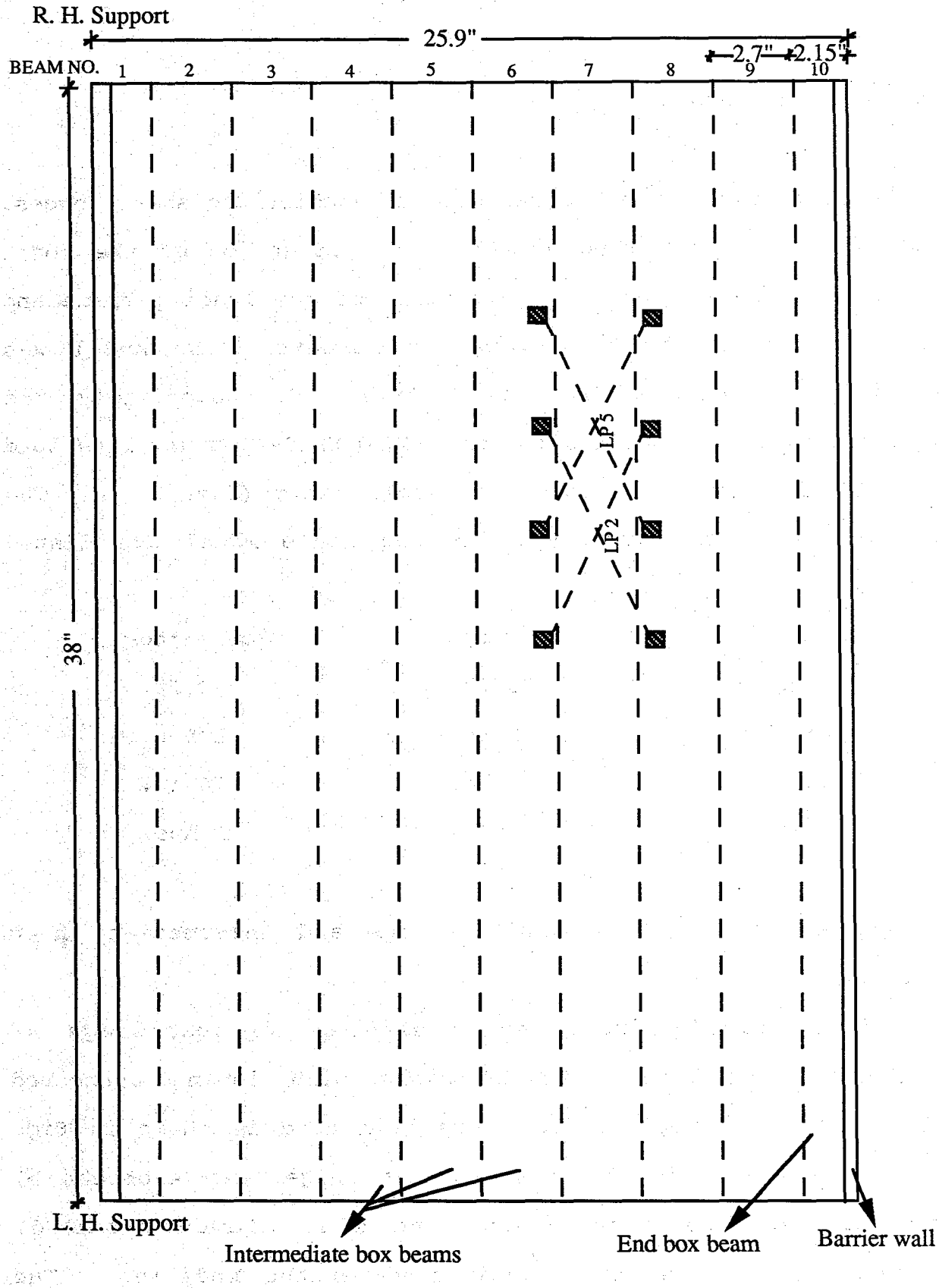

Fig. 3.4 Location of the loading device for the acrylic model test -load positions 2 & 5

3.3 Concrete model

Grillage analogy method was used to predict the shear forces, bending moments, twisting moments, and deflection of the model bridge system. Due to the limitations of the loading frame and the capacity of the MTS hydraulic actuator, the model was designed to simulate a single truck live load. Accordingly, the concrete model was analyzed for an AASHTO HS20-44 truck live load for a 75 ft. prototype and 1:2.5 scale ratio (Fig. 1.1). The particulars of the prototype and the scale model are listed below:

	Prototype	Scale model
Span	75 ft.	30 ft.
Width	38 ft. 8 in.	185.6 in.
Depth	40 in.	16 in.
Beams	9 nos.	9 nos.

Tables 3.2 and 3.3 show the edge and intermediate beam properties.

The bridge structure was modeled as an assemblage of longitudinal beam elements and transverse slab elements connected at their ends to form joints. The grid used is shown in Fig. 3.5. Four types of elements, i.e. a) edge beam elements b) intermediate beam elements c) end slab elements and d) intermediate slab elements were used in the modeling. The assemblage consisted of 178 members with 99 joints of which 16

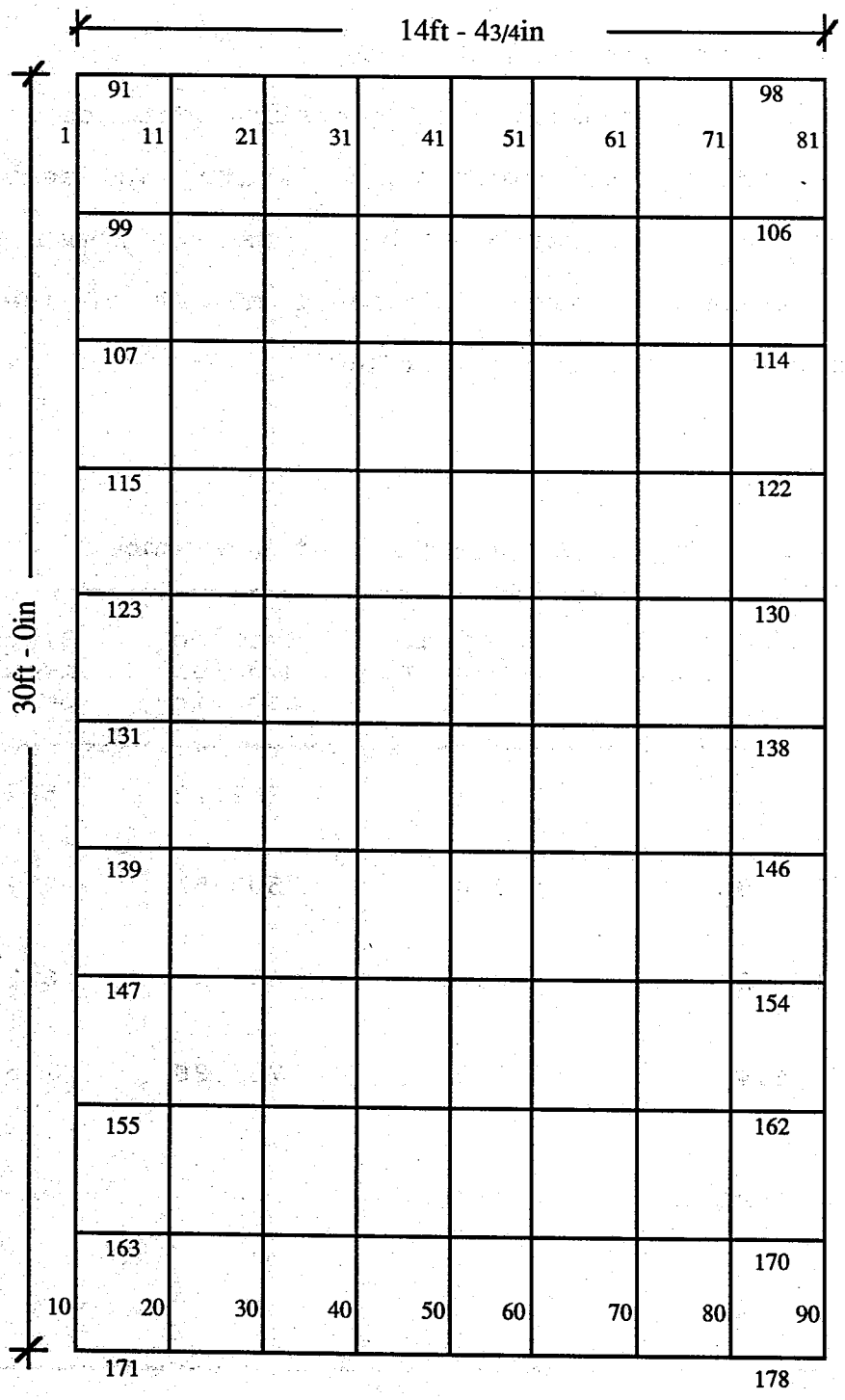

Fig. 3.5 The grillage model

joints at the ends were simply supported.

The input parameters consisted of geometric data consisting of coordinates of joints and member connectivity, and sectional properties of elements represented by cross sectional area, centroid, second moment of area, torsional moment of inertia, density, Young's modulus and shear modulus.

Table 3.2 Physical properties of the member

Member	Area of cross section (in^2)	Centroid from bottom (in.)	Section modulus top (in^3)	Section modulus bot(in^3)
Edge beam	150.44	7.49	512.42	582.79
Intermediate beam	156.90	7.02	509.51	652.60
Composite edge beam	164.22	8.09	637.26	622.77
Composite intermediate beam	184.46	8.16	765.86	735.28
Transverse end slab	82.80	8.74	-	-
Transverse intermediate slab	165.6	8.74	-	-

Table 3.3 Torsional moment of inertia of members (membrane analogy method)

Member	Torsional moment of inertia (in^4)
Composite edge beam	1424.85
Composite intermediate beam	1449.38
End slab element	138.92
Intermediate slab element	293.37

3.3.1 Loads acting on the model bridge system

The actual loads acting on the prototype were initially computed and the model loads derived using the similitude theory. The model loads were obtained by dividing the prototype values by the square of the linear scale. The following loads were considered in the design:

Dead load

Live load due to single HS 20-44 truck

Impact factor due to.live load

Dead Load:

Table 3.2 gives the cross sectional areas and centroid of the edge and intermediate beams. The self weight of the edge and intermediate beams are respectively 13.06 and 13.62 lb/in.

Live Load:

Fig. 3.6 shows the weight and geometric particulars of the

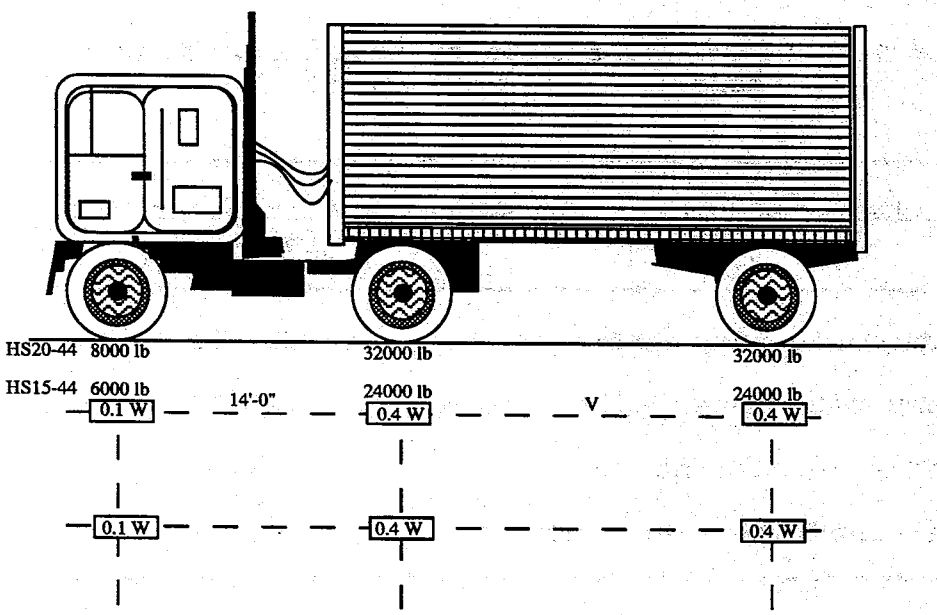

W = Combined weight on the first two axles which is the same as for the corresponding H (M) truck.

V = Variable spacing - 14 feet to 30 feet inclusive spacing to be used is that which produces maximum stresses.

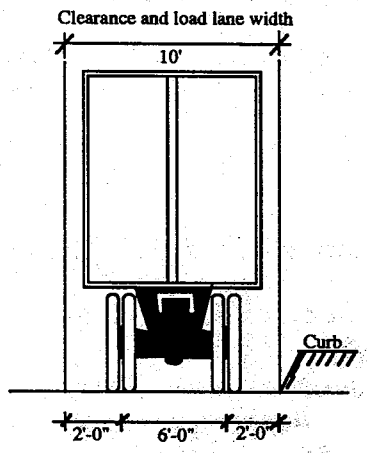

Fig. 3.6 AASHTO HS 20 - 44 truck load

HS 20-44 truck. For the case of the model, the total load of the truck is considered to be acting at the two rear axle positions.

Impact Factor:

The impact allowance is determined as a fraction of the live load stress by the formula

$$I = 50/(L+125) = 0.25 \quad (3.1)$$

Total live load acting on the prototype = 72 * 1.25

= 90 Kips

Live load acting on the model = 90/2.52 = 14.4 Kips

Tables 3.4 and 3.5 provide the typical input and output for the grillage analysis.

Table 3.4 Typical input data

```
Firm:  Florida Atlantic University
Name:  Ramkumar
Date:  March 18, 1988
Job Number: 1
Job Title:  Multi-Box Beam Bridge Analysis

Print Data, Summary Results Coordinates

Structure Bridge Deck

Type plane grid
Method stiffness joints

Tabulate all

Number of joints 99
Number of members 178
Number of supports 18
Number of loadings 1
```

Table 3.4 Typical input data (contd.)

```
Joint coordinates

1   Thru 9   X    0.0  Y  0.0   YL  172.8      Support
10  Thru 82    Step 9  X  36.0  Y   0.0   XL   324.0
11  Thru 83    Step 9  X  36.0  Y   21.6  XL   324.0
12  Thru 84    Step 9  X  36.0  Y   43.2  XL   324.0
13  Thru 85    Step 9  X  36.0  Y   64.8  XL   324.0
14  Thru 86    Step 9  X  36.0  Y   86.4  XL   324.0
15  Thru 87    Step 9  X  36.0  Y   108.0 XL   324.0
16  Thru 88    Step 9  X  36.0  Y   129.6 XL   324.0
17  Thru 89    Step 9  X  36.0  Y   151.2 XL   324.0
18  Thru 90    Step 9  X  36.0  Y   172.8 XL   324.0
91  Thru 99  X 360.0   Y  0.0   YL  172.8      Support

Joint releases

1   Thru 9  Moment X Y
91  Thru 99 Moment X Y

Member incidences

1   Thru 10  Range 1,10   82,91
11  Thru 20  Range 2,11   83,92
21  Thru 30  Range 3,12   84,93
31  Thru 40  Range 4,13   85,94
41  Thru 50  Range 5,14   86,95
51  Thru 60  Range 6,15   87,96
61  Thru 70  Range 7,16   88,97
71  Thru 80  Range 8,17   89,98
81  Thru 90  Range 9,18   90,99
91  Thru 98  Range 1,2    8,9
99  Thru 106 Range 10,11  17,18
107 Thru 114 Range 19,20  26,27
115 Thru 122 Range 28,29  35,36
123 Thru 130 Range 37,38  44,45
131 Thru 138 Range 46,47  53,54
139 Thru 146 Range 55,56  62,63
147 Thru 154 Range 64,65  71,72
155 Thru 162 Range 73,74  80,81
163 Thru 170 Range 82,83  89,90
171 Thru 178 Range 91,92  98,99

Constants E  4.28E+6 All G  1.78E+6 All density 0.0868 All
```

Table 3.4 Typical input data (contd.)

```
Member Properties

1   Thru  10  AX 164.22   IX 1424.85   IY 5039.445  CZ -8.092
11  Thru  80  AX 184.46   IX 1449.38   IY 6002.06   CZ -8.163
81  Thru  90  AX 164.22   IX 1424.85   IY 5039.445  CZ -8.092
91  Thru  98  AX 82.8     IX 138.92    IY 3857.44   CZ -8.74
99  Thru 170  AX 165.6    IX 293.37    IY 7714.89   CZ -8.74
171 Thru 178  AX 82.8     IX 138.92    IY 3857.44   CZ -8.74

Loading Case 1
Member loads

34   Force Z Concentrated P -2666.67  L 19.2
44   Force Z Concentrated P -2629.6   L 19.2
54   Force Z Concentrated P -2703.7   L 19.2
37   Force Z Concentrated P -2666.67  L 14.4
47   Force Z Concentrated P -2629.6   L 14.4
57   Force Z Concentrated P -2703.7   L 14.4

Solve
Finish
```

3.3.2 Results of the analysis

The analysis was carried out for dead load and different cases of live load to generate the moment and shear envelope. Live load was assumed to be carried by beam elements and equivalent wheel loads acting on respective beam elements were determined. The output from the grillage analysis consisted of shear force, bending moment, torsional moment and deflection at 3 ft. intervals. Fig. 3.7 shows the five truck load positions for the generation of the envelope and Tables 3.6 and 3.7 provide the resulting shear forces and bending moments. Figs. 3.8 and

Table 3.5 Typical Output Data

FLORIDA ATLANTIC UNIVERSITY
MULTI-BOX BEAM BRIDGE ANALYSIS/BRIDGE DECK

JOINT	X ROTATION	Y ROTATION	Z DISPLACEMENT
81	-.000002893	-.000338958	-.026871432
82	.000001881	-.000377525	-.013895495
83	.000001793	-.000376546	-.013855390
84	.000001446	-.000375670	-.013819795
85	.000000813	-.000375055	-.013794890
86	.000000000	-.000374833	-.013785914
87	-.000000813	-.000375055	-.013794890
88	-.000001446	-.000375670	-.013819795
89	-.000001793	-.000376546	-.013855390
90	-.000001881	-.000377525	-.013895495
91	.000000030	-.000390212	.000000000
92	.000000006	-.000389035	.000000000
93	.000000010	-.000387991	.000000000
94	.000000005	-.000387261	.000000000
95	.000000000	-.000386998	.000000000
96	.000000005	-.000387261	.000000000
97	-.000000010	-.000387991	.000000000
98	-.000000006	-.000389035	.000000000
99	-.000000030	-.000390212	.000000000

LOADING CASE 1/MEMBER FORCES

MEMBER	JOINT	TORSION	BENDING MOMENT	SHEAR FORCE
1	1	4238.6826	461.3181	1318.4843
	10	-4238.6826	-47926.7535	-1318.4843
2	10	2215.3433	48641.7515	1163.5798
	19	-2215.3433	-90530.6230	-1163.5798
3	19	-406.7960	90698.5855	613.6837
	28	406.7960	-112791.1976	-613.6837
4	28	-2024.1665	112489.8233	156.6477
	37	2024.1665	-118129.1414	-156.6477
5	37	-2182.6081	117648.1614	-323.1108
	46	2182.6081	-106016.1714	323.1108
6	46	-1392.7599	105639.3372	-586.7461
	55	1392.7599	-84516.4769	586.7461
7	55	-592.9873	84326.8038	-633.5216
	64	592.9873	-61520.0262	633.5216
8	64	-127.1932	61459.4861	-601.9866
	73	127.1932	-39787.9695	601.9866

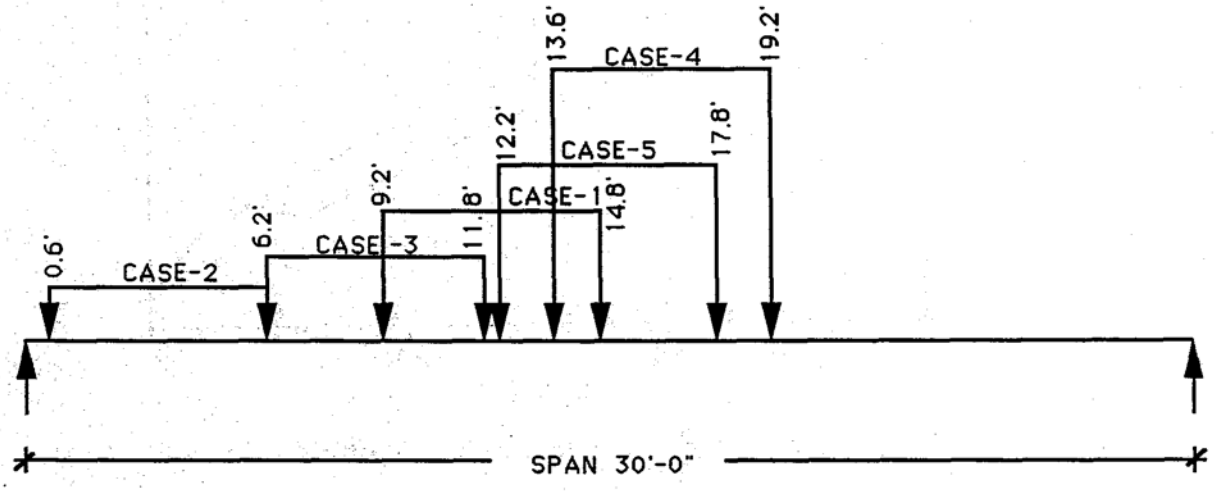

Fig. 3.7 Truck axle positions for live load analysis

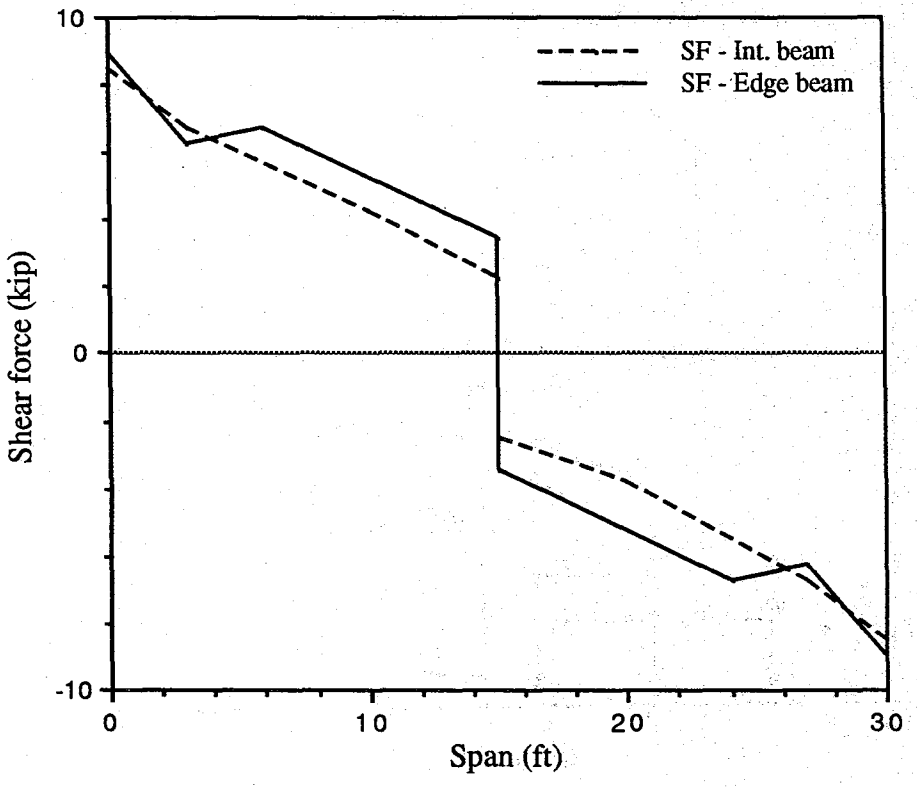

Fig. 3.8 Shear force envelope

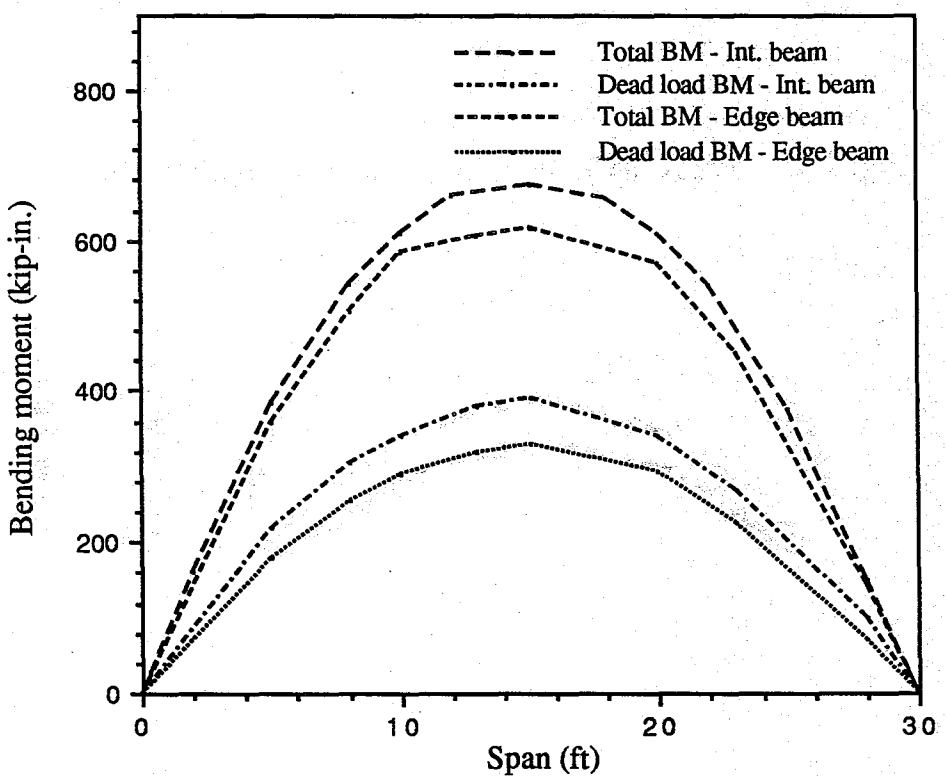

Fig. 3.9 Bending moment envelope

3.9 show the resulting shear and bending moment envelopes respectively for the bridge system.

3.3.3 Design of the model

The design of the nine pre stressed beams was carried out according to working stress method and was subsequently checked for ultimate strength.

3.3.3.1 Allowable stresses

The design of the prestressed beams was based on concrete strength f'c, 5000 psi. The stresses in concrete at different stages of beam fabrication are given by the following:

Specified 28 day compressive strength of concrete	= f' c
Compressive strength of concrete at release of prestress (f'ci)	= 0.8 f'c
Allowable compressive stress at release	= 0.6 f'ci
Allowable tensile stress at release	= $3\sqrt{f'ci}$
Allowable compressive stress at service	= 0.4 f'c
Allowable tensile stress at service	= 200 psi

Table 3.6 Shear force under five load cases (kips)

Span (ft.)	Dead load	Live load case 1	case 2	case 3	case 4	case 5
Intermediate beam						
0	4.21	1.68	4.25	2.80	2.23	1.77
3	3.64	1.72	1.70	2.97	2.34	1.83
6	2.76	1.81	1.82	3.18	2.57	1.97
9	1.88	2.88	0.85	0.86	2.81	2.23
12	1.01	0.76	0.66	1.81	0.52	2.48
15	0.14	0.55	0.53	1.57	2.15	0.29
Edge beam						
0	3.52	1.73	5.46	2.91	2.27	1.81
3	3.00	1.78	1.97	3.32	2.44	1.87
6	2.30	1.92	2.76	4.24	2.94	2.08
9	1.57	1.72	1.24	1.18	3.88	2.58
12	0.84	2.43	0.74	2.82	0.82	3.53
15	0.11	1.57	0.53	1.89	3.18	0.47

Table 3.7 Bending moment under five load cases (in-kips)

Span (ft.)	Dead load	Live load case 1	case 2	case 3	case 4	case 5
Intermediate beam						
0	0.0	0.0	0.0	0.0	0.0	0.0
3	141.3	60.6	78.5	100.8	80.3	63.8
6	250.9	122.6	151.4	207.8	164.5	129.7
9	328.9	187.8	115.6	232.5	257.1	200.7
12	375.7	246.9	91.9	257.1	268.8	281.0
15	391.3	266.5	73.0	200.7	281.0	280.6
Edge beam						
0	0.0	0.0	0.0	0.0	0.0	0.0
3	117.5	60.2	83.0	102.2	79.1	62.8
6	209.6	120.1	151.4	216.9	162.0	125.5
9	275.5	185.2	114.8	231.5	263.4	196.2
12	315.1	244.0	87.8	262.1	265.7	285.8
15	328.3	262.9	69.4	195.0	285.2	276.5

3.3.3.2 Stress inequality conditions and plots

The four governing equations of stress inequality are given below:

$-P/A + P*e/Z_{lt} - M_d/Z_{lt} < 3\sqrt{f'ci}$ (3.2)

$P/A + P*e/Z_{lb} - M_d/Z_{lb} < 0.6\ f'ci$ (3.3)

$a*P/A - a*Pe/Z_{lt}+M_d(B+S)/Z_{lt}+M_1/Z_{2t} < 0.4\ f'ci$ (3.4)

$-a*P/A - a^{*}P*e/Z_{lb}+M_d(B+S)/Z_{lb}+M_l/Z_{2b} < 2.00$ psi (3.5)

where

P = Prestressing force in the beam

A = Area of cross section of he beam

a = Factor to account for loss in prestressing force

e, = Eccentricity of the prestressing force

Ma = Moment due to dead load of the beam

Md(B+S) = Moment due to dead load of beam and slab

M_l = Moment due to the live load

Z_{lb}, Z_{lt} = Section modulus at the bottom and top of the beam respectively

Z_{2b}, Z_{2t} = Section modulus of the composite section at bottom and top respectively

Equations (3.2) and (3.3) consider the prestressing force and the stress due to dead load at transfer in the top and bottom fibers respectively. Equations (3.4) and (3.5) take into account the effects of prestress losses, the superimposed dead load due to the cast in-situ slab and the live load in the top and bottom fibers respectively. The stress values at different.

locations in the span were, substituted into these equations and plotted to determine the required amount of prestressing forces. Fig. 3.10 gives the stress inequality conditions at midspan which indicated maximum prestressing force requirement. Tables 3.8 and 3.9 provide the stresses at different locations in the span due to dead load, dead load and cast in-situ slab, and that due to live load in the edge and intermediate beams respectively.

3.3.3.3 Selection of prestressing strands

The stress inequality equations and the plots indicate a prestressing force requirement of 83.2 kips in the edge beam and 91 kips in the intermediate beam. Three tendons with 1/2 in. diameter, 7 wire strand having an ultimate strength of 270 ksi was selected for each beam. The tendons are stressed to 70 percent and 75 percent of the ultimate strengths for the edge and intermediate beam respectively. Fig. 3.11 shows the tendon locations in the intermediate and the edge beam respectively. The detailed structural drawing is shown in Fig. 3.12.

3.3.3.4 Estimation of prestress losses

The loss of prestress in the edge and intermediate beams due o all causes excluding friction was estimated according to

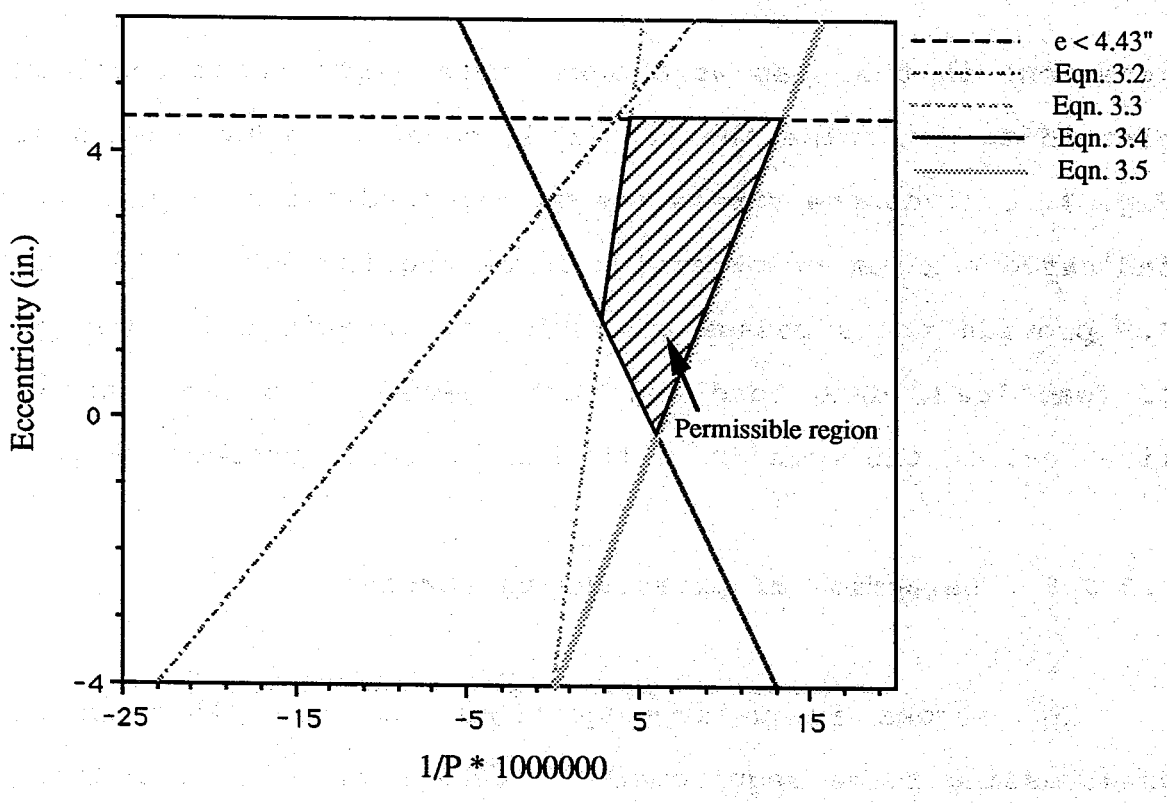

Fig. 3.10 Stress inequality plot

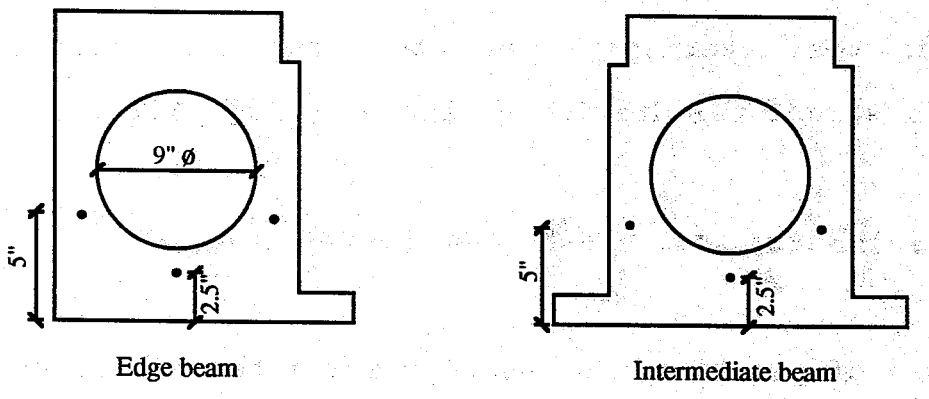

Fig. 3.11 Prestressing strand location

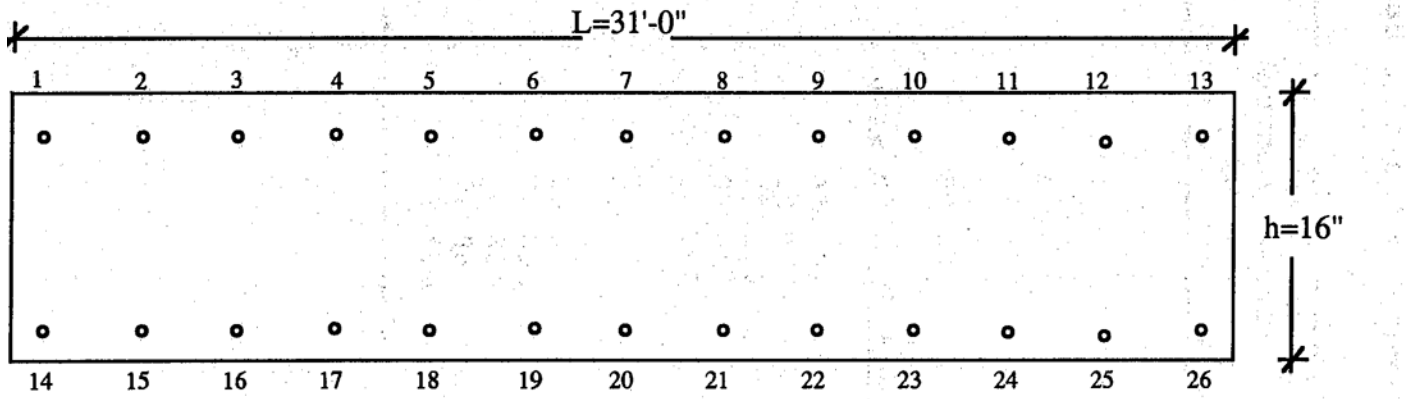

Strands 1 , 13 , 14 , 26	----	12.3 kips
Strands 2 , 12 , 15 , 25	----	17.6 kips
Strands 3 - 11 and 16 - 24	----	13.2 kips

Fig. 3.12 Lateral post - tensioning forces in the strands

Table 3.8 Stress in the edge beam

Span (ft.)	Moment (kip-in.)	Stress (bottom) (psi)	Stress (top) (psi)
Due to dead load			
3	76.17	130.7	148.6
6	135.4	232.34	264.25
9	177.72	304.95	346.82
12	203.11	348.51	396.37
15	211.57	363.03	412.89
Due to dead load of beam + cast in-situ slab			
3	117.47	201.56	229.24
6	209.56	359.59	408.97
9	275.50	472.73	537.65
12	315.10	540.68	614.93
15	328.31	563.33	640.70
Due to live load			
3	102.19	164.09	160.36
6	216.93	348.33	340.41
9	263.43	423.0	413.38
12	285.80	458.91	448.48
15	285.20	457.96	447.55

Table 3.9 Stress in the intermediate beam

Span (ft.)	Moment (kip-in)	Stress (bottom) (psi)	Stress (top) (psi)
Due to dead load			
3	79.43	121.71	155.9
6	141.21	216.38	277.15
9	185.34	284.0	363.76
12	211.82	324.58	415.73
15	220.64	338.1	433.05
Due to dead load of beam + case in-situ slab			
3	141.34	216.58	277.40
6	250.89	384.45	492.41
9	328.92	504.02	645.57
12	375.69	575.68	737.35
15	391.27	599.56	767.94
Due to live load			
3	100.78	137.06	131.59
6	207.79	282.6	271.32
9	257.13	349.7	335.73
12	280.99	382.16	366.9
15	280.98	382.15	366.89

AASHTO 9.16 (Ref. 36).

Total loss = $SH + ES + CR_c + CR_s$ .....(3.6)

SH = Loss due to concrete shrinkage in psi.

ES = Loss due to elastic shortening in psi.

CR_c = Loss due to creep of concrete in psi.

CR_s = Loss due to relaxation of prestressing steel in psi

$SH = 17000 - 150\ RH$ .....(3.7)

(RH = mean ambient relative humidity in percent)

$ES = (E_s/E_{ci})f_{cir}$ .....(3.8)

E_s = modulus of elasticity of prestressing strand $= 28 \times 10^6$ psi

E_{ci} = modulus of elasticity of concrete at transfer of stress $= 33w_c^{1.5}\sqrt{f'_{ci}}$

f_{cir} = concrete stress at the center of gravity of the prestressing steel due to prestressing force and dead load of beam immediately after transfer

$CR_c = 12f_{cir} - 7f_{cds}$ .....(3.9)

f_{cds} = concrete stress at the center of gravity of the prestressing steel due to all loads except the dead loads present at the time the prestressing force is applied.

$CR_s = 20{,}000 - 0.4ES - 0.2\ (SH + CR_c)$ .....(3.10)

Table 3.10 provides the summary of the losses computed using the above equations, in both the edge and intermediate beams.

Table 3.10 Prestress losses

Item	Intermediate beam (lb.)	Edge beam (lb.)
Shrinkage	5000	5000
Elastic shortening	4526.3	4635.2
Creep (concrete)	6694.8	6995.2
Relaxation of steel	15850.5	15746.9
Total	32071.6	32377.3
Percentage loss	16.97	17.13

3.3.3.5 Estimation of lateral post tensioning force

The post tensioning force was estimated based on achieving an effective concrete stress in the transverse direction of 200 psi. At the supports and 150 psi. in the mid 80 percent of span. Losses in post tension are attributed to friction and low average stress in strands.

Loss due to friction:

$$T_o = T_x e(\mu\alpha + kx)$$

$$\approx T_x (1+\mu\alpha+kx) \qquad (3.11)$$

T_o = force at Jacking end

T_x = force at other end

μ = primary curvature coefficient

k = secondary curvature coefficient

α = total angle change

x = distance from the jacking end to other end in feet

Substituting $\alpha = 0$, $K = 0.0014$ in Eqn. (3.11)

gives $T_o = 1.02 \quad T_x$

Other losses:

When the post-tensioning average stress is about 250 psi, the losses will be around 1.5 percent based on experimental results.

Accordingly, the required force at jack T_o 1.17 Tx. Fig. 3.12, shows the required force, in each post-tension tendons.

3.3.3.6 Determination of cracking moment

The cracking moment is the moment for which the tensile stress- on the extreme- fiber of. the concrete section reaches a value equal to the modulus of rupture of the concrete. Considering the bottom fiber of a prestressed concrete section the cracking moment, M_{cr} is determined using the following equation:

$P/A + Pe/Z_{lb} - M_d(g)/Z_{lb} - M_{d(S)}/Z_{2b} - M_l/Z_{2b} = - f_{cr}$,

f_{cr} = modulus of rupture = $7.5 \sqrt{f'c}$

The first two terms on the left hand side of the Equation (3.12), give the stress due to the prestressing force. The third and fourth term represent the stress due to dead load of the beam and cast-in-situ slab respectively. The fifth term is the stress due to the cracking moment just before cracking. For a typical intermediate beam, the values are,

$P = 3 \times 31{,}000 = 93{,}000$ lbs $\qquad A = 156.9$ in^2

$e = 2.85$ in. $\qquad Z_{lb} = 652.60$ in^3, $\qquad Z_{2b} = 735.28$ in^3

f'c = 8200 psi $\qquad f_{cr} = 7.5\ \sqrt{8200} = 679.2$ lb/in^2

The moment at midspan due to self weight of the beam is computed to be 220.644 in-kips and that due to cast-in-situ slab is 170.629 in-kips. The live load moment at first cracking is determined as 689.74 in.-kips, by substituting the above values in Equation (3.12).

A grillage analysis was carried out for a typical line load of 18.6 kips distributed over the width of the bridge model at midspan and the maximum moment in an intermediate beam was determined to be 197.17 in-kips. The required line load to cause cracking was determined from the ratio of live load moment to cause cracking to the moment due to the applied load of 18.6 kips.

Line load to cause cracking = 689.74 X 18.6 / 197.17

= 65.07 kips

3.3.3.7 Determination of ultimate load

The ultimate moment capacity can be computed by using the rectangular stress distribution in. concrete (Fig. 3.13). The reinforcement ratio p x f*su /f'_c must be below 0.3 (AASHTO 9.18.1) tonsure yielding of the reinforcement at the section of maximum bending moment at midspan.

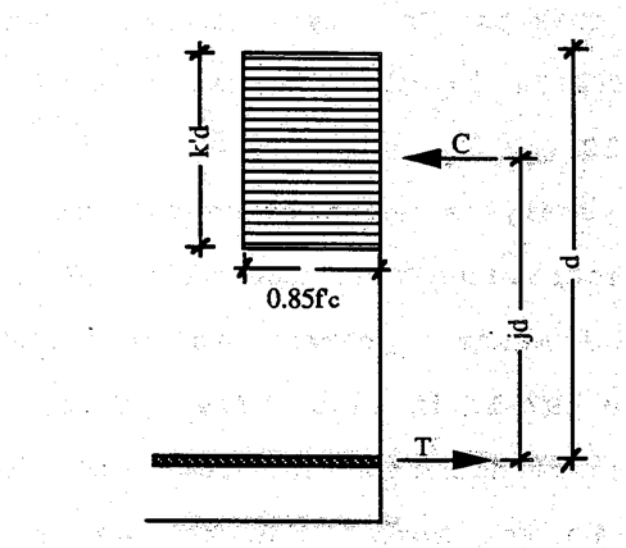

Fig. 3.13 Rectangular stress block

Midspan section:

$e = 2.85$ in., $d = 11.83$ in.,

$A = 0.459$ in^2, $b = 22.6$ in.

$f'_c = 8200$ psi

$p = A_s / (b \times d) = 0.001717$ (AASHTO 9.17)

$0.5 \times p \times f'_s / f'_c = 0.0283$

$f^*_{su} = f'_s [1 - (0.5 \times p \times f'_s / f'_c)] = 262.4$ ksi

$p \times f^*_{su} / f'_c = 0.055 < 0.3$ 0.K

$T = 0.459 \times 262.4 = 120.44$ kips

$k' \times d = 120.44 /(0.85 \times 8.20 \times 22.6 = 0.765$ in < Slab thickness

Hence a rectangular section

$j \times d = 11.83 - 0.765 / 2 = 11.45$ in.

$M_u = 11.45 \times 120.44 = 1379.2$ in - kips

Considering 9 beams, $M_u = 12412.8$ in - kips

Moment due to dead load = 1759.22 in - kips

Required live load moment = 10653.6 in - kips

Required ultimate live line load = 118.4 kips

3.4 Acoustic Emission Technique for Crack Monitoring (38)

Acoustic emission (AE) is the characteristic and irreversible sound emitted by a material when it is deformed. When a solid is subjected to stress at a sufficiently highlevel, sound is generated in the material and emitted in the form of elastic waves. There are two types of acoustic emission (AE) continuous and burst type. Continuous emission is a low energy emission and can be eliminated from the data acquisition system along with other unwanted filter noises by setting an appropriate threshold. Burst type emissions can be mathematically described as decaying sinusoids. These burst type emissions are significant for AR analysis. AE sources can be distinctly classified into the four groups:

i) Dislocation movements

ii) Phase transformations

iii) Friction mechanisms

iv) Crack formation and extension

For the AE monitoring of the ultimate load test of the model bridge system the crack formation and extension (fourth category) is of particular relevance.

One of the parameters for measuring AE activity is the detection of ringdom counts. A single burst type emission is termed an event, and the number of times the signal crosses the threshold is taken as the number of counts 3.14. More the number of counts in an event, more intense is the damage.

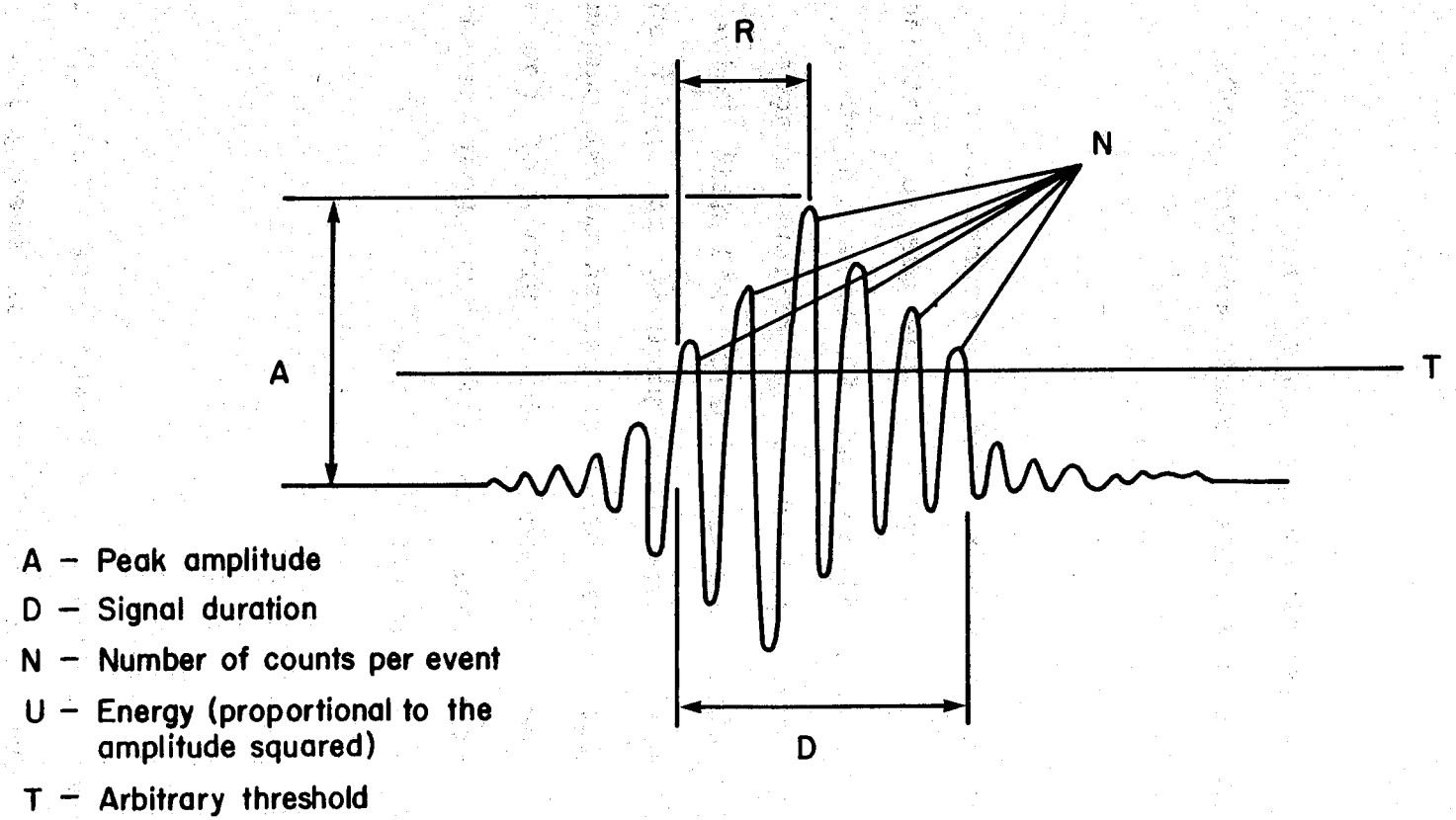

Fig. 3.14 Acoustic emission signal parameters

CHAPTER 4

FABRICATION AND TESTING OF THE ACRYLIC AND PRECAST PRESTRESSED CONCRETE MULTI-BOX BRIDGE SYSTEMS MODELS

4.1 Introduction

The details of fabrication, and instrumentation of the acrylic and concrete models as well as the static, fatigue and ultimate load tests are discussed in this chapter. The fabrication of the models was done in various stages. The acrylic model was fabricated at Florida Atlantic University whereas nine prestressed beams were precast at the plant of STRESSCON, Hialeah. They were then transported to FAU campus and erected under the loading frame. The pouring of top: slabs connecting the multi-box beams, the transverse post tensioning and grouting were done at the FAU test site.

4.2 Acrylic Mode

4.2.1 Fabrication

Rectangular beams, 1.5" x 1.75" x 40" size, were first cut using a band saw from the thick sheet of plexiglass. The surfaces were then machined to obtain a size of 1.5" x 1.6" x 38" with a smooth finish, Fig. 4.1. One in holes were drilled for

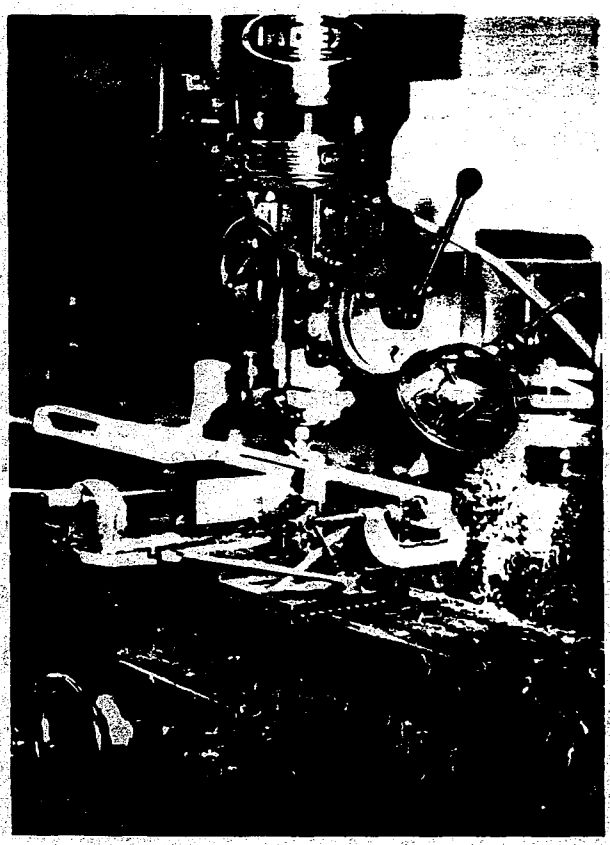

Fig. 4.1 Preparation of the acrylic model

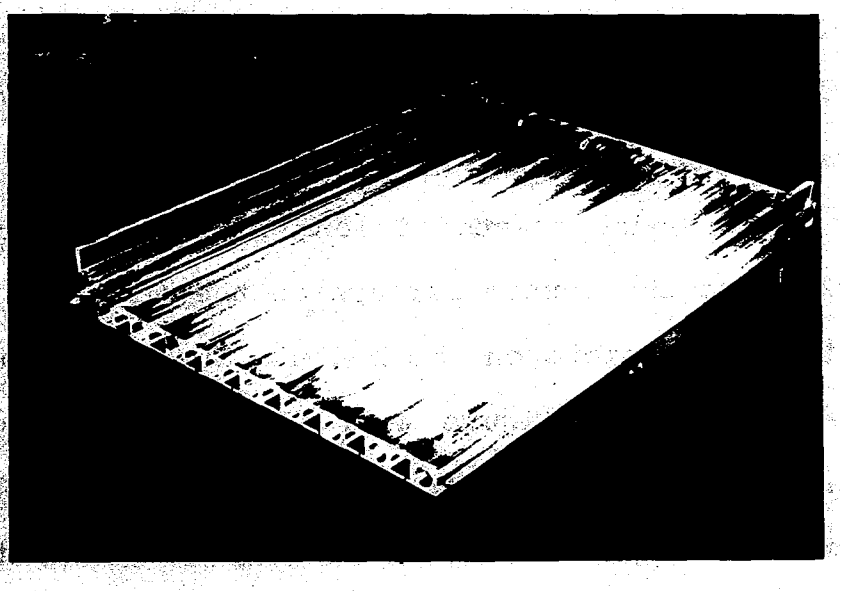

Fig. 4.2 Acrylic model

the entire span length of the beam. This involved drilling holes from either end of the beam and the drilling was continued from both ends until the holes meet at the beam center. This required considerable skill and long machining time to align the hole from either end to minimize the mismatch at the center. This was achieved by first drilling a hole of 1/2 in. diameter and then enlarging it to a 1 in. diameter. This technique reduced the vibration and provided for greater accuracy. The drilling was carried out at low speed to minimize the induced thermal stresses.

Once the beams were drilled, the model deck was assembled together with flanges and slab elements glued in place. The assembled model is shown in Fig. 4.2.

4.2.2 Test Set-up

The existing loading frame in the laboratory was modified to facilitate the testing of the 1/20 scale model. A hydraulic jack of 5 ton capacity was installed for load application.

4.2.3 Instrumentation

Strain gages for measurements of longitudinal and transverse strains were glued to the bottom surface of the deck, at the midpoint and quarter-span points on the beams. The locations of the strain gages are shown in Figure 4.3. In addition to these, strain gages and rosettes were also installed on the webs of the beams to measure the shear strains. The location of the dial gages is shown in Fig. 4.4. The instrumentation also included

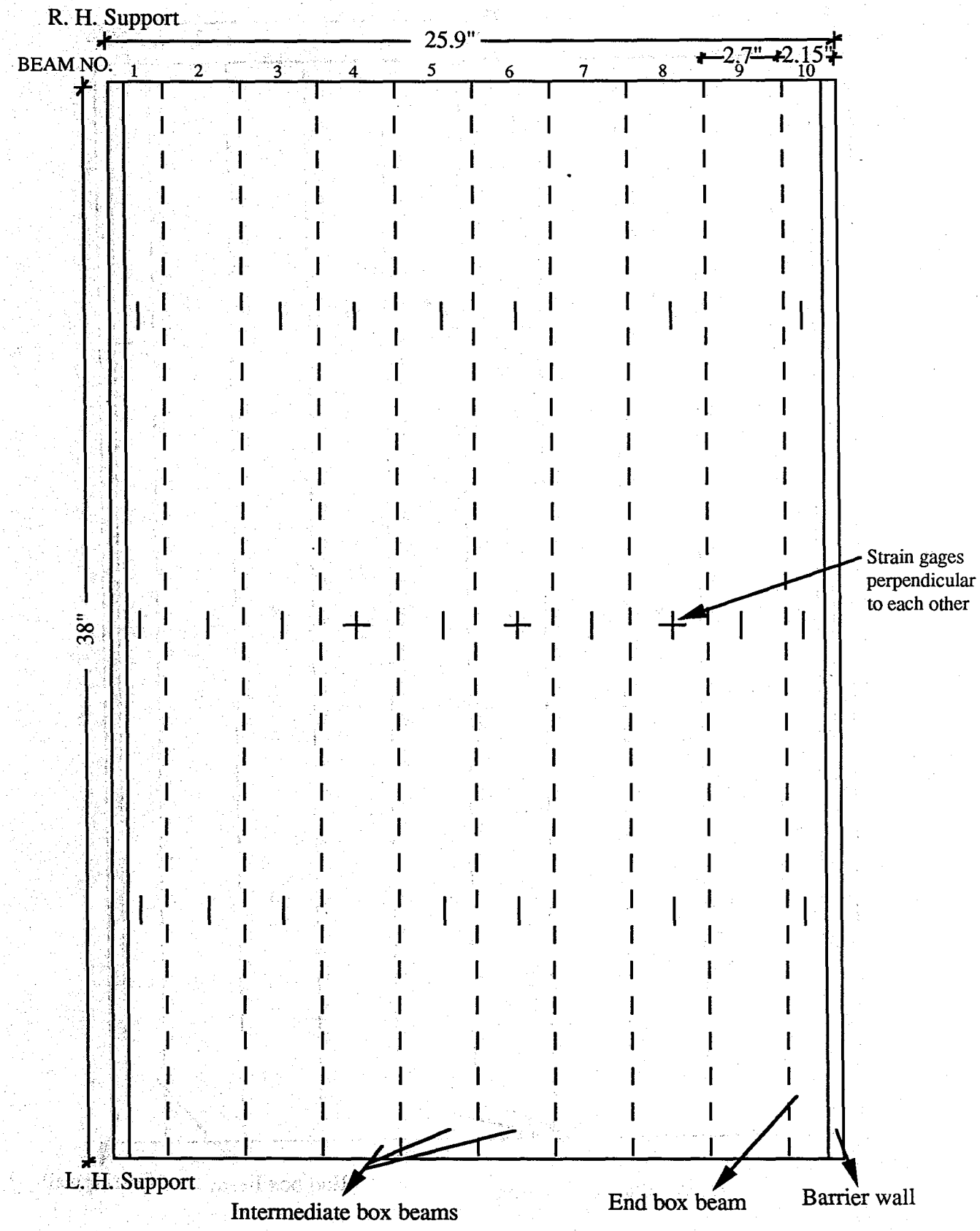

Fig. 4.3 Location sketch of the strain gages

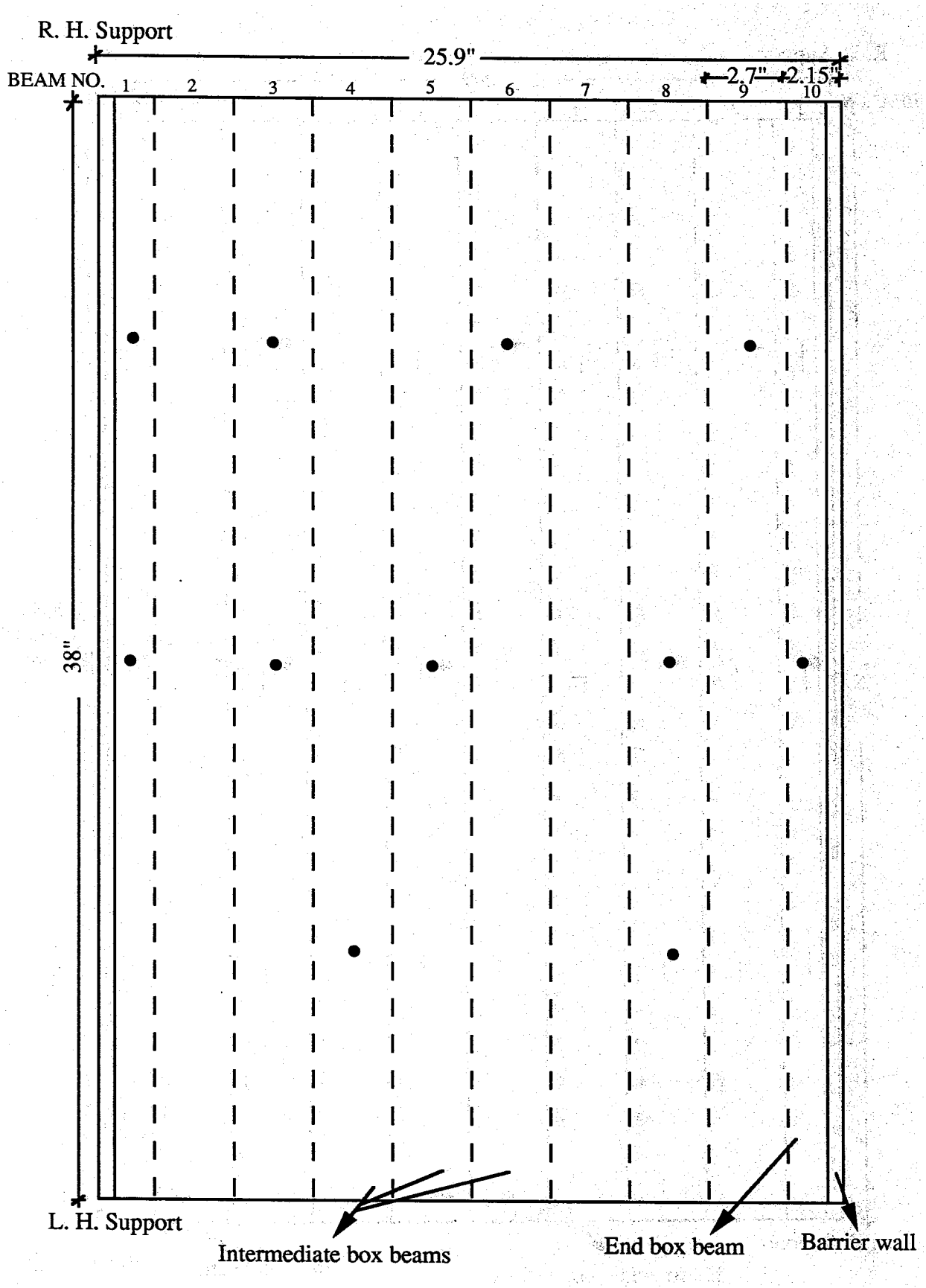

Fig. 4.4 Location sketch of the deflection gages

deflection gages mounted at various points under the model. The modified loading frame and typical deflection gage locations are shown in Figs. 4.5 and 4.6.

4.2.4 Load locations

Seven load positions were selected on the bridge deck based on considerations of maximum moment, torsion and shear. The load locations were also selected with the objective of obtaining load distribution coefficients. The locations of the loading device for the seven load positions are shown in Figures 3.2, 3.3, and 3.4.

4.2.5 Test procedure

The strain gages were connected to four units of 10 channel strain indicators. The model under test is shown in Figure 4.7. The model was tested using incremental loading to a maximum load of 400 lb. The strain gage and dial gage readings were recorded for each stage of loading. This procedure was repeated for each test corresponding to the other load locations.

4.3 Concrete Model Multi-Box Bridge System

4.3.-1 Fabrication of the precast prestressed beams

The two end and seen intermediate prestressed beams were cast one per day in a specially erected wooden formwork, at the

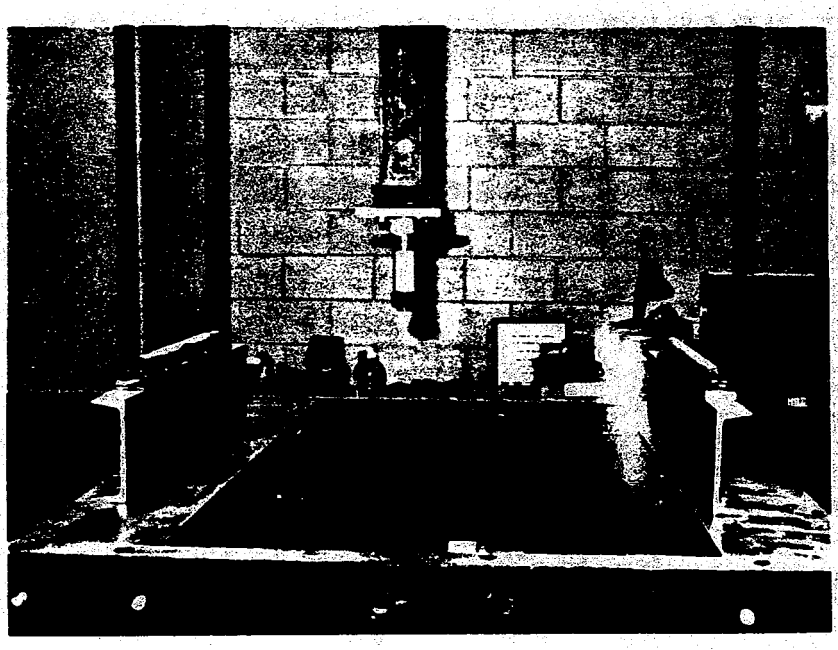

Fig. 4.5 Loading frame for acrylic model test

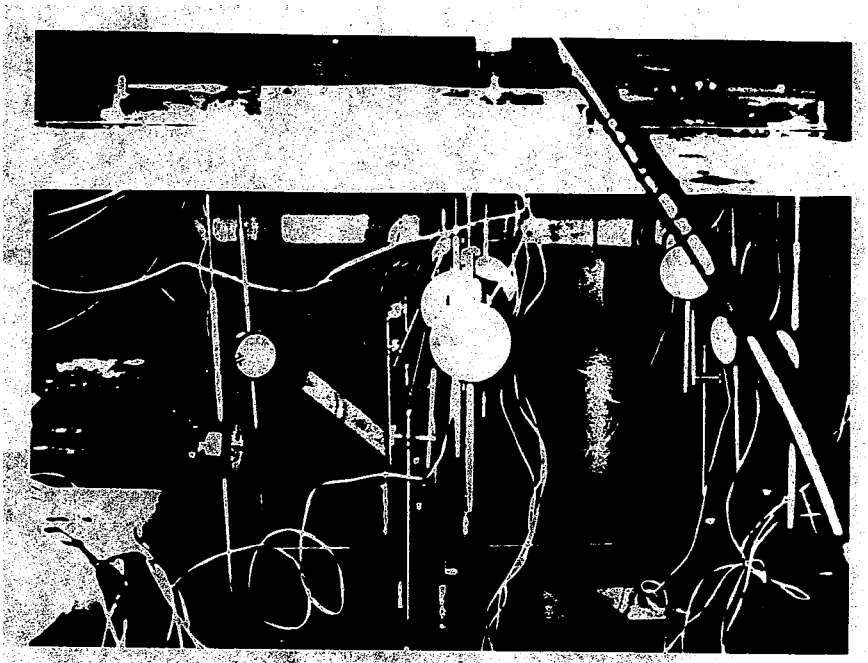

Fig. 4.6 Location of deflection gages

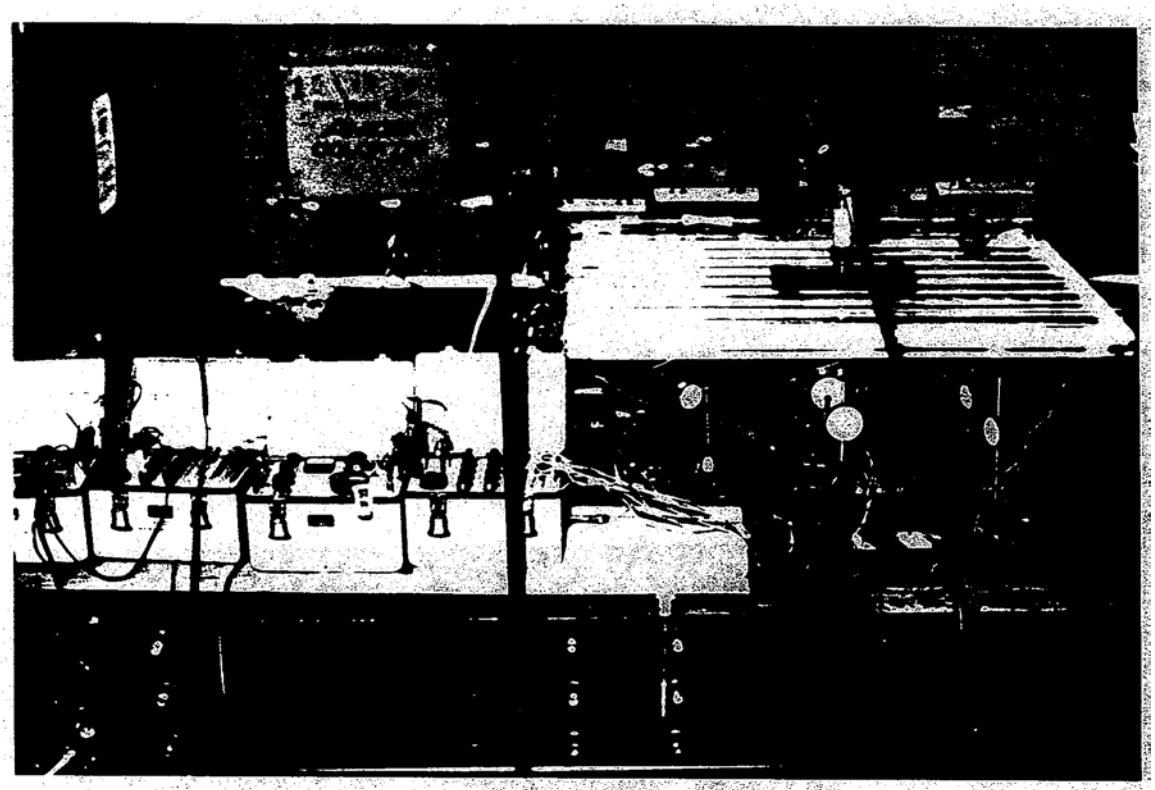

Fig. 4.7 Acrylic model under test

Fig. 4.8 Formwork and the prestressing bed

prestressing bed in the STRESSCON plant. Figure 4.8 shows the wooden formwork and the prestressing bed. The special features of the fabrication were:

a) an 8. inch internal diameter, 30 ft. long PVC pipe with a splice of 20 ft. used for the circular void and b) 3/4 inch diameter corrugated metal ducts placed and aligned transversely for the 13 post tensioning ducts both in the top and at the bottom. Special junction boxes were provided, in the bottom row of the 3/4 inch diameter ducts for injecting grout from the bottom. Similar arrangements were made in the top row at site before pouring the slab. These details are shown in the fabrication drawing enclosed (Figure 4.9). Figure 4.10 shows the top view of the form, with the PVC pipe and the post tensioning duct.

Special polyester mold electrical resistance strain gages of type PML-60 marketed by Texas Measurements, Inc. were embedded in the concrete at three depths as shown in Figure 4.11 to measure the concrete strains. This embedded gage is designed to measure interior strains in concrete during loading. The gage and lead wires are hermetically sealed between thin resin plates, completely water proofing, the whole unit. It is coated with a coarse grit to eliminate bond failures with the concrete. The sequence of casting of the beams was as follows:

The form work was prepared and strands tensioned each morning and the strain gages were installed subsequently ensuring that the gages would stay in place during concreting. Concrete was

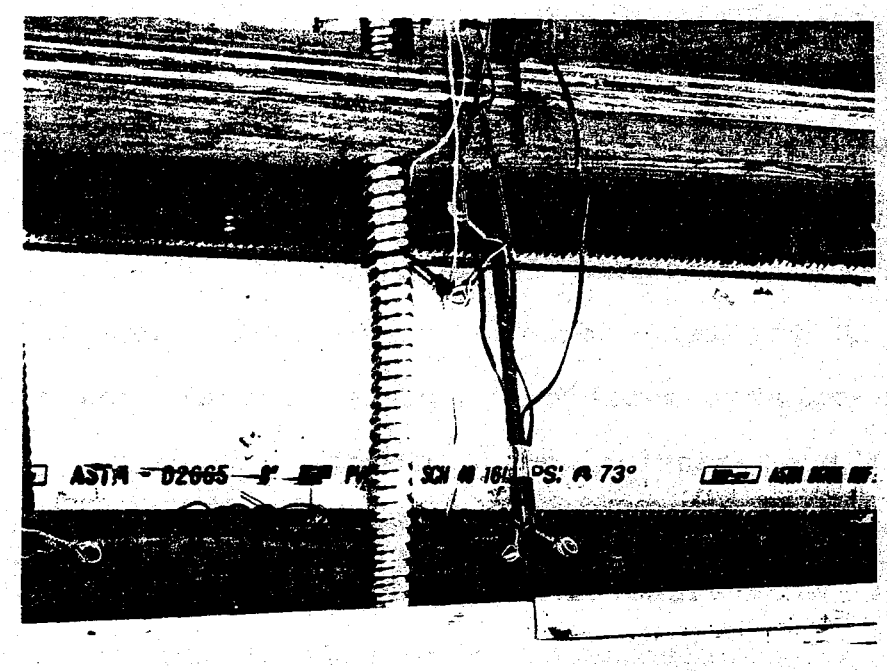

Fig. 4.10 View of the form showing the PVC pipe and lateral post-tensioning duct

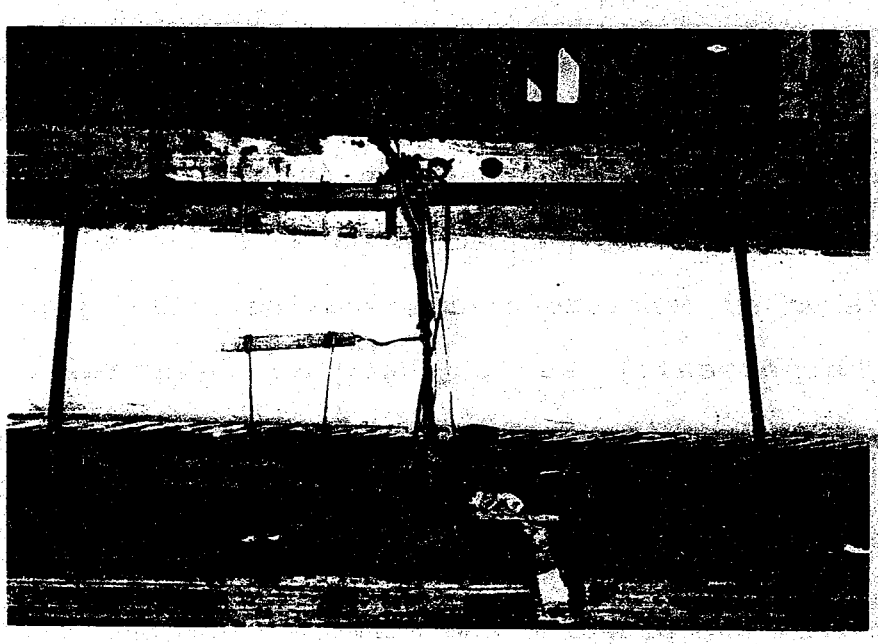

Fig. 4.11 Strain gage embedded in the concrete

poured same day. The strands were released the following day morning and beams removed to the curing yard. The schedule of casting is given, in Table 4.1 with the 28 day cylinder strength of concrete. Figure 4.12 shows the casting of the beams.

Table 4.1 Schedule of casting of the beams and the 28 day cylinder strength of concrete

Beam No.	Date of casting	f'_c (psi)
1	5-24-88	8232
2	5-25-88	8143
3	5-26-88	8223
4	5-27-88	8241
5	5-31-88	8188
6	6-01-88	8144
7	6-03-88	8214
8	6-07-88	8232
9	6-09-88	8117

4.3.2 Erection of the precast beams

The existing 10 feet wide supporting piers at the FAU test site were widened to 16 feet and repositioned to suit the span of 3.0 feet. A 6 inch wide reinforced bearing pad was provided on the support. Figure 4.13 shows the supporting wall with the

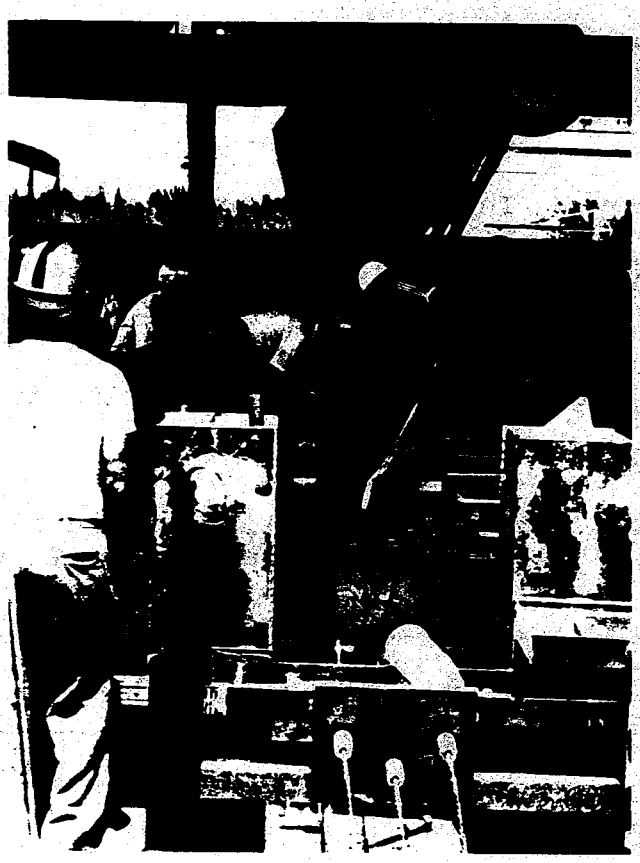

Fig. 4.12 Casting of the concrete

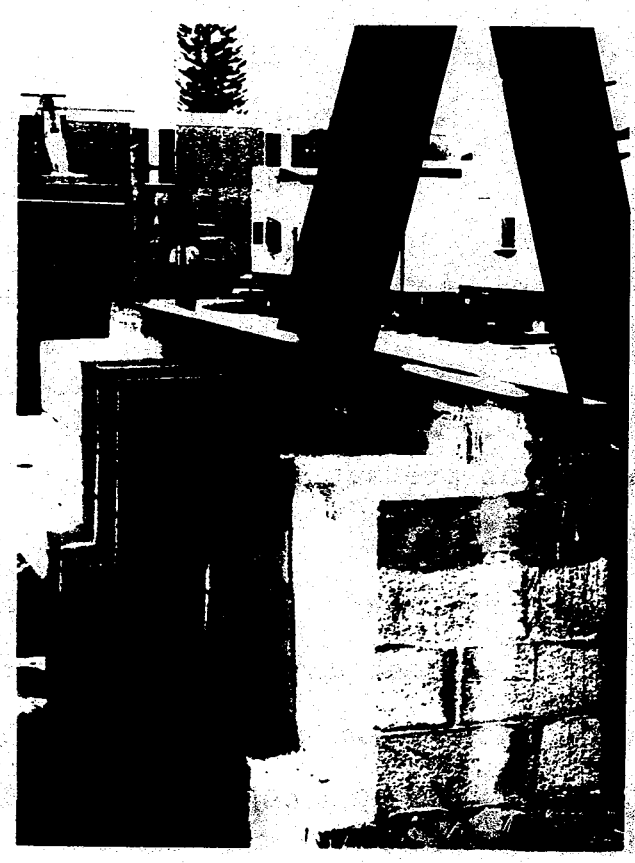

Fig. 4.13 Supporting wall with the bearing pad in position

bearing pad in position. The nine precast beams were transported by truck to FAU and erected under the loading frame. Figures 4.14. and-4.15 show the handling and erection respectively of the beams. Figure 4.16 shows the beams assembled in place.

4.3.3 Joint grouting, cast-in-situ slab and post tensioning

The bottom transverse post tensioning ducts were jointed using couplers at the 'V' joint and the strands placed in position. Subsequently the bottom joints were cement grouted. Then the top strands were kept in position and the cast-in-situ slab was poured. The average cylinder strength of the concrete in cast-in-situ slab was determined to be 4680 psi after 5 days. The forces in the transverse post tensioning strands at the top and bottom of the beams :are shown in Figure. 3.12. The top and bottom ducts were subsequently grouted to ensure bond between the ducts and the tendons.

4.3.4 Experimental set up

4.3.4.1 static and fatigue load tests

Twenty three concrete piles of size 14" x 14" each weighing 4 kips were placed over the HP beams to provide adequate capacity of dead load for application n of gravity loading in the test frame. The wheel loads of HS20-44 truck was simulated by

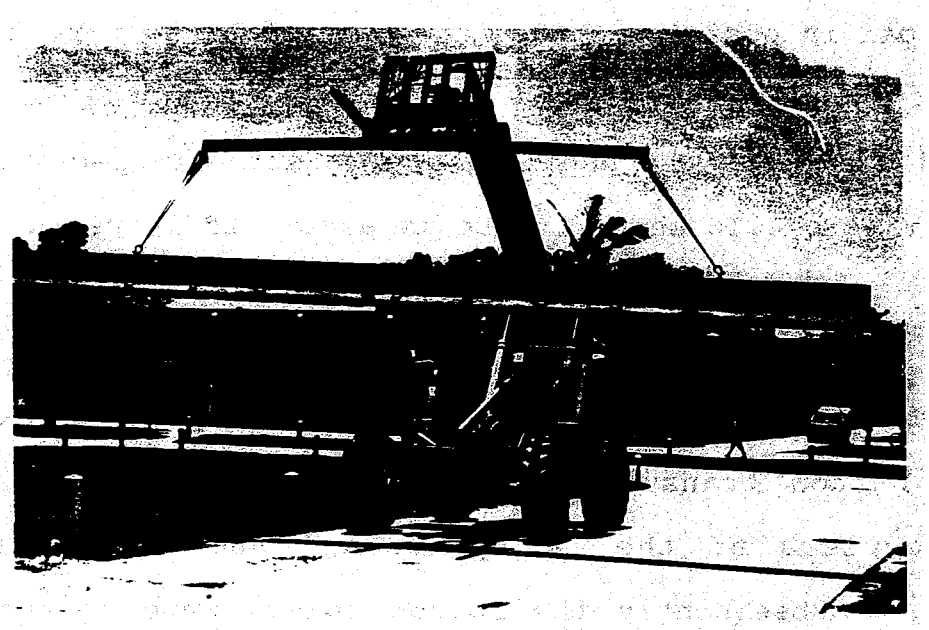

Fig. 4.14 Handling of the precast beams

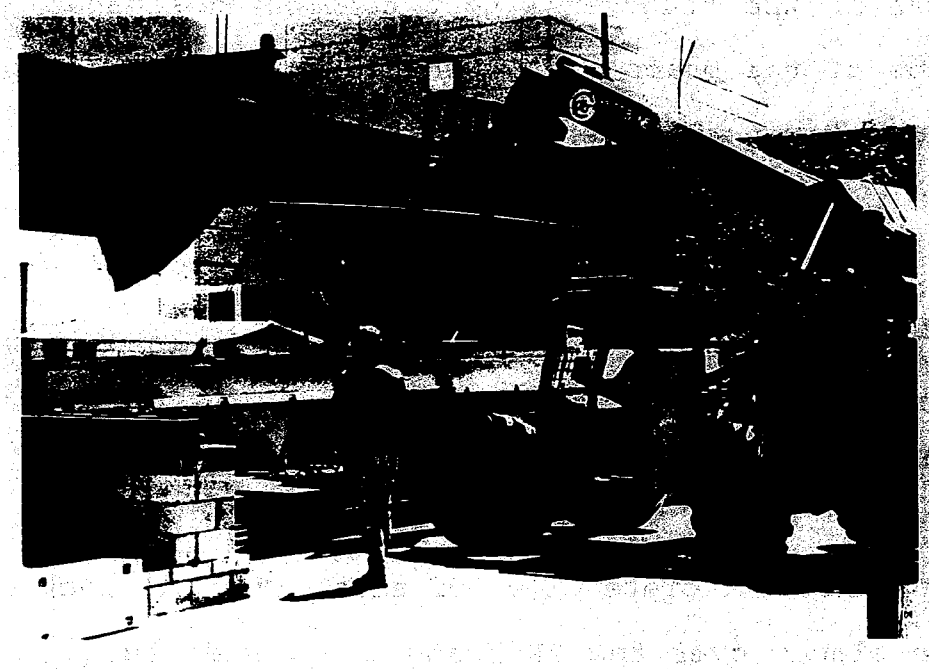

Fig. 4.15 Erection of the precast beams

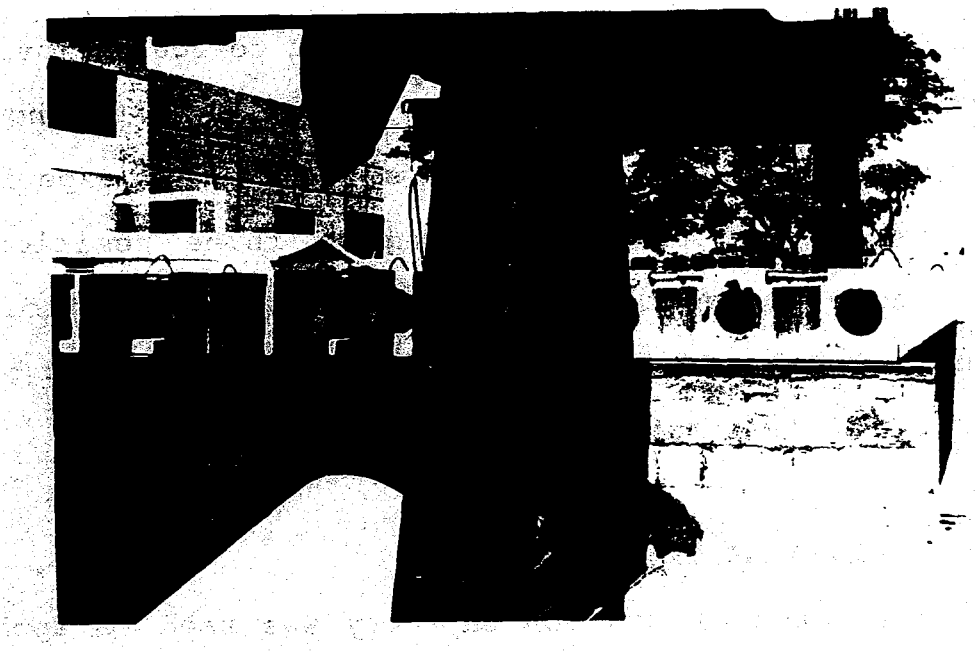

Fig. 4.16 Beams assembled in place

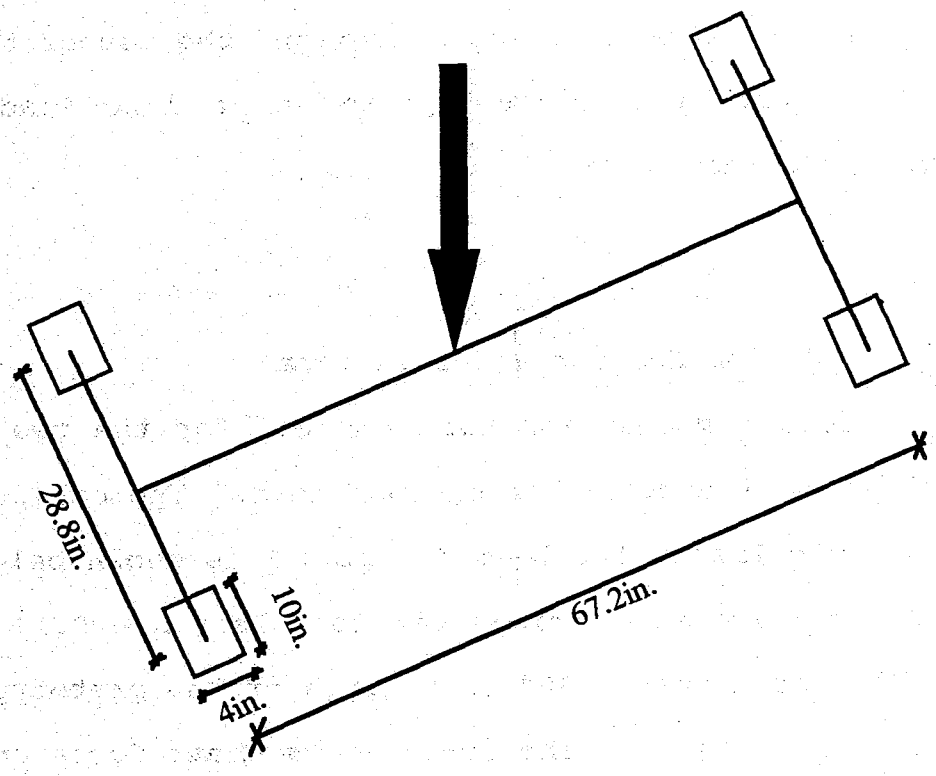

Fig. 4.17 Truck load simulation

distributing the MTS hydraulic actuator load to four points using the arrangement shown in Figure 4.17. Figure 4.18 shows the concrete model and the experimental set up. The experimental program consisted of fatigue testing at three positions and static testing at three other positions shown in Figure 4.19. Measurements, of deflections, concrete strains, and joint opening were made in both the static and fatigue tests.

4.3.4.2 Ultimate load test

A hydraulic jack of 200 ton capacity was used to apply the loading on the-model bridge system. A specially built-up loading arrangement consisting of I-sections was attached to the bottom of the HP sections comprising of the load frame and the hydraulic jack placed between this built-up system and the top of the model bridge. The ultimate load was applied as a line load on the bridge Fig. 4.20a and 4.20b.

4.3.5 Dead load compensation and load data

The dead load compensation was computed for the two fatigue load positions to determine the minimum load. Typical dead load compensation calculation for load position 1 is shown below:

Dead load of prototype bridge per foot length ,= 9.14 kips/ft. Dead load shear at distance 80" (2'x depth of the prototype) from the support = 281.9 kips. The scaled down shear force on the

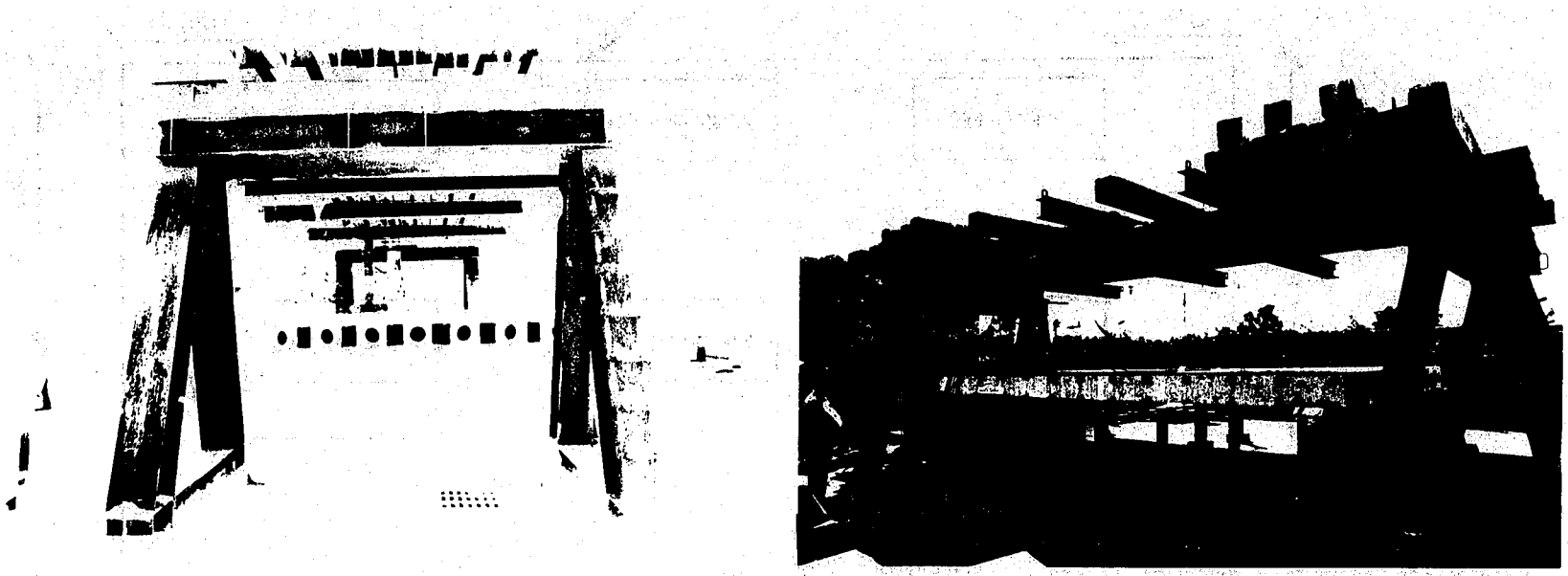

Fig. 4.18 Concrete model and the experimental set up

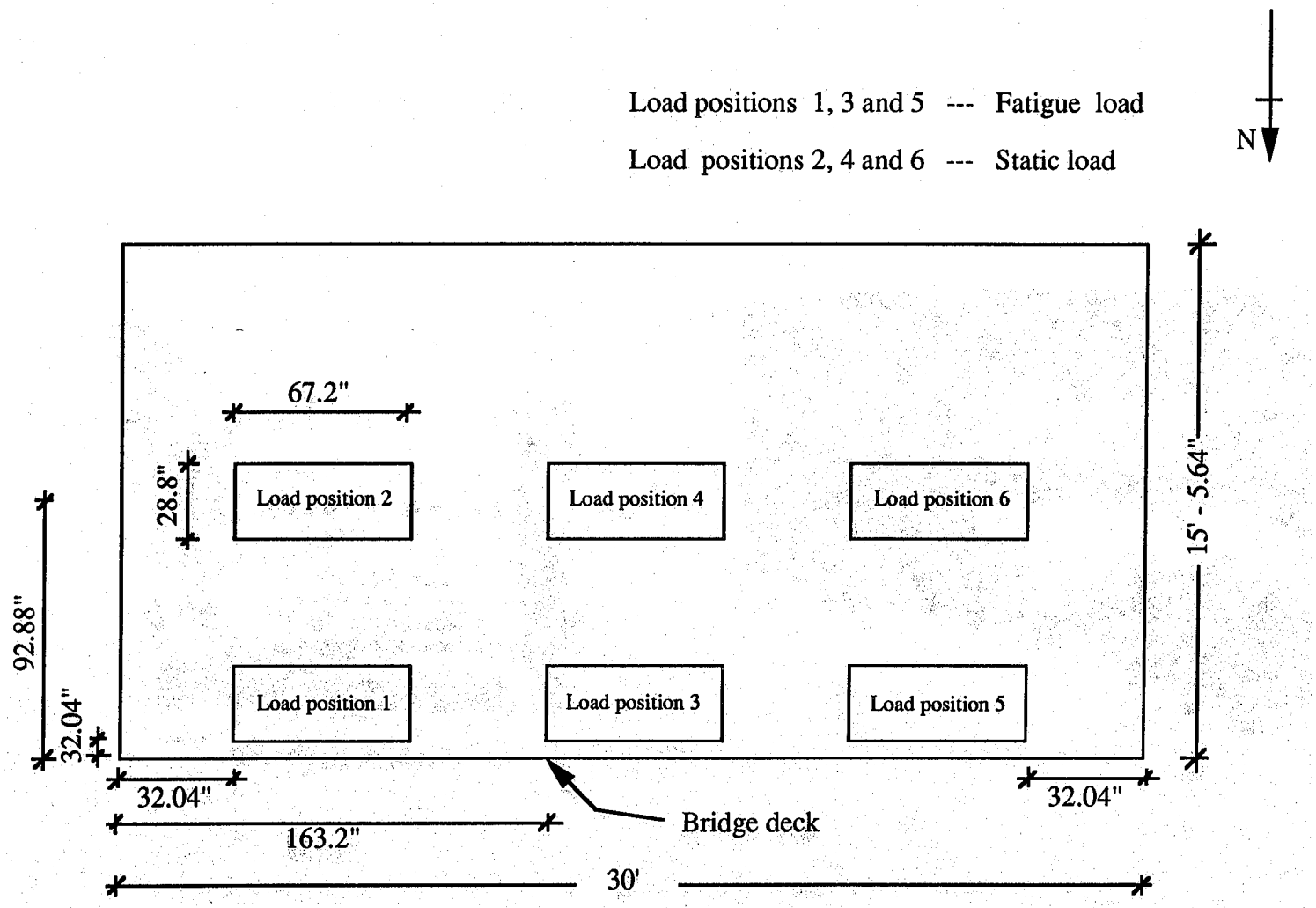

Fig. 4.19 The load positions for the model concrete bridge system

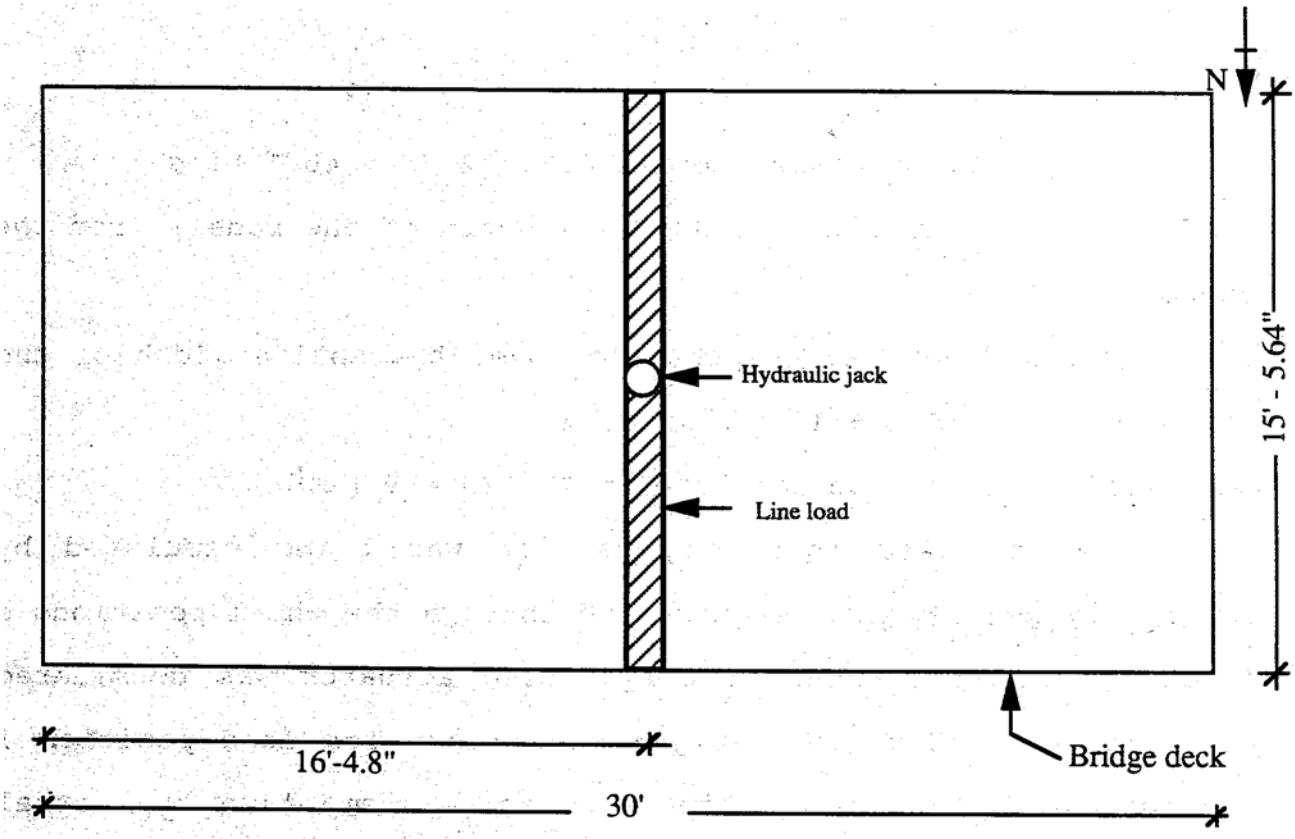

Fig. 4.20a Plan showing ultimate load position

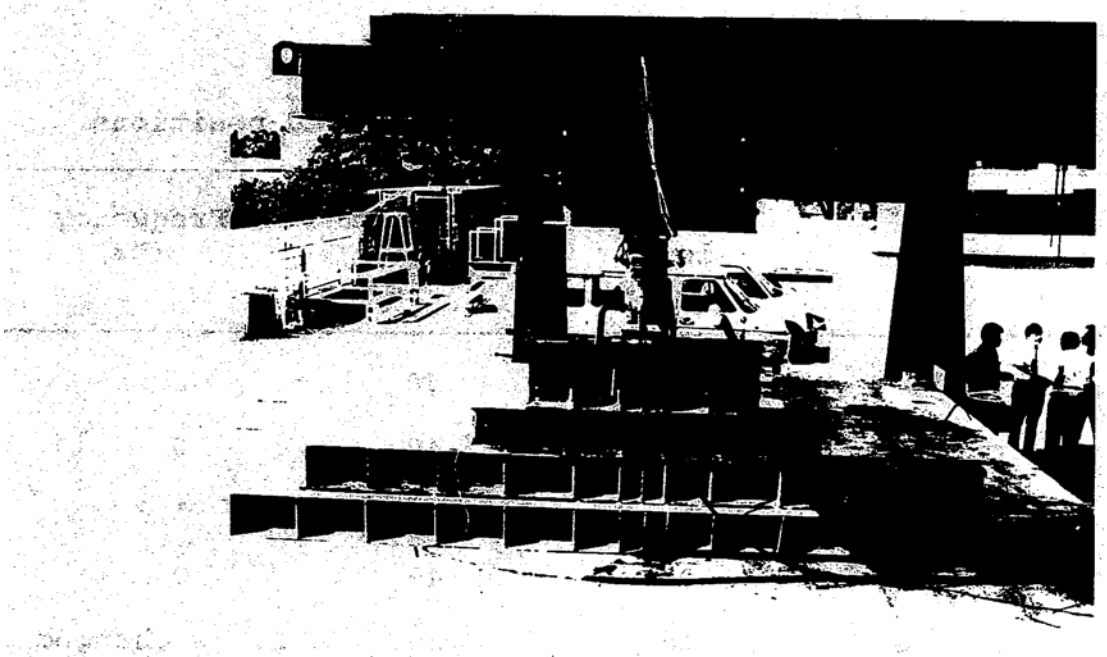

Fig. 4.20b Built-up section for application of line loading for ultimate strength test

1:2.5 scale model = $281.5/2.5^2$ = 45.1 kips

Dead load shear at distance 32" (2 x depth of the model) from the support = 18 kips

The required dead load compensation over the entire width, of the bridge model = 45.1 - 18 = 27.1 kips

Dead load compensation per lane = 27.1/3 9 kips

Since the dead load compensation was being simulated by additional concentrated static load through the wheel positions a force of 15 kips through the hydraulic actuator was considered satisfactory. Thus the fatigue load range for load position 1was set at 15 kips to 30 kips, the range simulating the actual HS20 - 44 truck load. Similarly the dead load compensation for load position 3 was determined to be 5 kips at the hydraulic actuator. The applied loads and their frequencies for the six load positions are given in Table 4.2

Table 4.2 Applied load data for the four load positions

Load position	Type of load	Minimum load (kips)	Maximum load (kips)	Frequency (Hz)
1	Fatigue	15	30	2.2
2	Static	0	49	0
3	Fatigue	5	20	1.8
4	Static	0	49	0
5	Fatigue	15	30	2.2 & changed to 2.0 @442200 cycles
6	Static	0	49	0

4.3.6 Instrumentation

The cyclic and static loads were applied using an MTS 55 kips capacity hydraulic actuator and the controller unit is shown in Figure 4.21. The built-in load cell and the digital indicator was calibrated using a flat external load cell for the entire range of loading to ensure accuracy of applied loads. The strain gages embedded in concrete were connected to strain indicators. Figure 4.22 shows the location of strain gages in the beams. Deflection gages were set up to measure the deflections along the longitudinal and transverse directions and their positions are shown in Figure 4.23. Typical crack measuring gage fixed across the longitudinal joints at the bottom of the model is shown in Figure 4.24.

4.3.7 Acoustic emission (AE) monitoring set up

Three Dunegan/Endevco S14~OB/HS ceramic, type AE transducers were fixed by means of silicone sealant along the midspan line on the underside of the bridge model in the ultimate load test. Fig. 4.25 shows the section of the bridge and the transducer locations. A Dunegan/Endevco 950 AE Distribution Analyzer with Module 303 was used in conjunction with an IBM PC/XT, to monitor the AE counts.

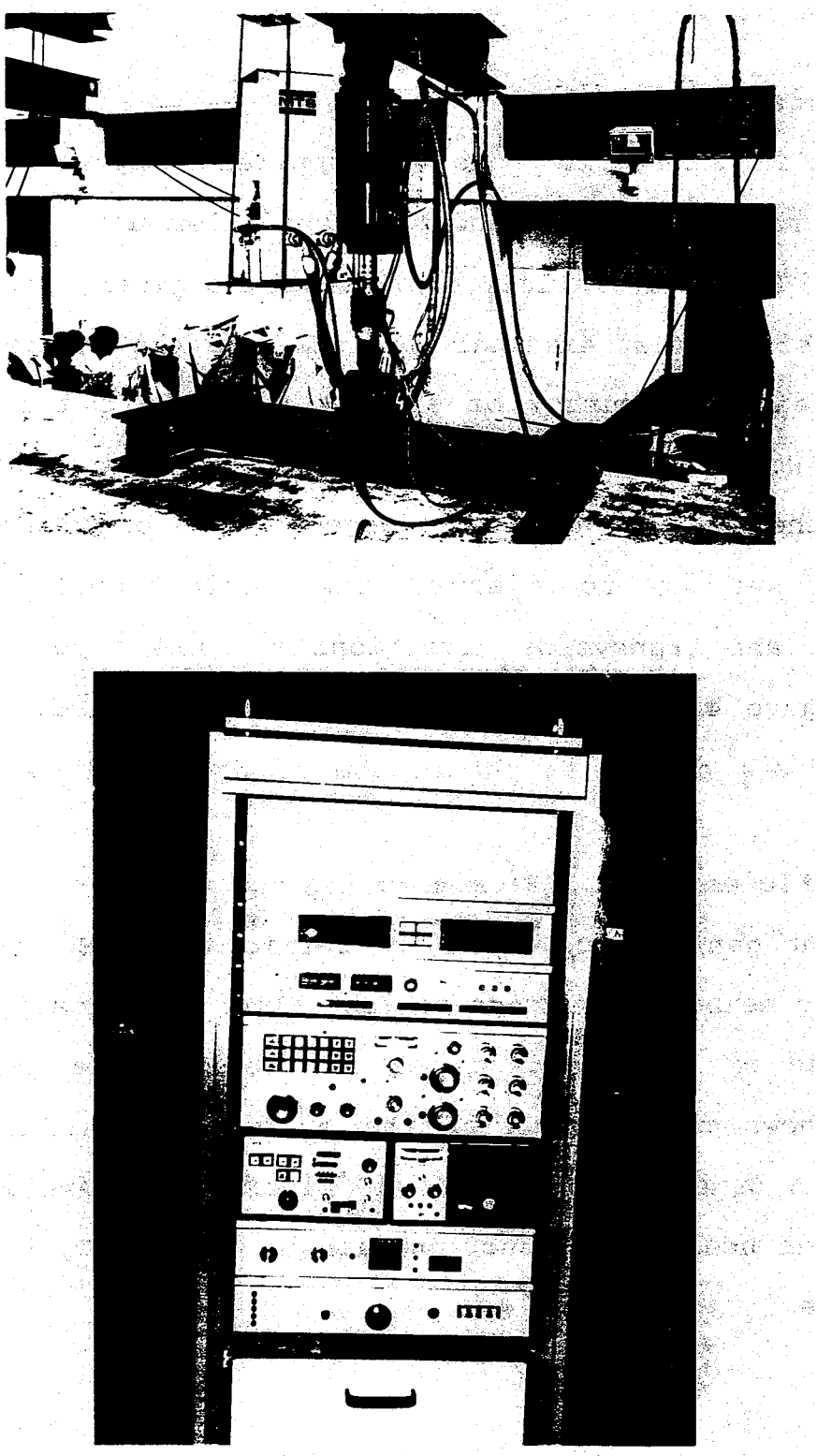

Fig. 4.21 The MTS hydraulic loading equipment

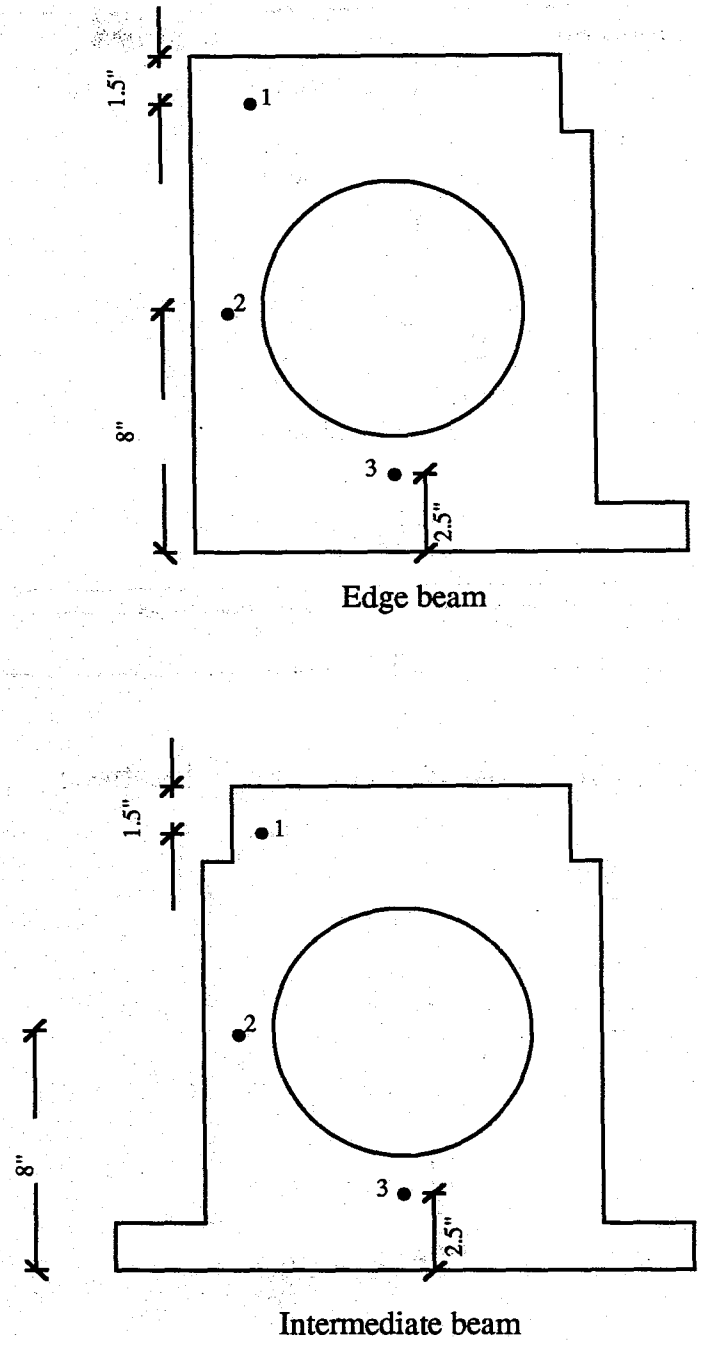

Fig. 4.22 The strain gage location across the depth at midspan

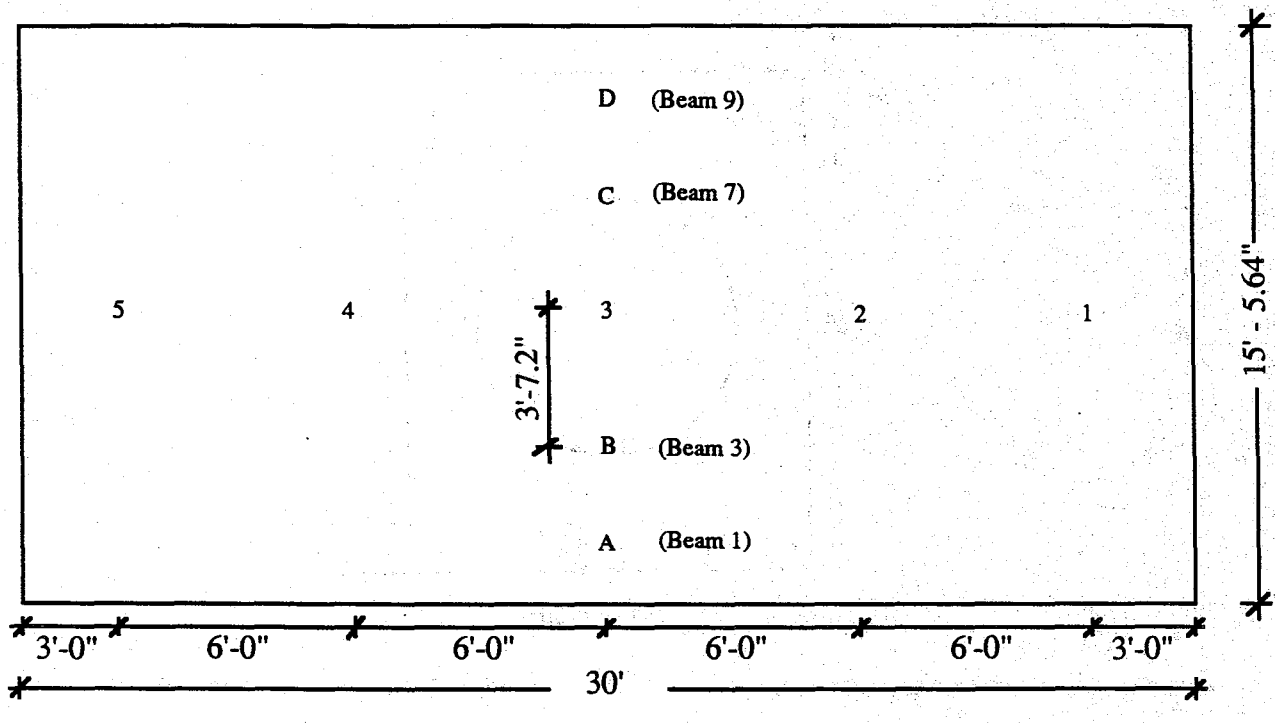

Fig. 4.23 The deflection gage locations

Fig. 4.24 The crack measuring gage

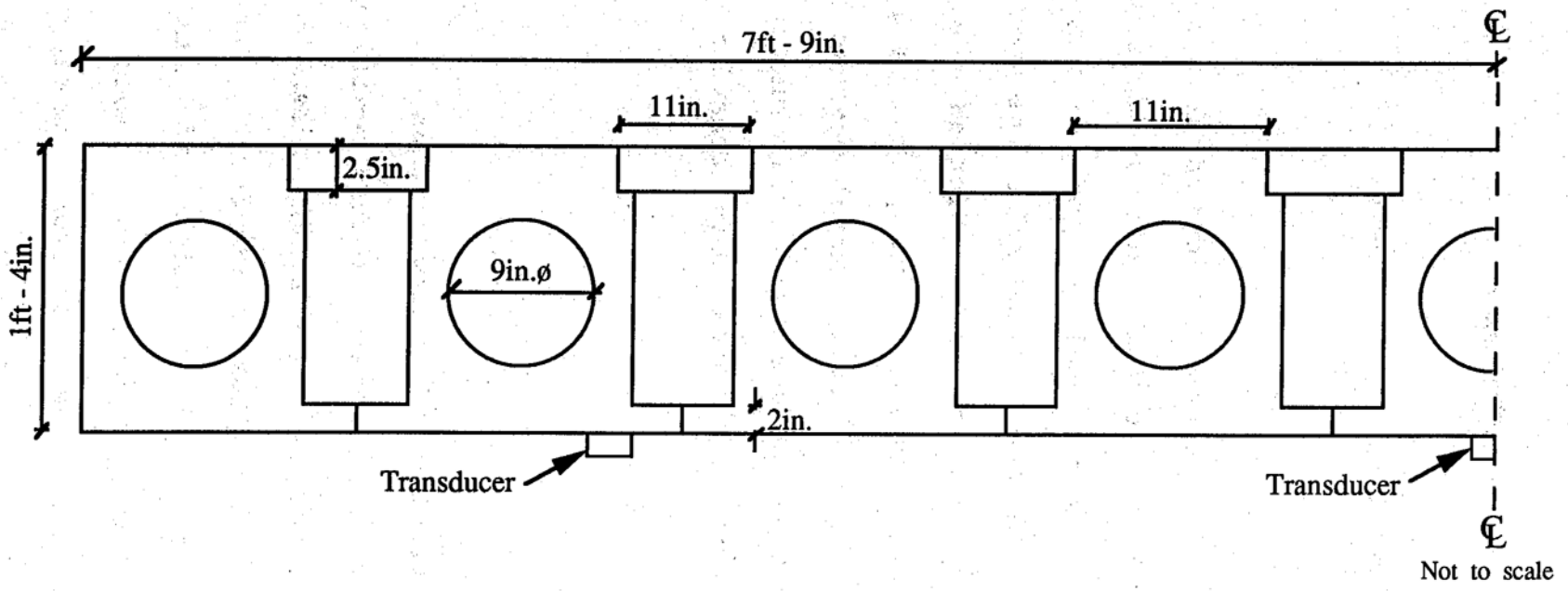

Fig. 4.25 Typical cross section of the multi-box bridge model showing the transducer locations

CHAPTER 5

RESULTS AND DISCUSSIONS

5.1 General

The behavior of the acrylic bridge deck and the multibox concrete bridge system models was studied under simulated AASHTO truck loadings. The experimental results are compared with the analytical values and the adequacy of the equivalent beam grillage analysis is evaluated in predicting the actual model behavior. The elastic behavior of the prototype multi-box beam bridge is studied using the acrylic model whereas the effect of shear and flexure in the concrete model is evaluated under fatigue loading with emphasis on longitudinal joint behavior.

5.2 Acrylic Model

5.2.1. Experimental results and interpretation

Typical strain vs. load curves for load positions 1 and 7 are shown in Figures 5.1 to 5.9. The strains seem to be uniformly distributed on all the individual beams for the load position 1, which corresponds to the location of maximum bending moment in the bridge deck. For load position 7, which corresponds to the maximum shear, the beams directly under the load are stressed more even though other

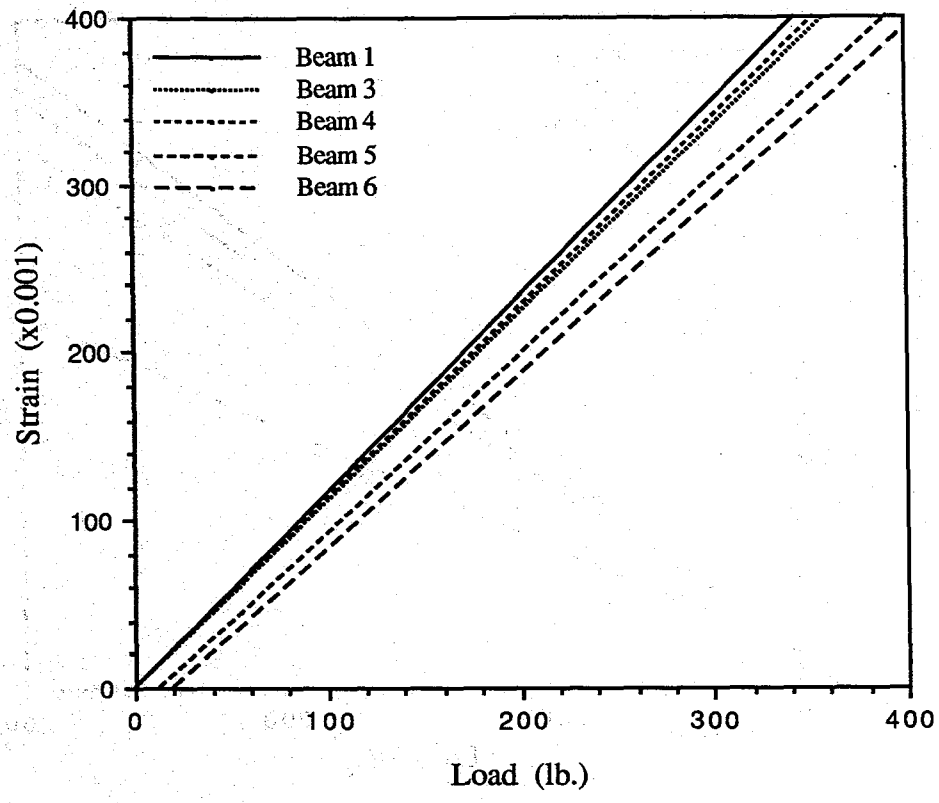

Fig. 5.1 Strain vs load at mid-point, load position 1

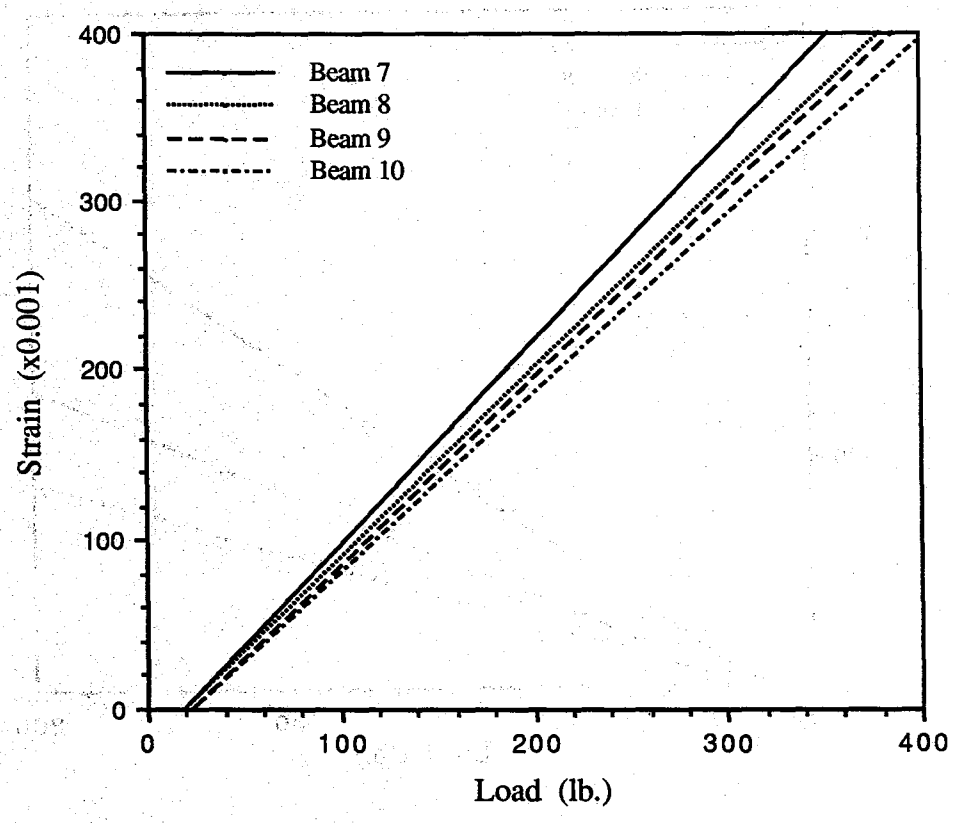

Fig. 5.2 Strain vs load at mid-point, load position 1

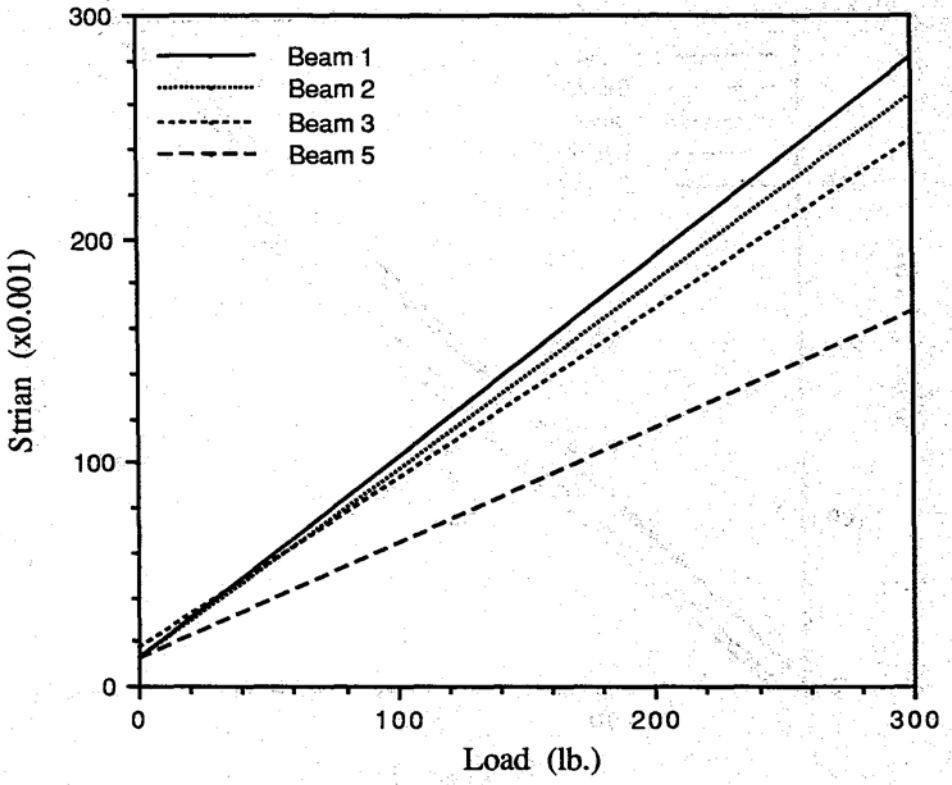

Fig. 5.3 Strain vs load at 0.25L from L.H. support, load position 1

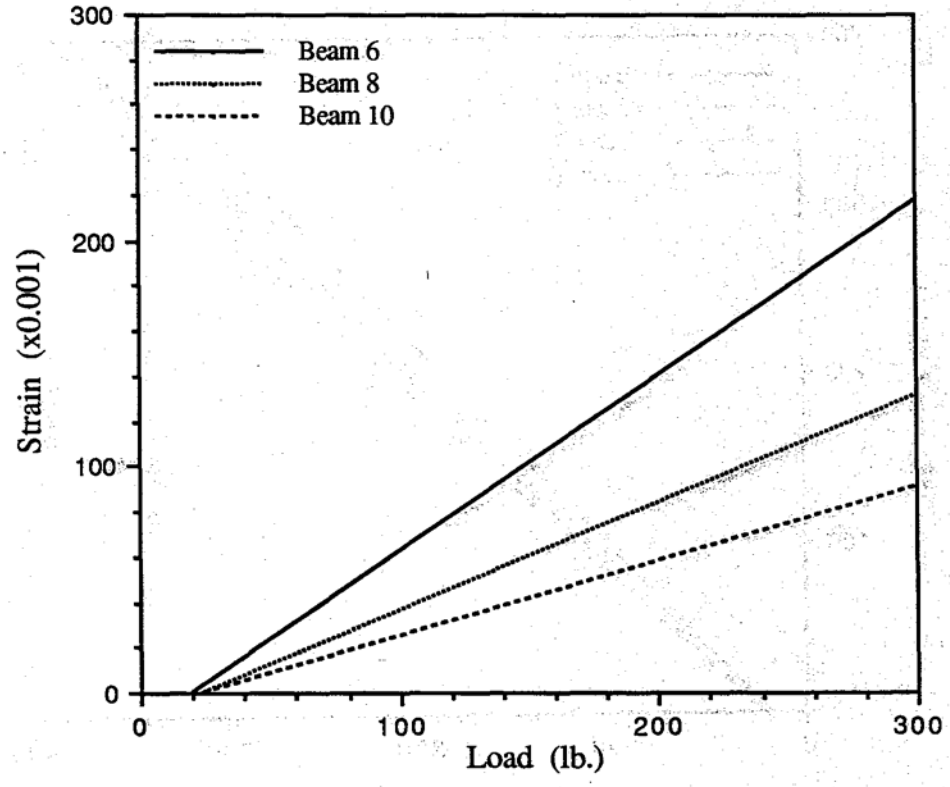

Fig. 5.4 Strain vs load 0.25L from L.H. support, load position 1.

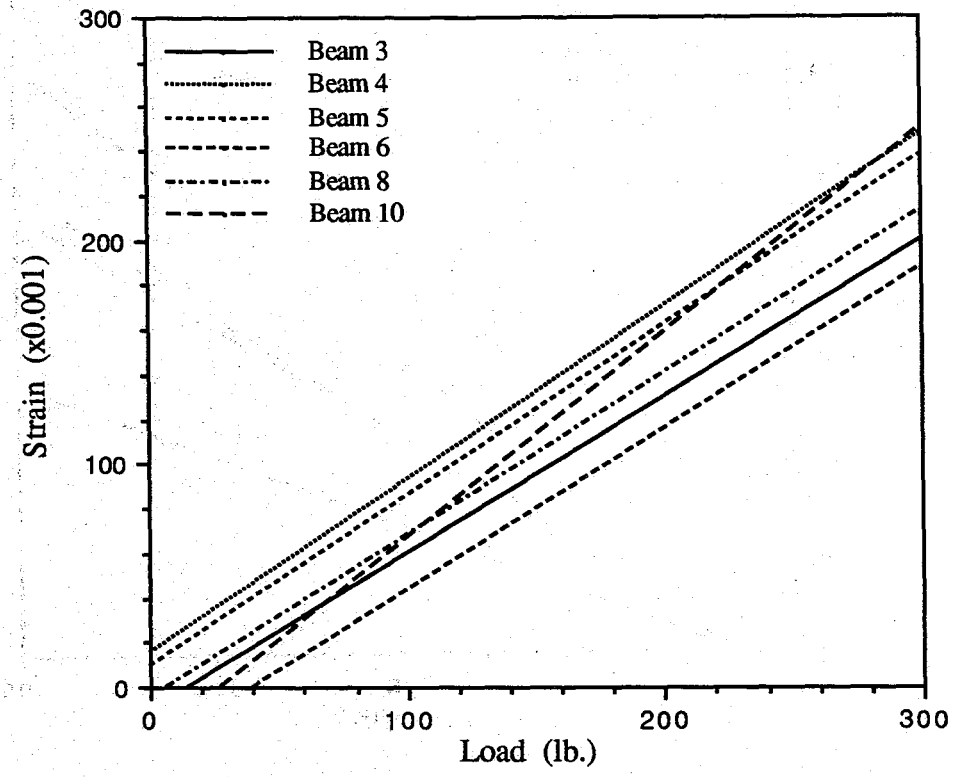

Fig. 5.5 Strain vs load at 0.25L from R.H. support, load position

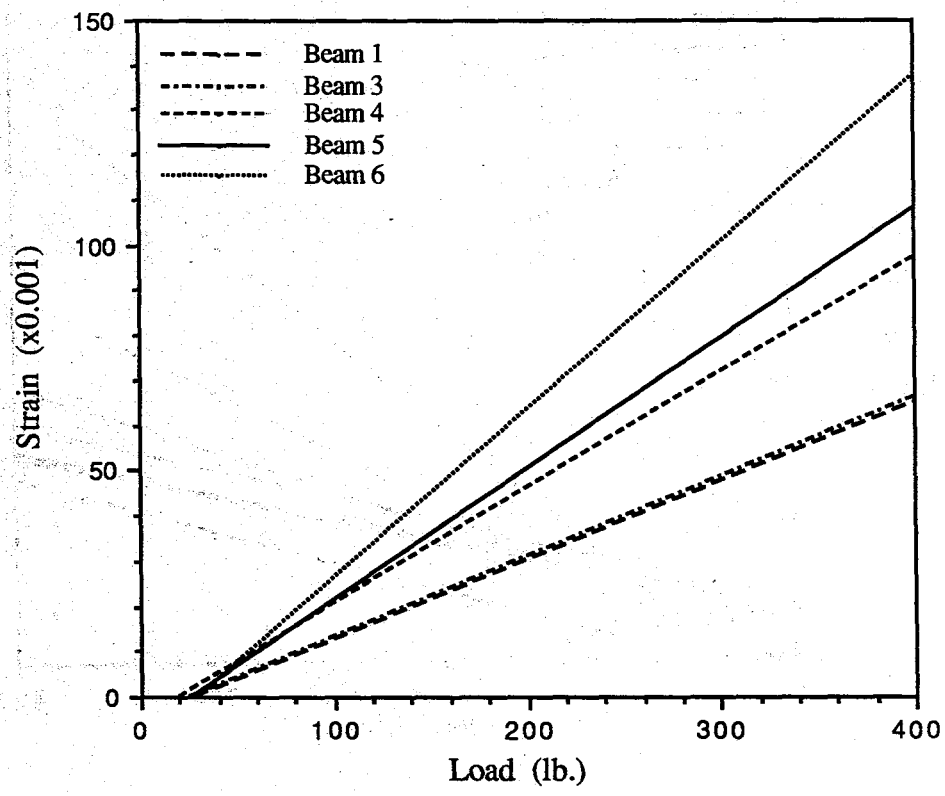

Fig. 5.6 Strain vs load at mid-point, load position 7

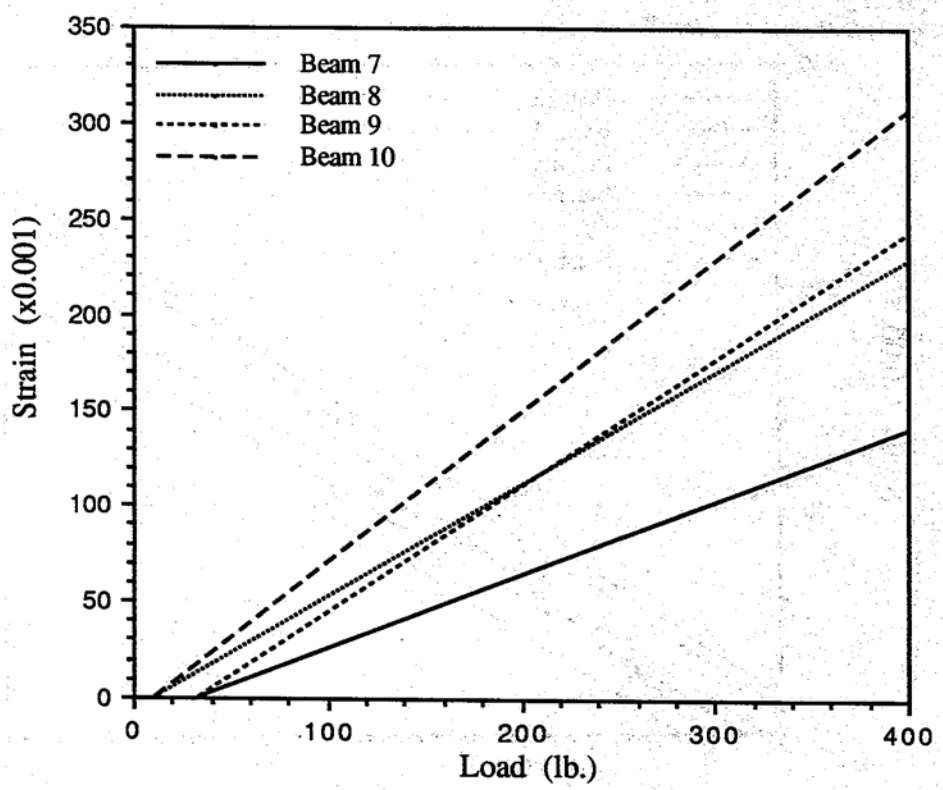

Fig. 5.7 Strain vs load at mid-point, load position 7

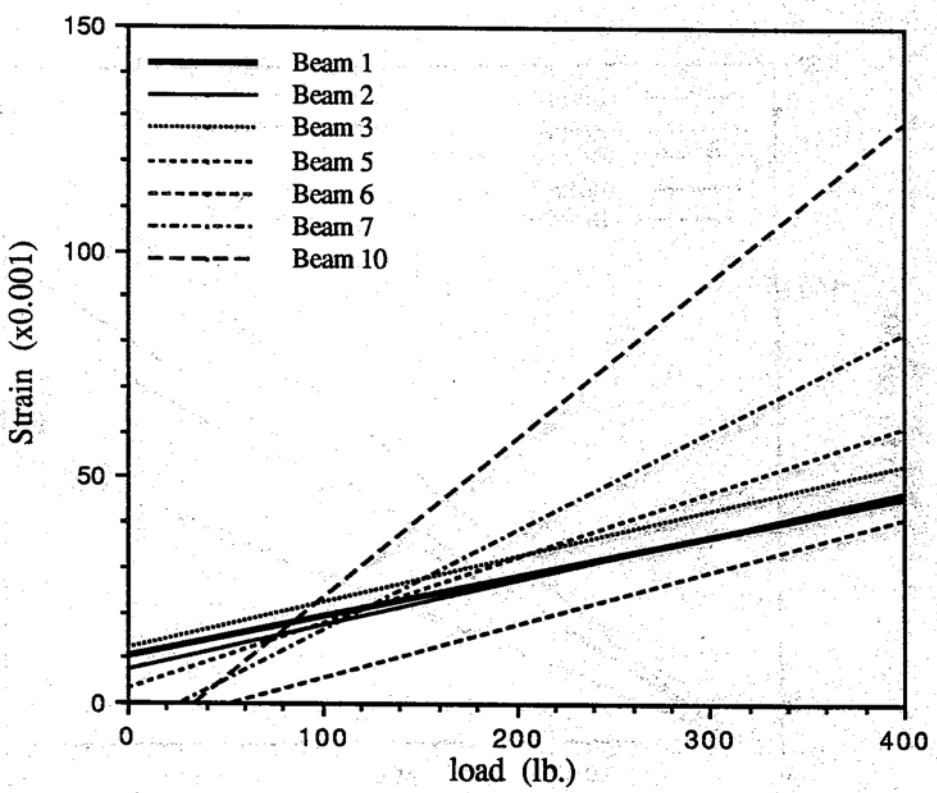

Fig. 5.8 Strain vs load at 0.25L from L.H. support, load position 7

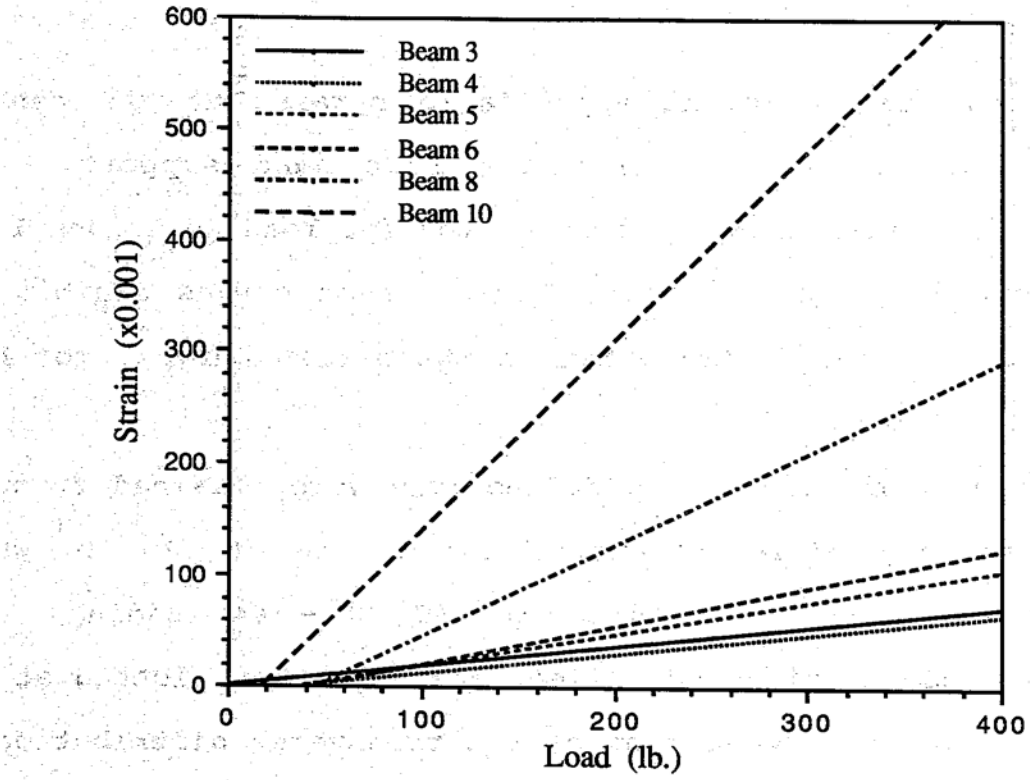

Fig. 5.9 Strain vs load at 0.25L from R.H. support, load position 7

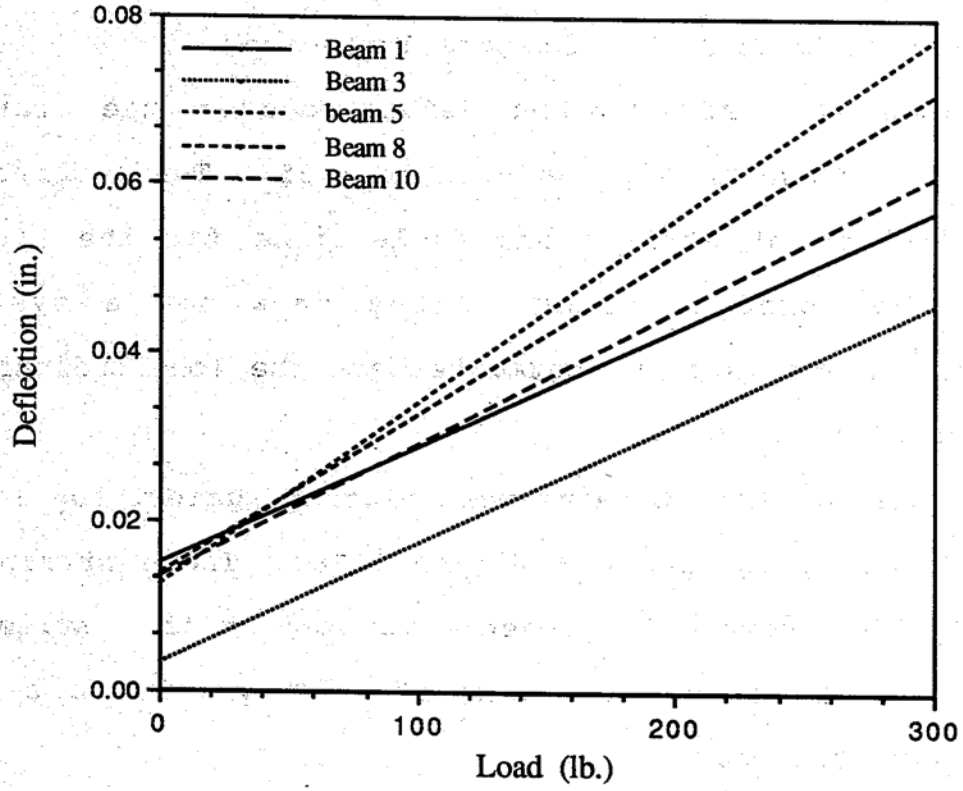

Fig. 5.10 Deflection vs load at mid-point, load position 1

beams appear to be taking appreciable strains at the central location, and at 0.25 L from the left hand support the corresponding deflection vs. load curves for load positions 1 and 7 are shown in Figures 5.10 to 5.15. These curves exhibit the same effect of load distribution as the strain curves for both the load positions.

The values of strains and deflections were obtained from the above curves for different beams, for a load of 180 lb. which corresponds to the simulated AASHTO HS 20 - 44 loading. The values, of these strains and deflections were then plotted at the beam locations, to give a plot of the transverse distribution of strains and deflections. Figures 5.16 to 5.20 show strain vs. beam location for load positions 1, 2, 3, 4, and 7 respectively. The corresponding deflection vs. beam location curves are shown, in Figures 5.21 to 5.25 for the same load cases.

The normalized strains and deflections in the transverse direction are shown in Figures 5.26 to 5.35. These curves give the distribution of strains and deflections for the prototype multibeam box bridge system. They show how a system of concentrated loads is distributed between the longitudinal beams of a bridge system.

The values of shear strains were plotted against the load for load positions 2, 3, and 7 - Figure 5.36. These strains were measured by the rectangular rosette mounted at the extreme beam (beam 10) at the right hand support. They exhibit a linear variation with the load.

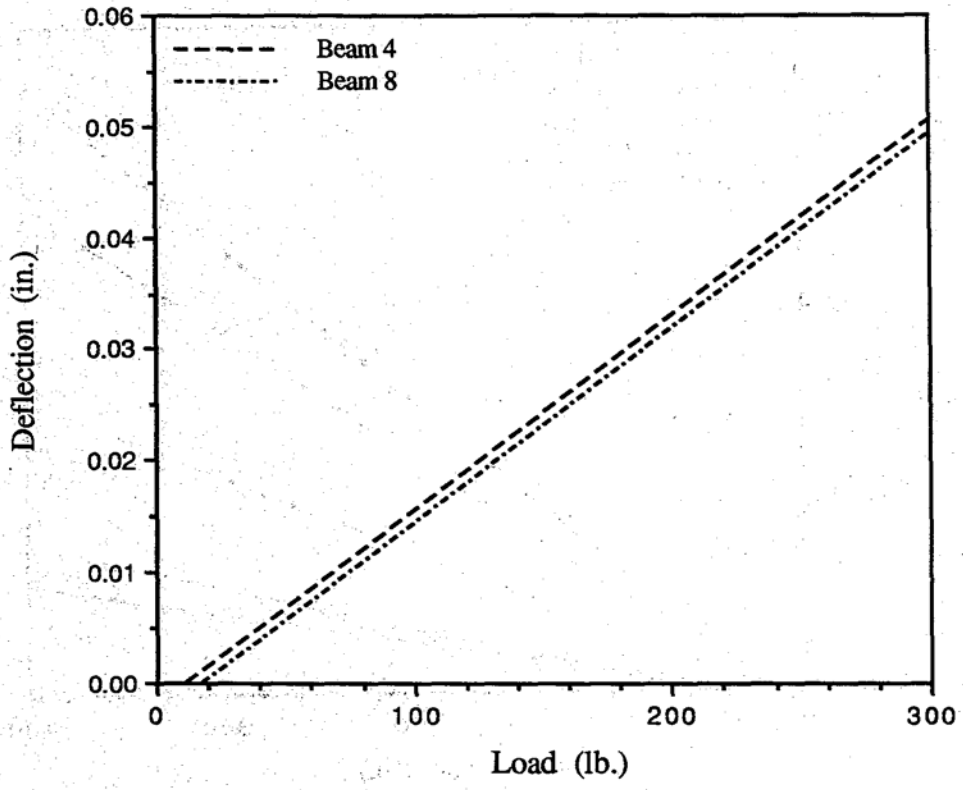

Fig. 5.11 Deflection vs load at 0.25L from L.H. support, load position 1

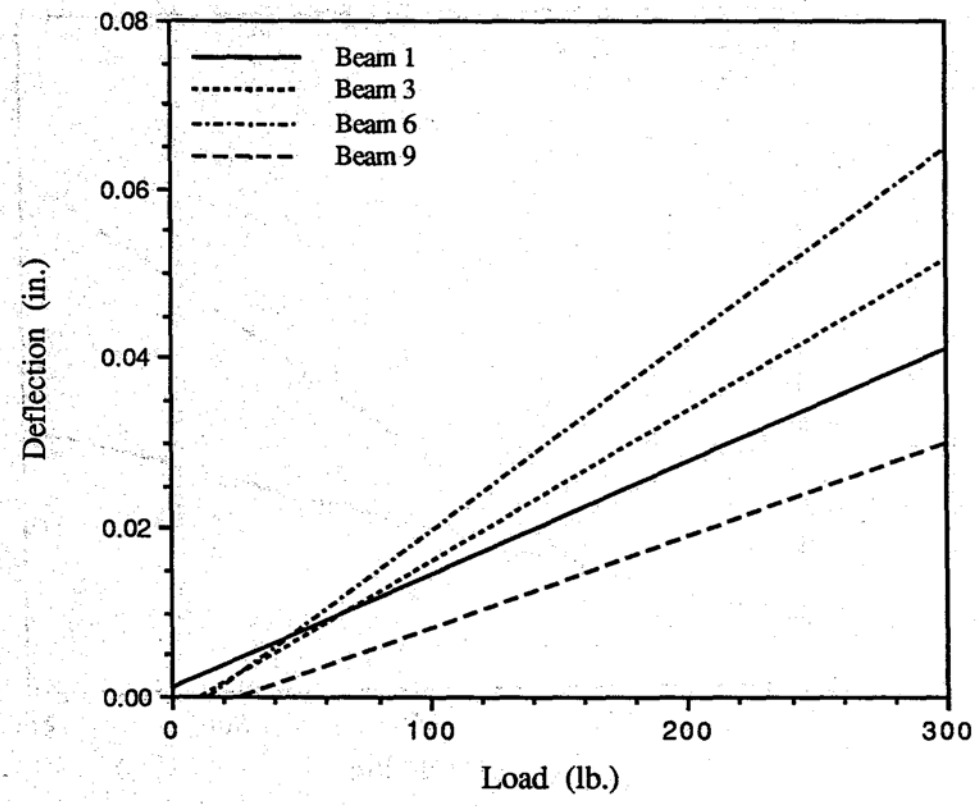

Fig. 5.12 Deflection vs load at 0.25L from R.H. support, load position 1

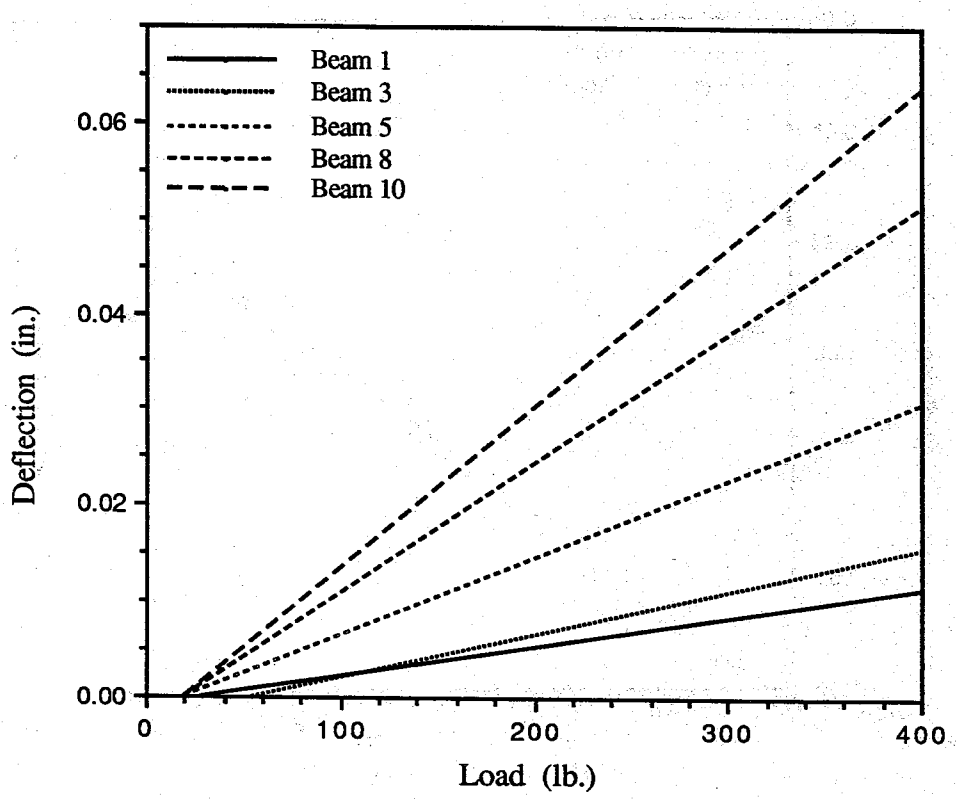

Fig.5.13 Deflection vs load at mid-point, load position 7

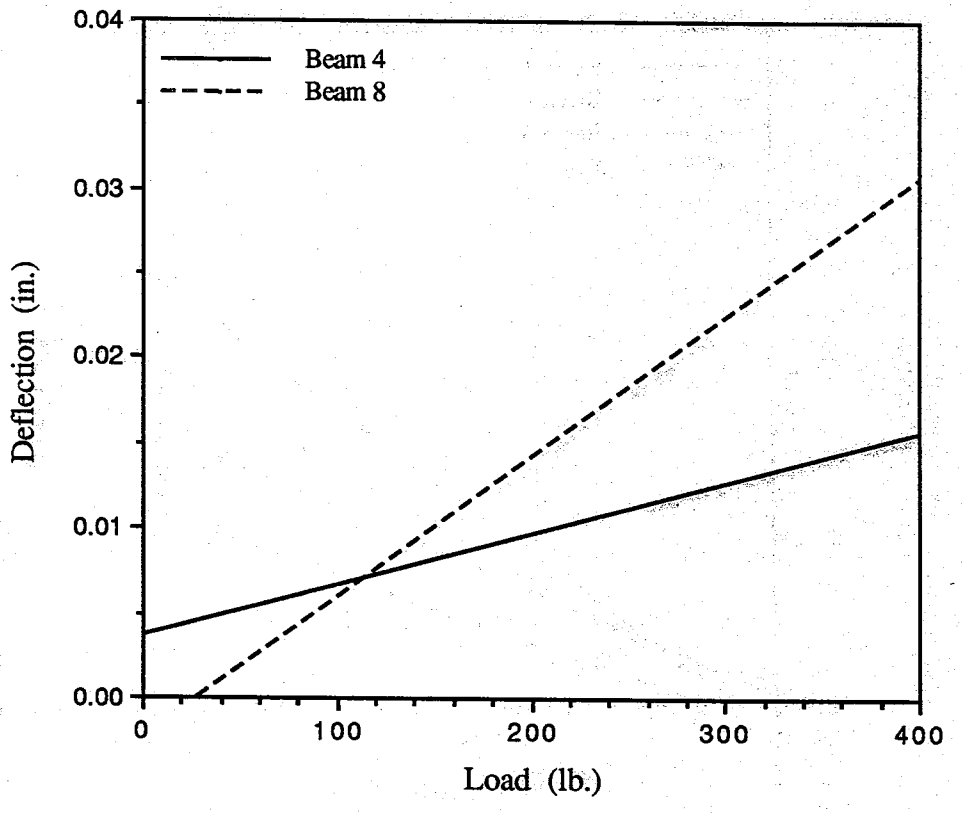

Fig. 5.14 Deflection vs load at 0.25L from L.H. support, load position 7

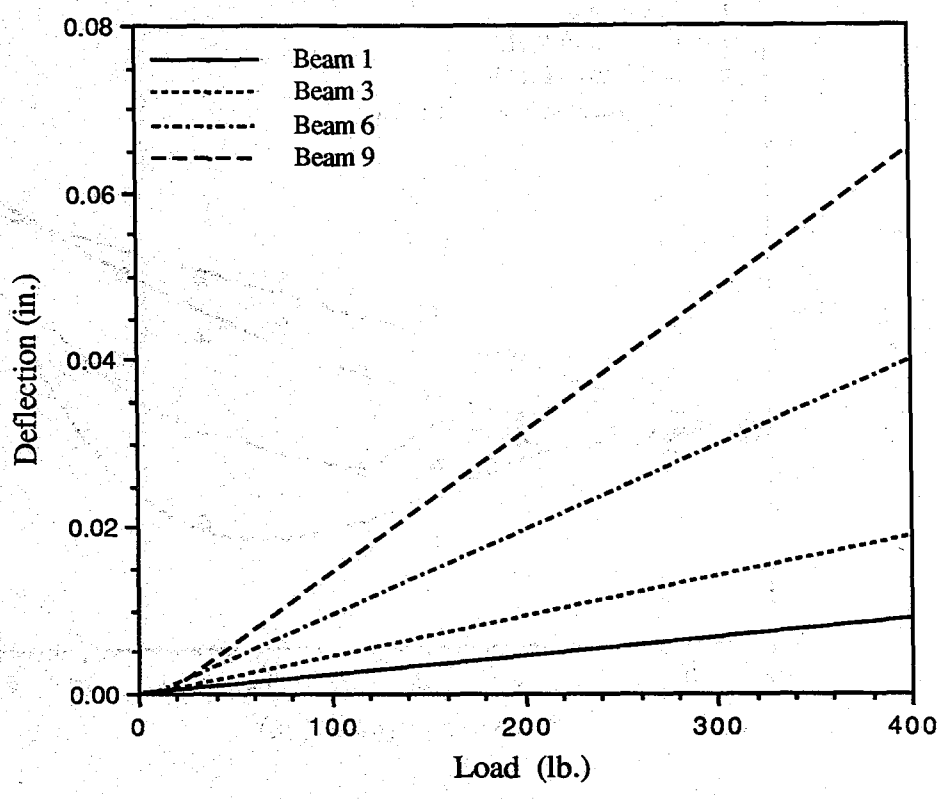

Fig. 5.15 Deflection vs load at 0.25L from R.H. support, load position 7

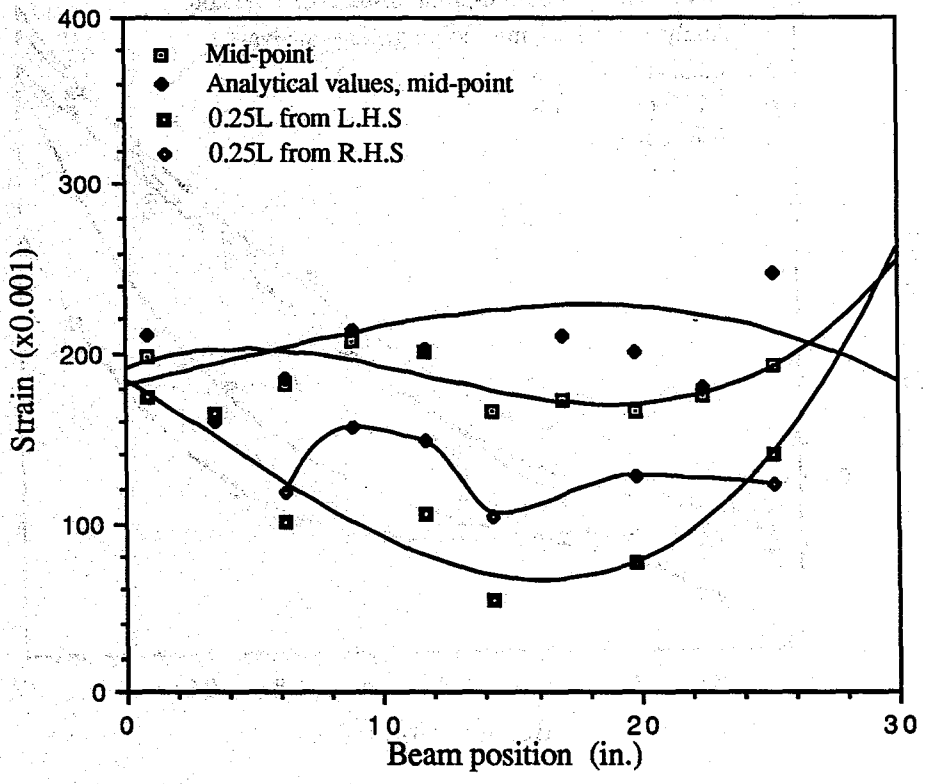

Fig. 5.16 Strain vs beam position, load position 1

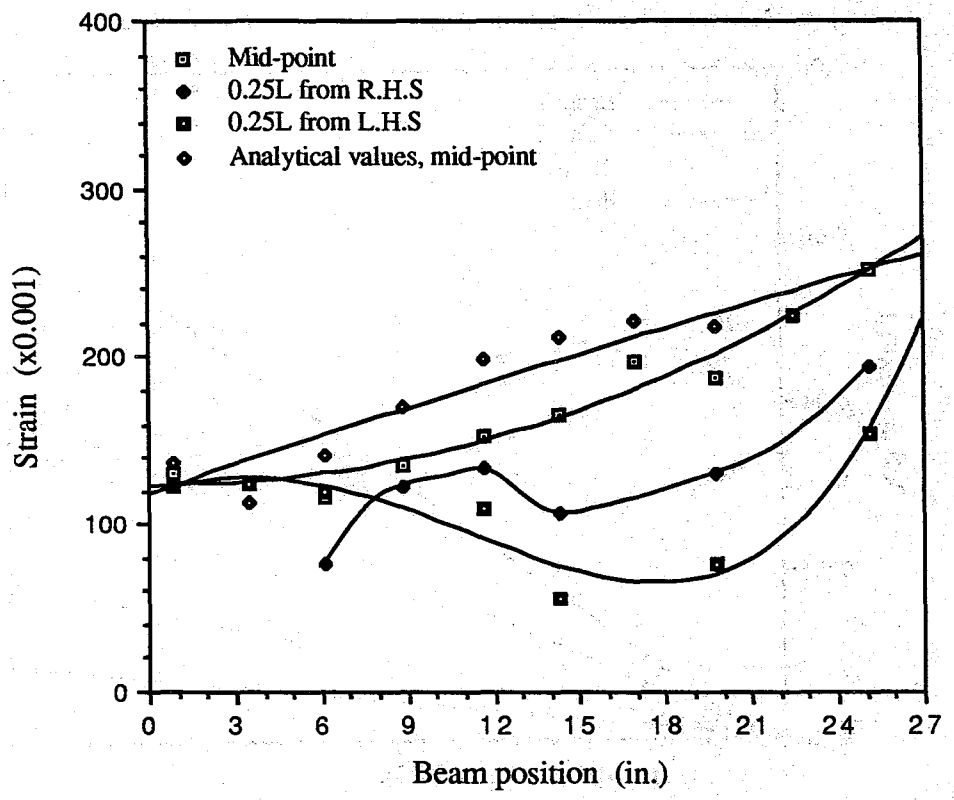

Fig. 5.17 Strain vs beam position, load position 2

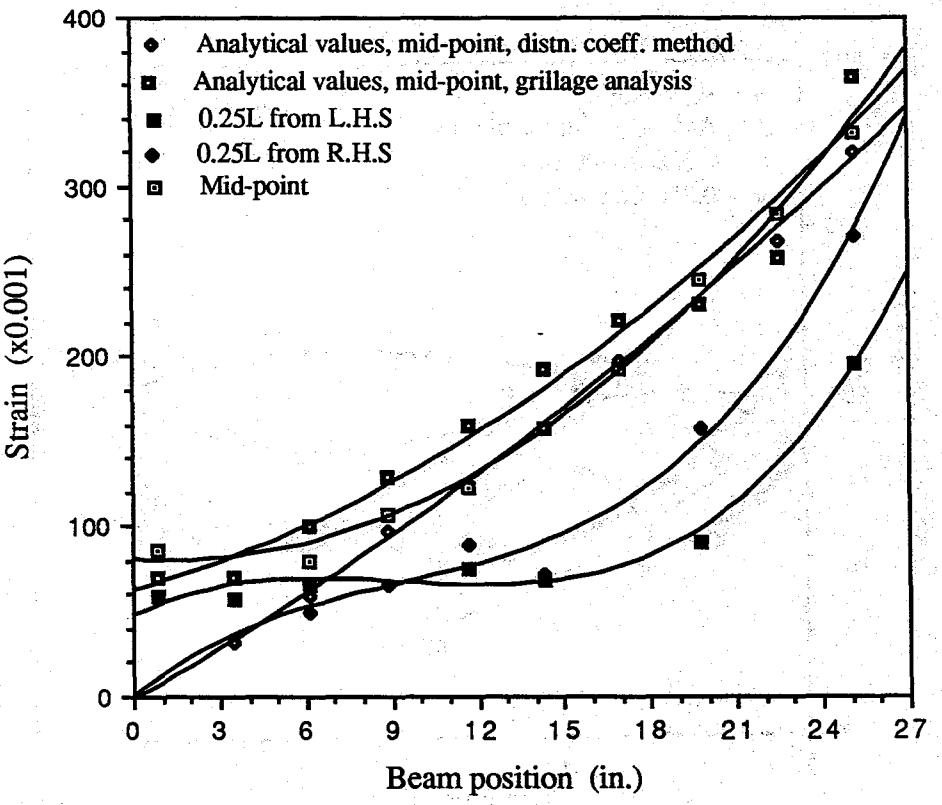

Fig. 5.18 Strain vs beam position, load position 3

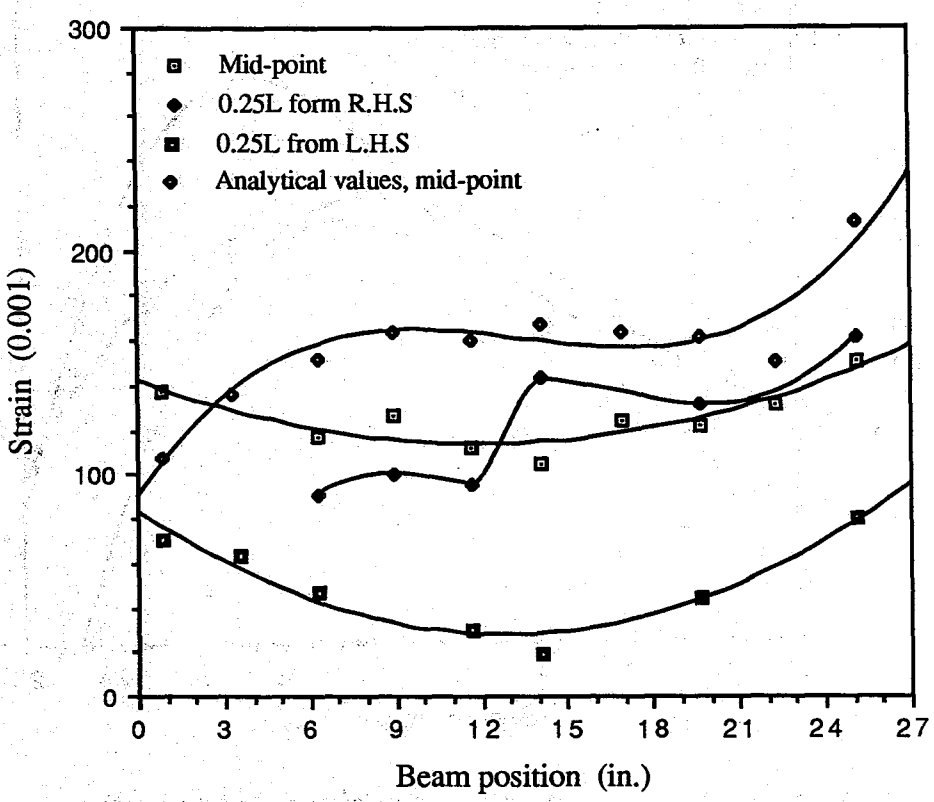

Fig. 5.19 Strain vs beam position, load position 4

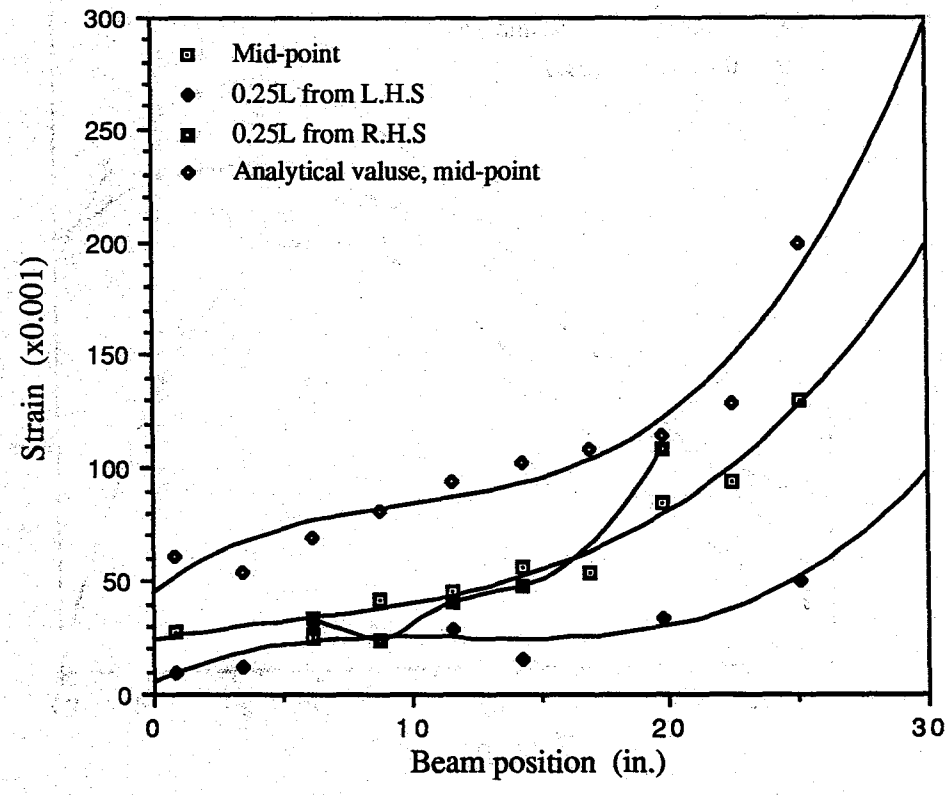

Fig. 5.20 Strain vs beam position, load position 7

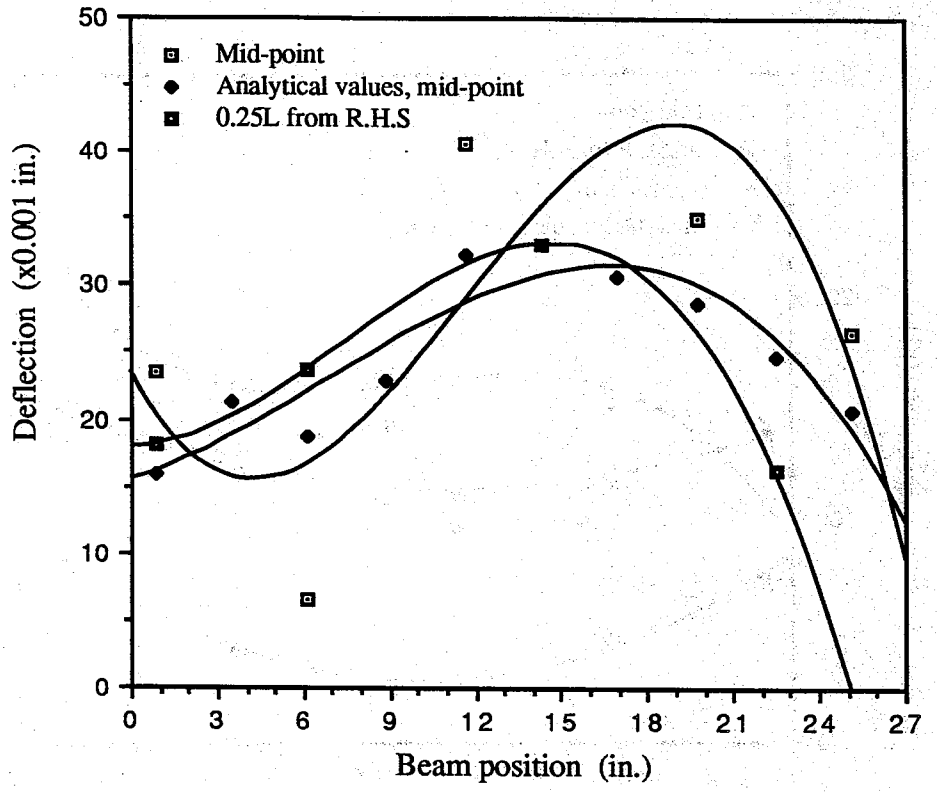

Fig. 5.21 Deflection vs beam position, load position 1

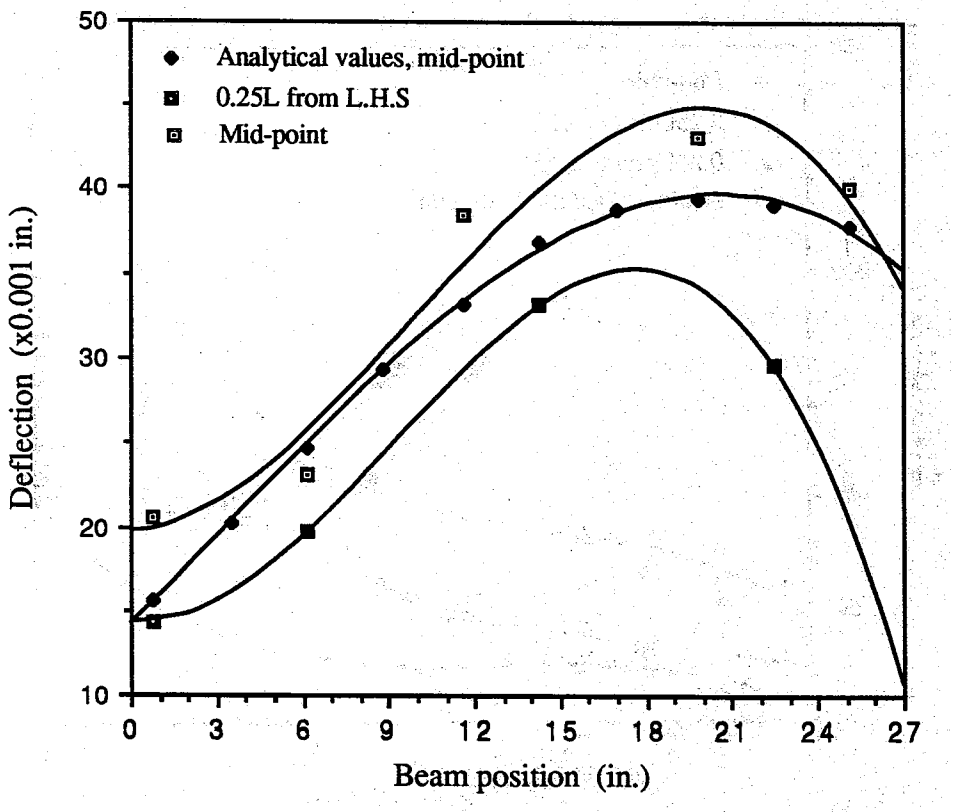

Fig. 5.22 Deflection vs beam position, load position 2

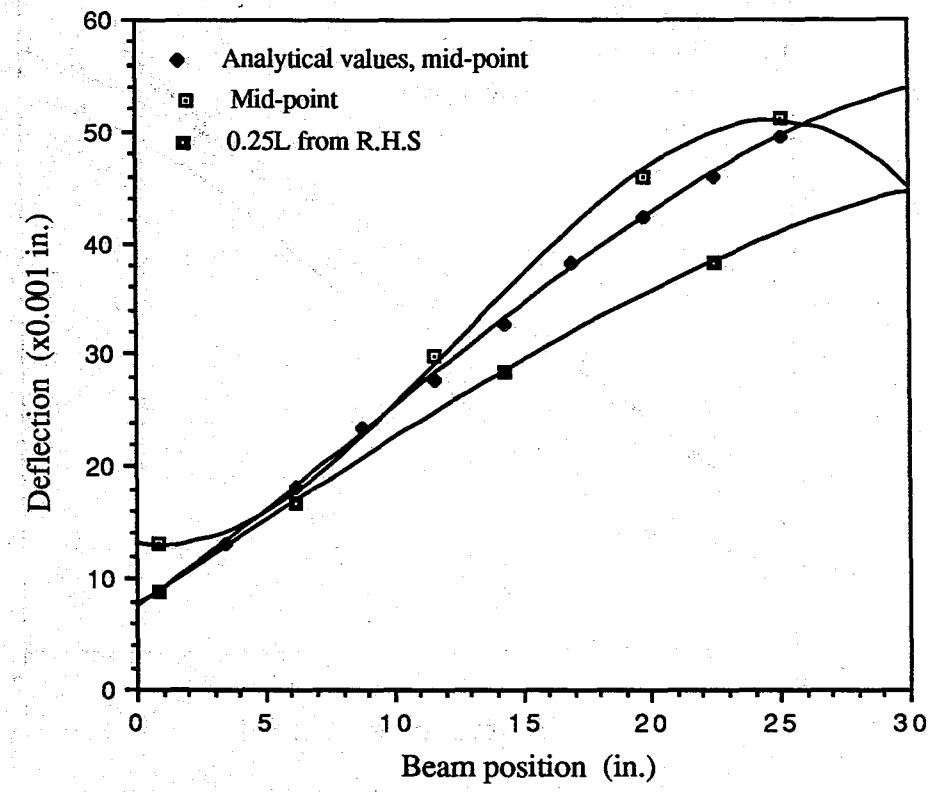

Fig. 5.23 Deflection vs beam position, load position 3

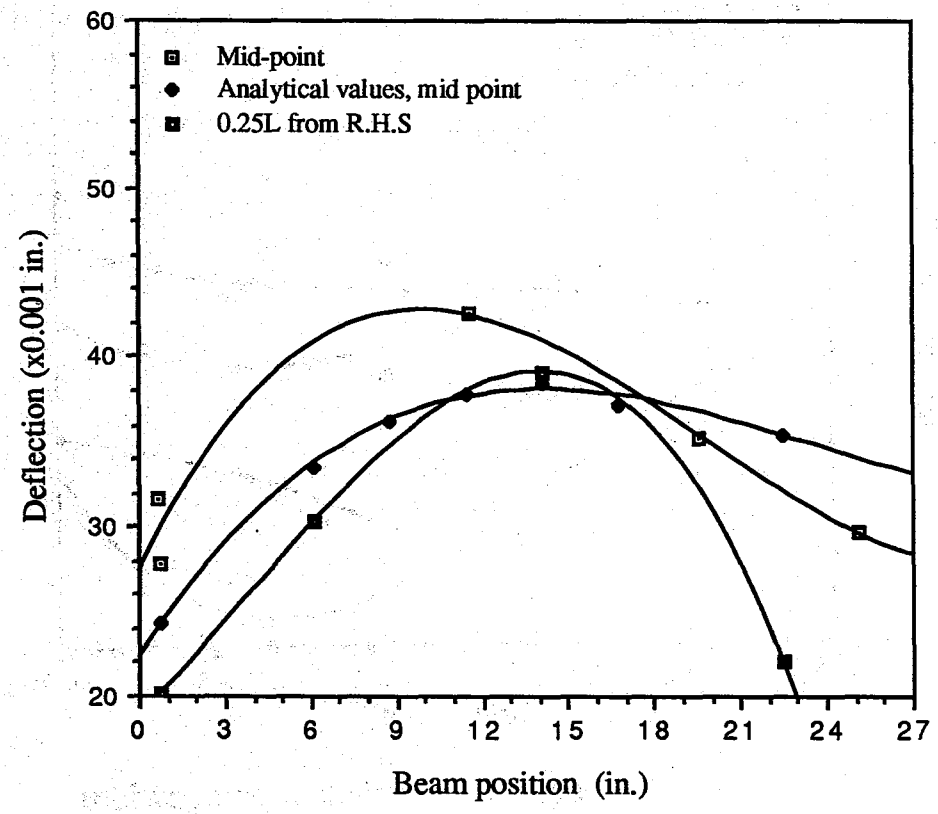

Fig. 5.24 Deflection vs beam position, load position 4

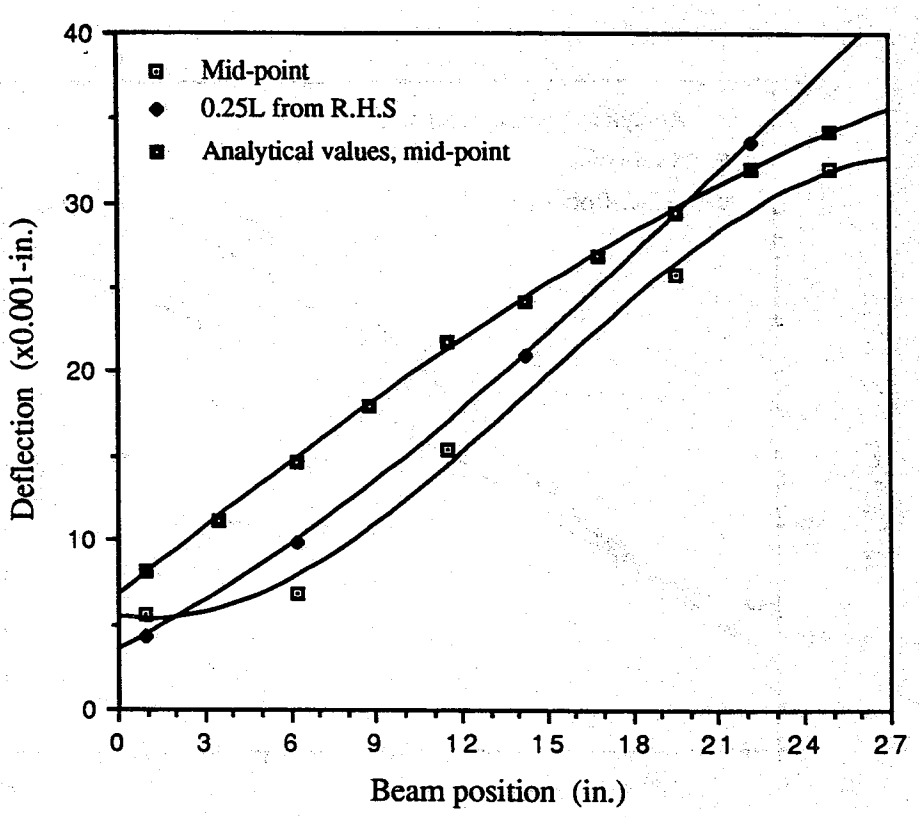

Fig. 5.25 Deflection vs beam position, load position 7

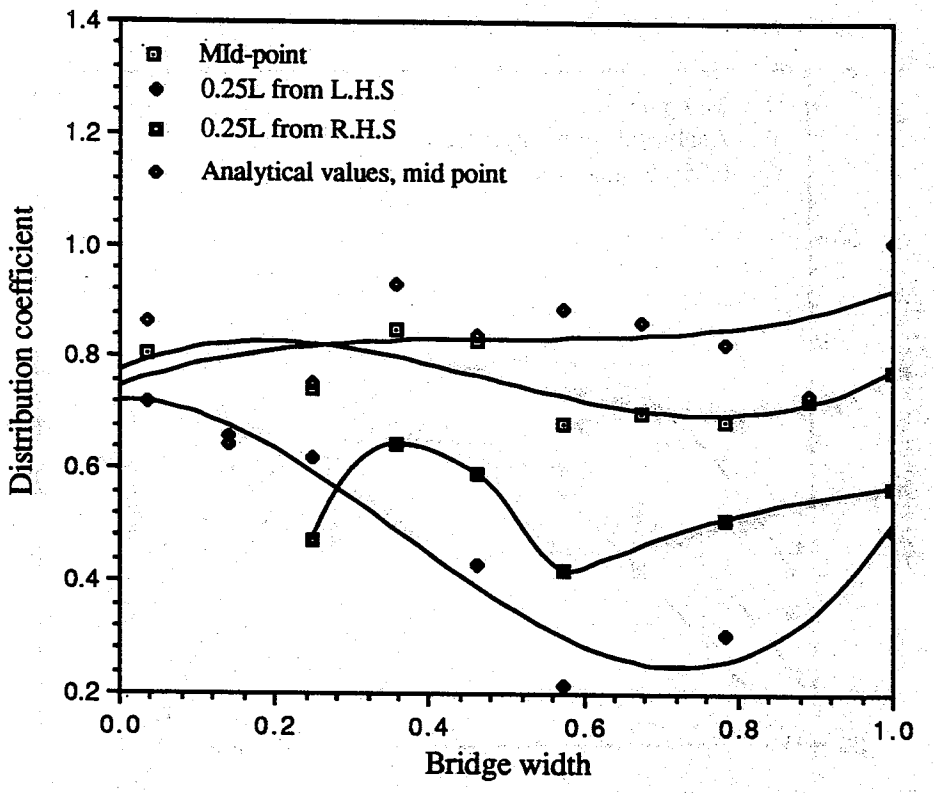

Fig. 5.26 Distribution coefficient vs bridgewidth for load position 1, based on strain data

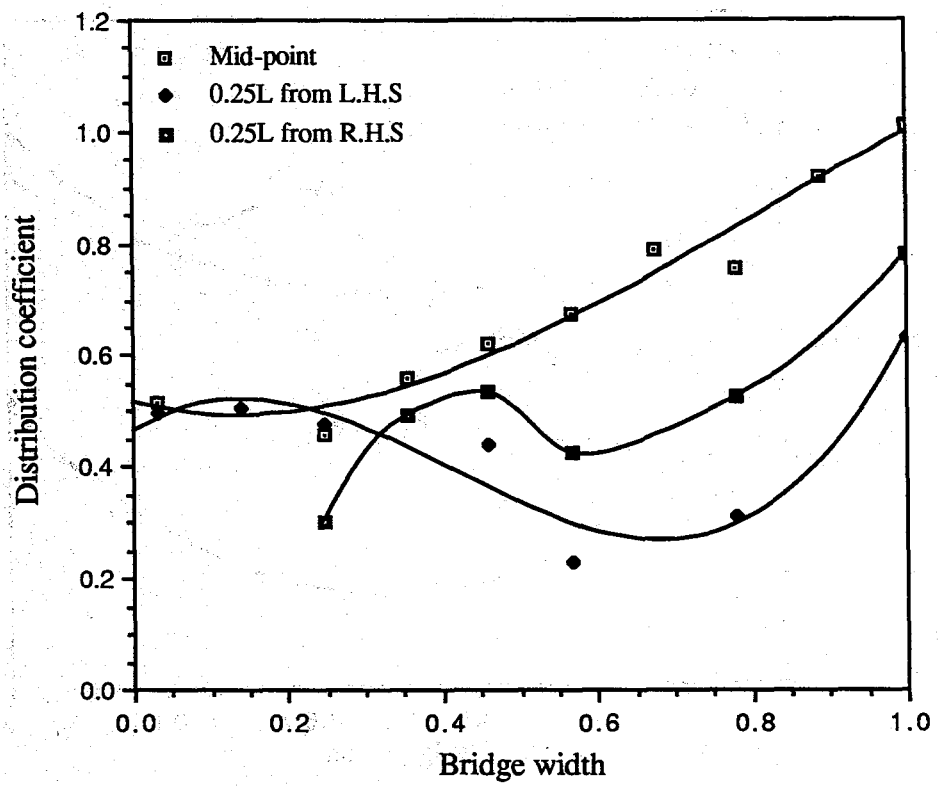

Fig. 5.27 Distribution coefficient vs bridge width for load position 2, based on strain data

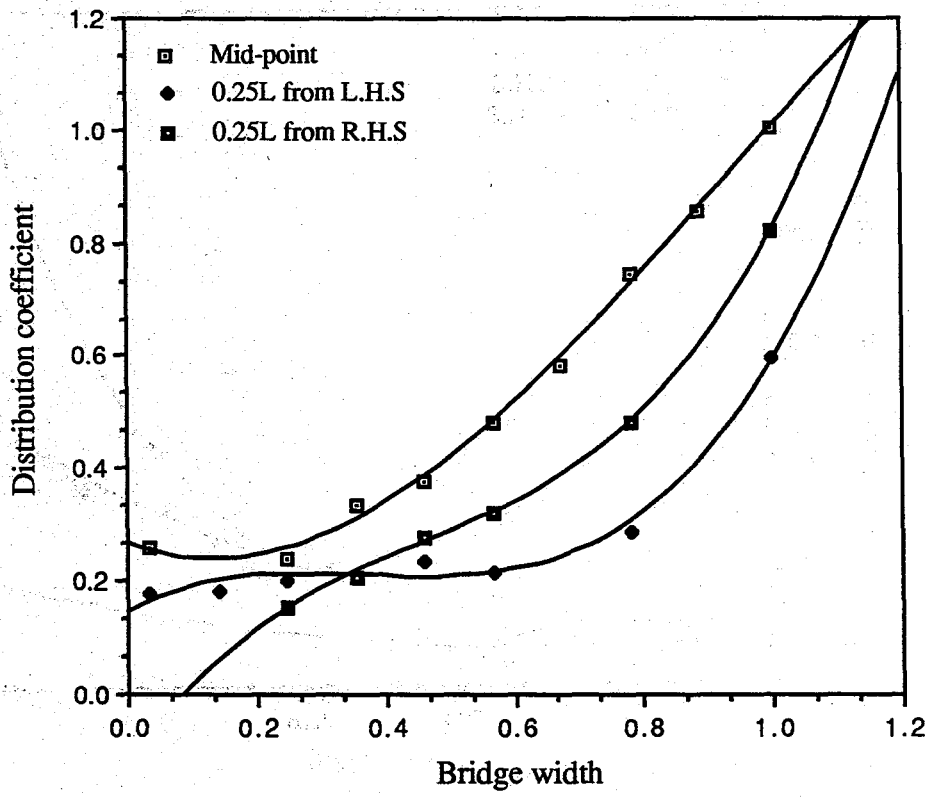

Fig. 5.28 Distribution coefficient vs bridge width for load position 3, based on strain data

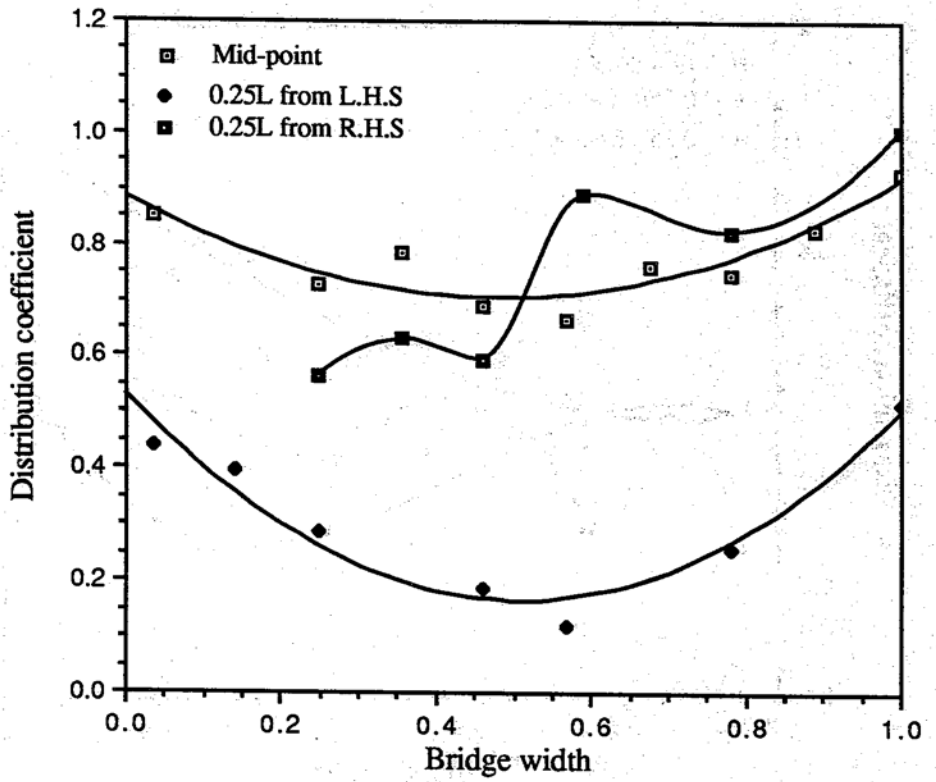

Fig. 5.29 Distribution coefficient vs bridge width for load position 4, based on strain data

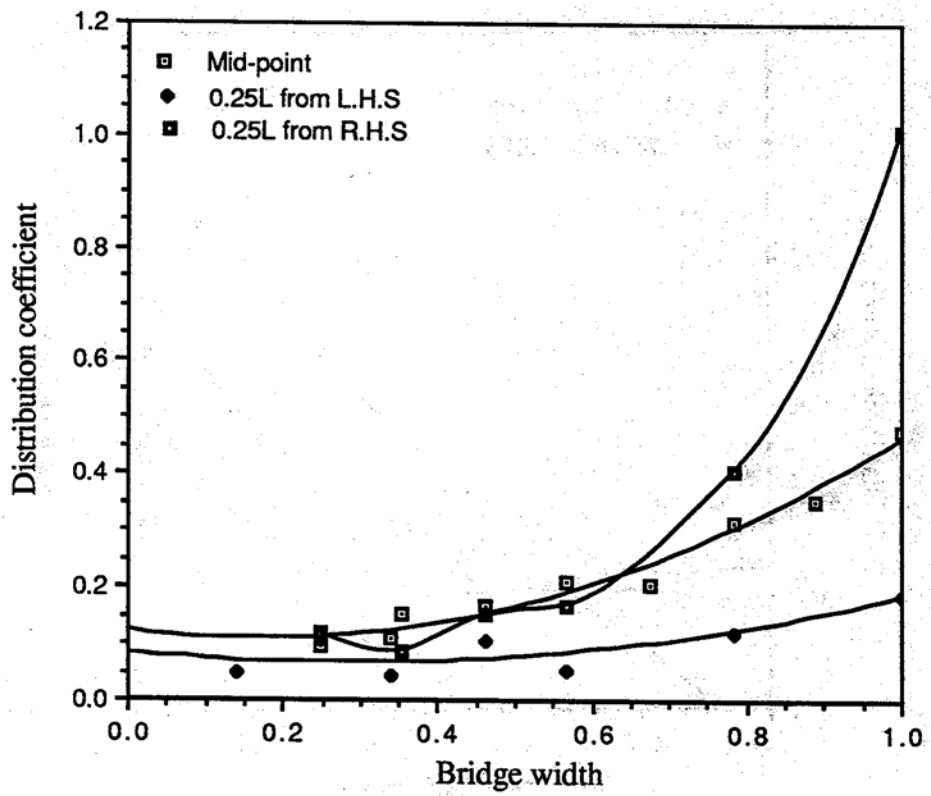

Fig. 5.30 Distribution coefficient vs bridge width for load position 7, based on strain data

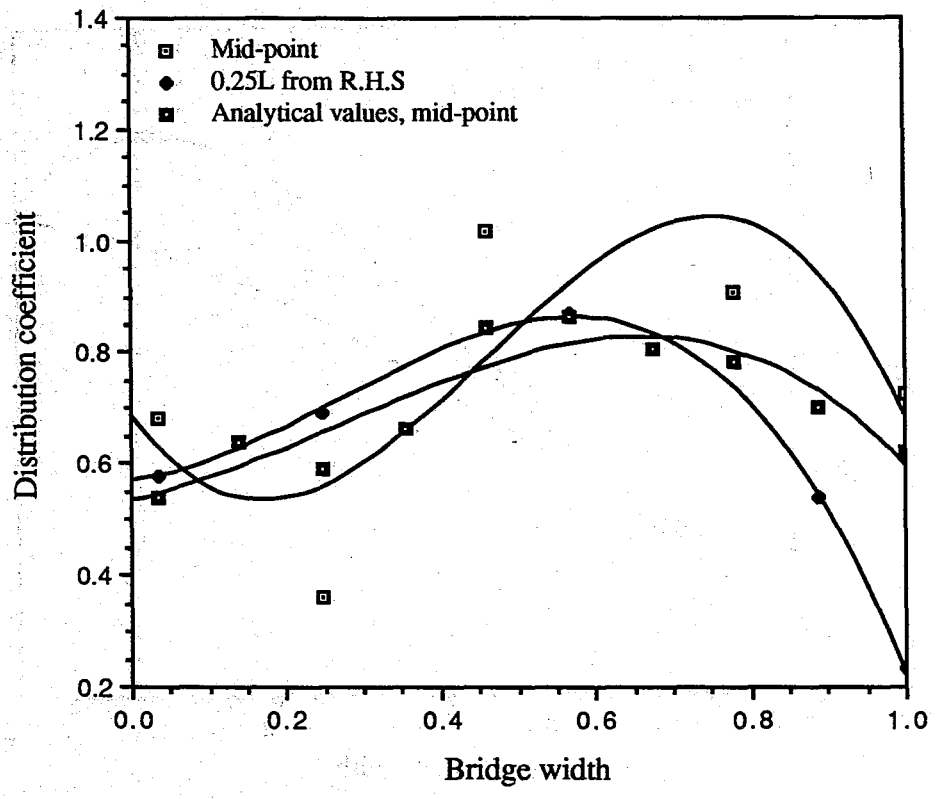

Fig. 5.31 Distribution coefficient vs bridge width for load position 1, based on deflection data

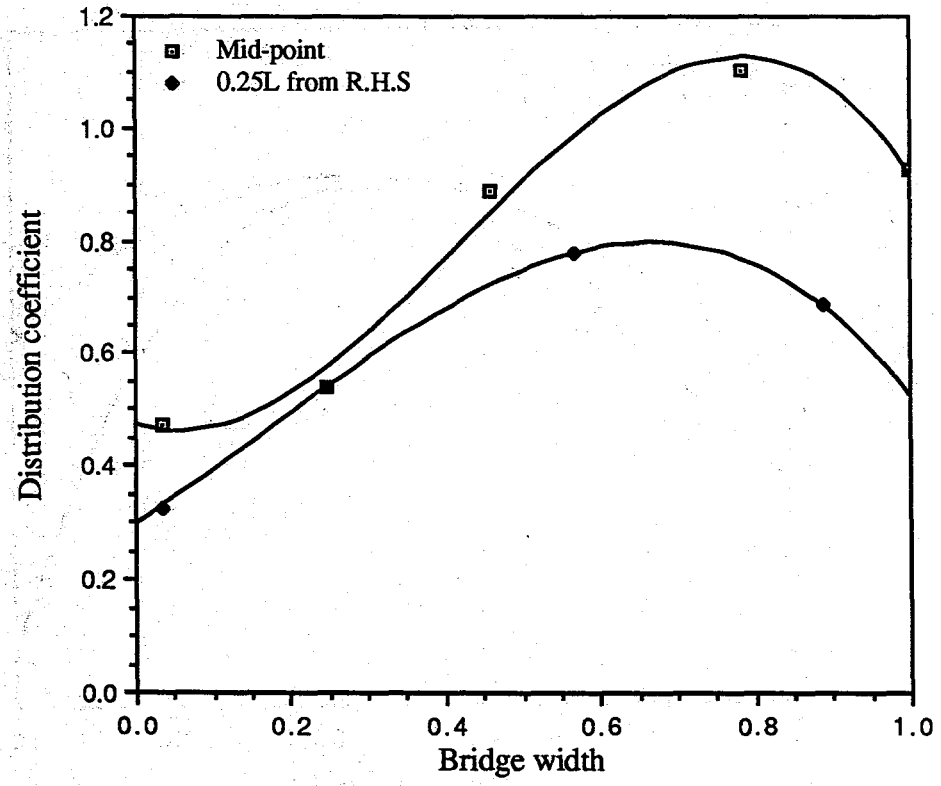

Fig. 5.32 Distribution coefficient vs bridge width for load position 2,based on deflection data

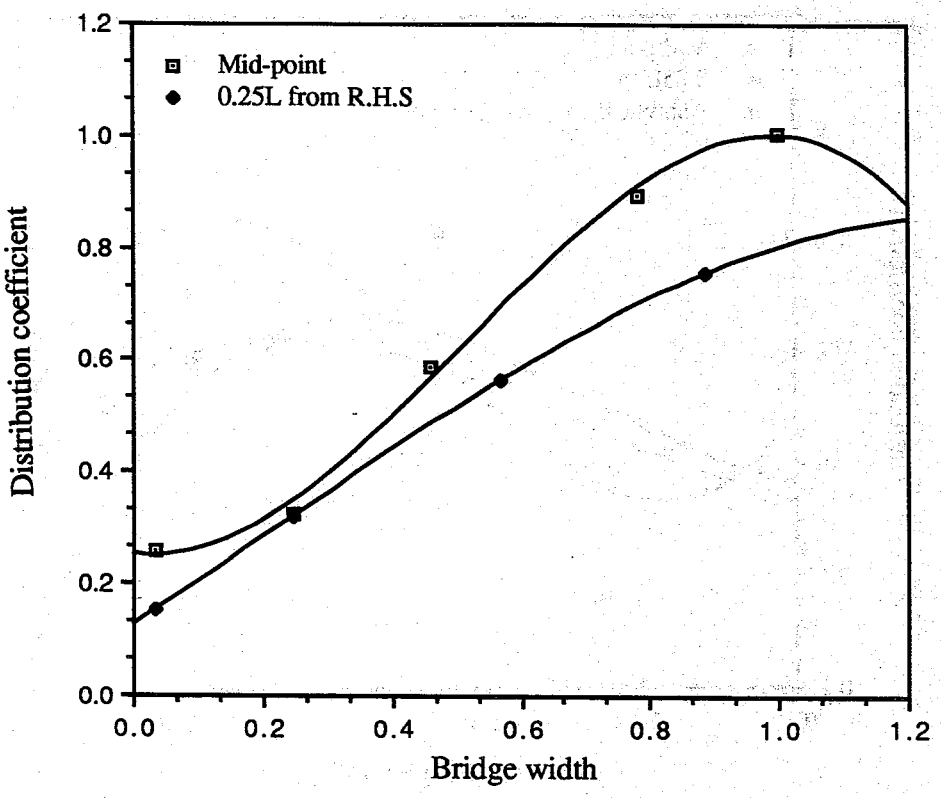

Fig. 5.33 Distribution coefficient vs bridge width for load position 3, based on deflection data

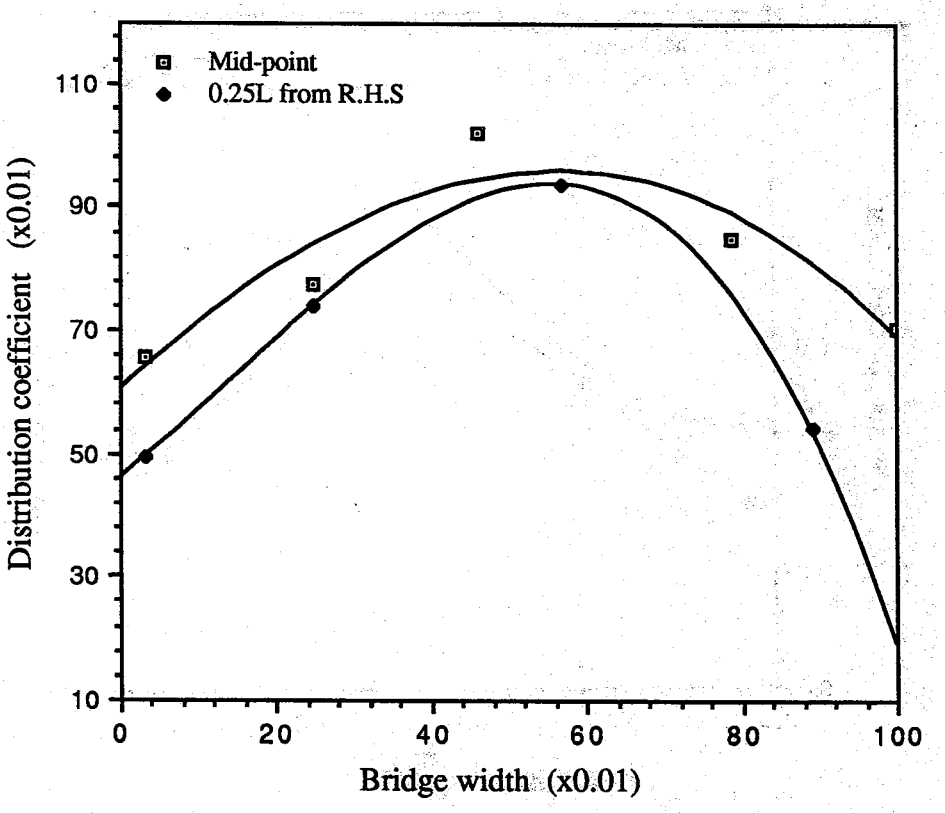

Fig 5.34 Distribution coefficient vs bridge width for load position 4, based on deflection data

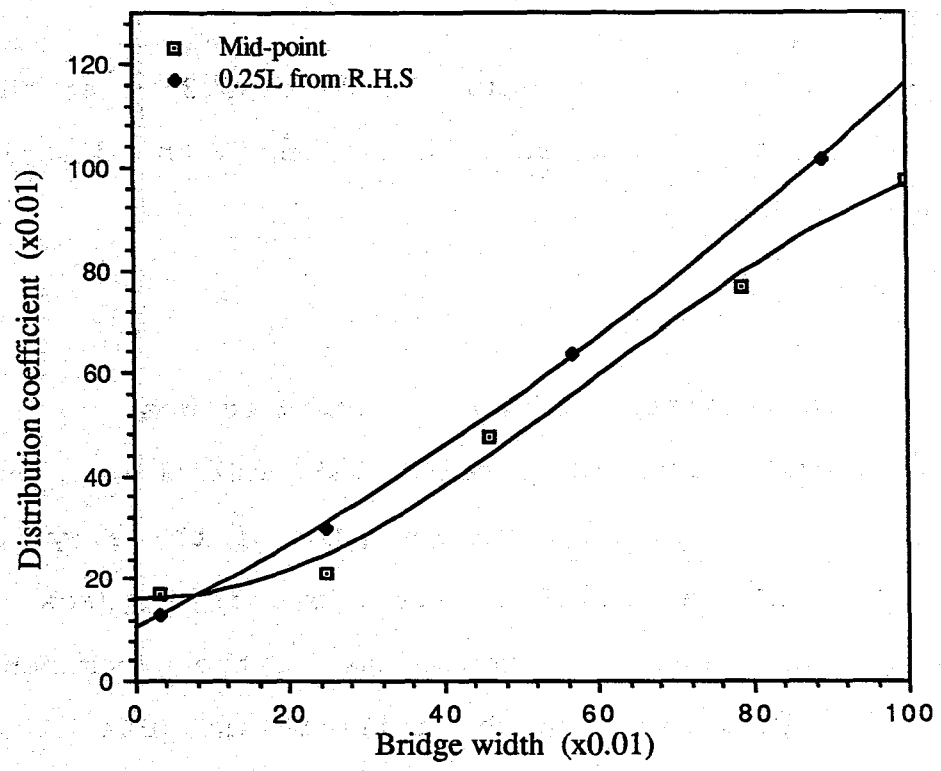

Fig. 5.35 Distribution coefficient vs bridge width for load position 7, based on deflection data

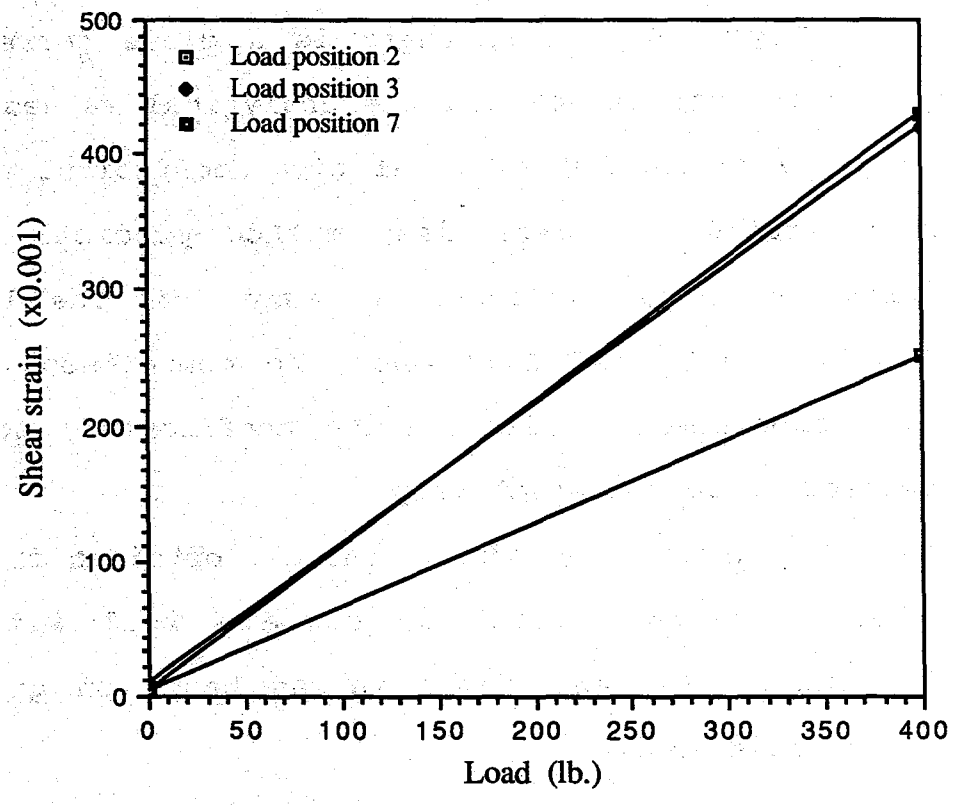

Fig. 5.36 Shear strain vs load for load positions 2,3,&7

It can also be seen from Figures 5.26 to 5.35 that there is some local effect of the applied load region on the distribution of strains and deflections.

5.2.2 Comparison of analytical and measured values

The analytical values of strains and deflections, obtained from the equivalent beam grillage analysis of the acrylic model plotted for the middle location, are shown in Figures 5.16 to 5.25.

Figure 5.18 shows the comparison of the experimental and the analytical values based on the grillage analysis as well as the distribution coefficient theory, Rowe [11]. It can be seen from these curves that grillage analysis is adequate to predict, the behavior of the bridge system in the elastic range. It is also clear from Figure 5.18 that there is a close correlation between the experimental values and the analytical values based on the grillage analysis and the distribution coefficient method, although the distribution coefficient method predicts lesser values at some locations on the deck, away from the loading location. Figures 5.26 and 5.31 show the comparison of the analytical and experimental distribution coefficients for the strain and deflection data respectively.

It can be seen that the analytical values, obtained from the equivalent beam grillage analysis, compare well with the experimental values. The analytical values based on grillage analysis are more conservative.

5.3 Multi-box Beam Concrete Model Bridge System

5.3.1 Static and fatigue testing

The effect of repetitive loading on the joint behavior and strength of multi-box beams are evaluated using the data from the fatigue test on the model. The static testing of the 1:2.5 scale model of the bridge system was carried out to study the structural integrity, load distribution, cracking behavior and ultimate load capacity.

5.3.2 Level of fatigue loading and stress range

Table 5.1 shows the level of fatigue loads and the stress levels for the load positions 1, 3, and 5. The stress ranges in the concrete are 260.8 psi in load positions 1 and 5 and 440.7 psi in load position 3. The stress range is computed based on strain compatibility, equilibrium of internal forces and the actual concrete and prestressing steel properties. The strand stress ranges in load positions 1 and 5 is 1020 psi and that in load position 3 is 1493 psi. The stress range in the strand is not significantly high since the model is subjected to a load range of only 15 kips corresponding to service load conditions. The ratio of strand stress range to the ultimate strength of the prestressing steel is seen to be in the range of 0.0038 to 0.005. The stress in the strands is much lower than the endurance limit given by f_r/f'_s 0.1 (Figure 5.37) as recommended by the guidelines of the American Concrete Institute (ACI) Committee 215 on Fatigue of Concrete [24].

Table 5.1 Fatigue loads and stress levels

Item	Load positions 1 and 5	Load position 3
Applied load (kips)		
P min.	15	5
P max.	30	20
Maximum moment (kip-in.)		
Under P min.	186.94	91.20
Under P max.	373.88	365.92
Cracking moment (M_{cr})	1081.01	1081.01
M max./M_{cr}	0.346	0.338
Maximum bottom fiber concrete stress (psi)		
Under P min.	280.5 (C)	375.67 (C)
Under P max	19.7 (C)	65.01 (T)
Stress range	260.8	440.68
Prestressing strand stress (bottom layer), ksi.		
Under P min.	171.22	170.7
Under P max.	172.24	172.19
Stress range (f_r)	1.02	1.49
f_r/f_{pu}	0.0038	0.0055

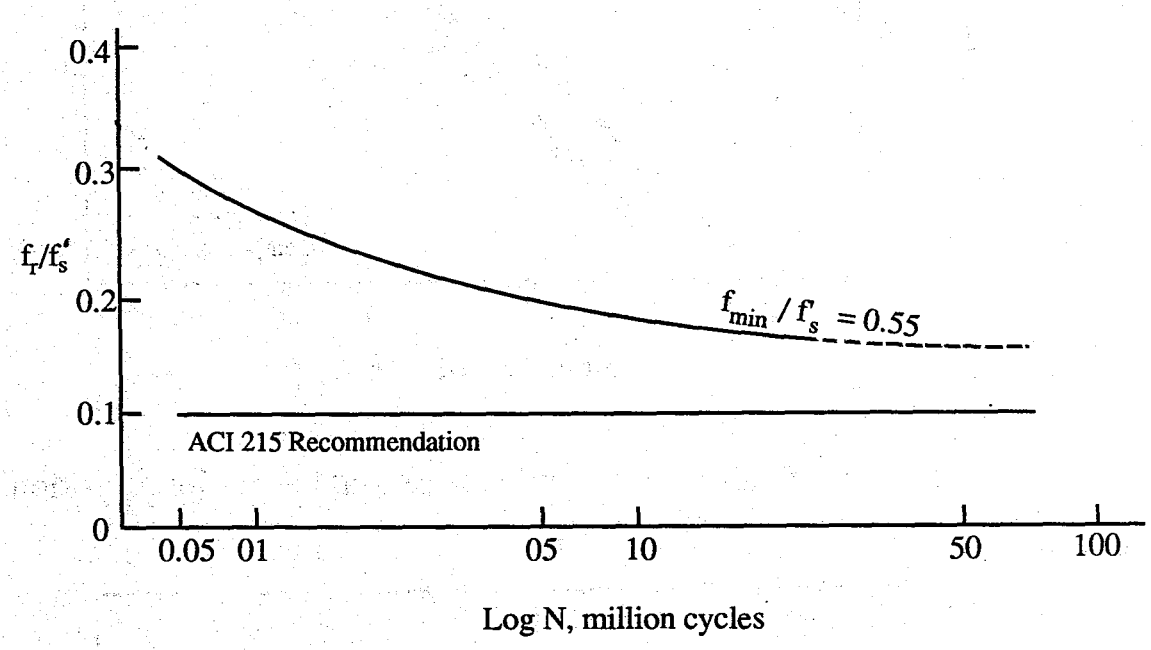

Fig. 5.37 S - N curve for prestressing strand

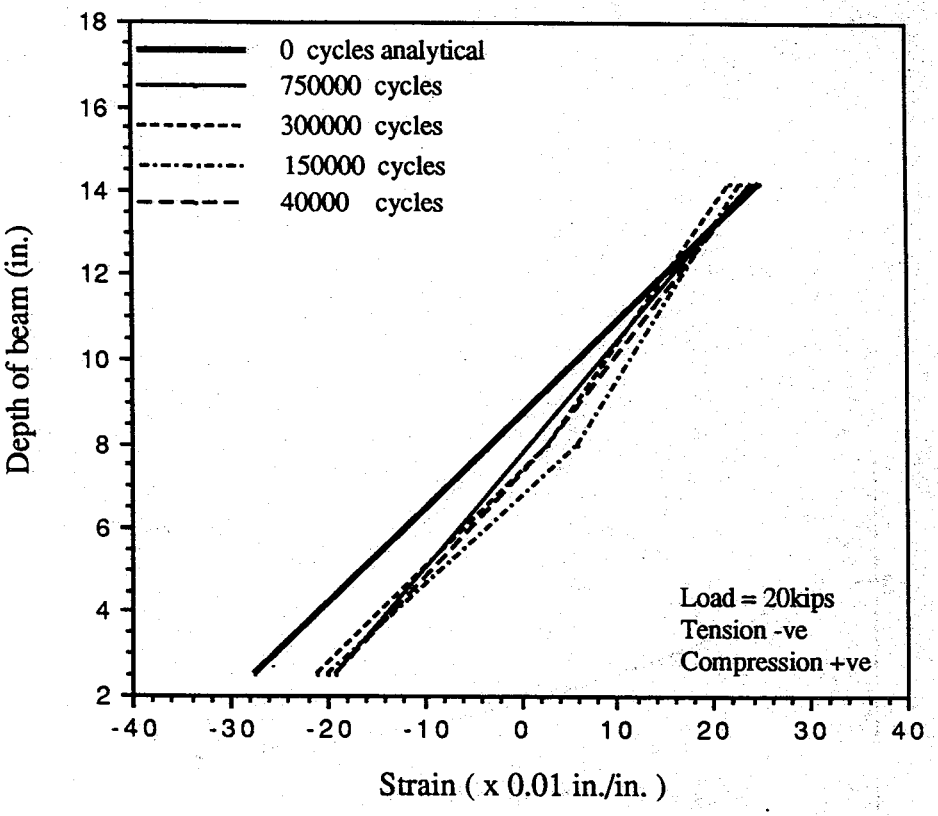

Fig 5.38 Strain at midspan in the central beam - load position 3

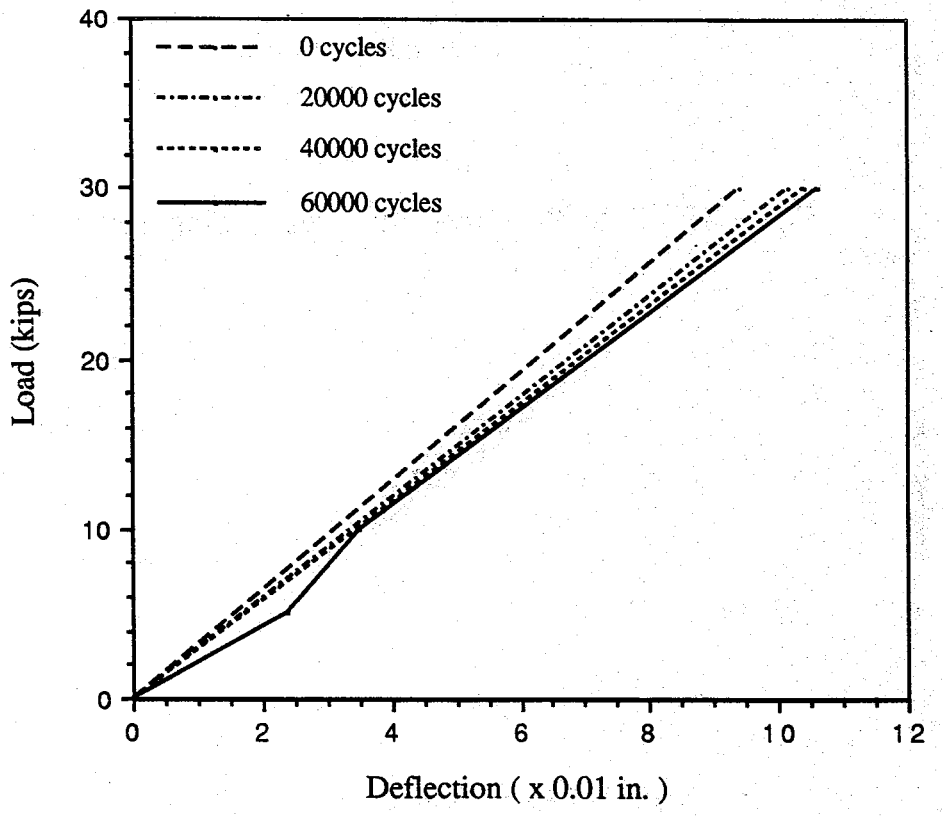

Fig 5.39 Load vs deflection for gage B - load position 3

5.3.3 Strains in concrete

The strains in concrete across the depth of the central beam at midspan for an load of 20 kips in shown in Figure 5.38. The analytical strain values are determined based on the computed. concrete stresses in the compression zone of the beam. The measured concrete strains compare reasonably well with the predicted values. They show a distinct linear variation of strains across the beam depth. However the increase in concrete strains with the increase in the number of cycles of fatigue loading is negligible.

5.3.4 Behavior of longitudinal joints

The crack gages installed across the bottom longitudinal joints did not indicate any signs of joint opening. These grouted joints which are subjected to an applied stress of 150 psi by transverse post tensioning did not develop any cracks and behaved monolithically with the beam. This could be attributed to the low stress values in the bottom fibers under the applied fatigue loads (Table 5.1) which are much smaller compared with the modulus of rupture of concrete.

5.3.5 Load deflection characteristics

Typical load deflection curves obtained at the beginning of repeated loading (0 cycles), and at increasing cycles for load positions 1 and 5 are, shown in Figs. 5.39 and 5.40. The apparent loss of stiffness is not significant since the loading level

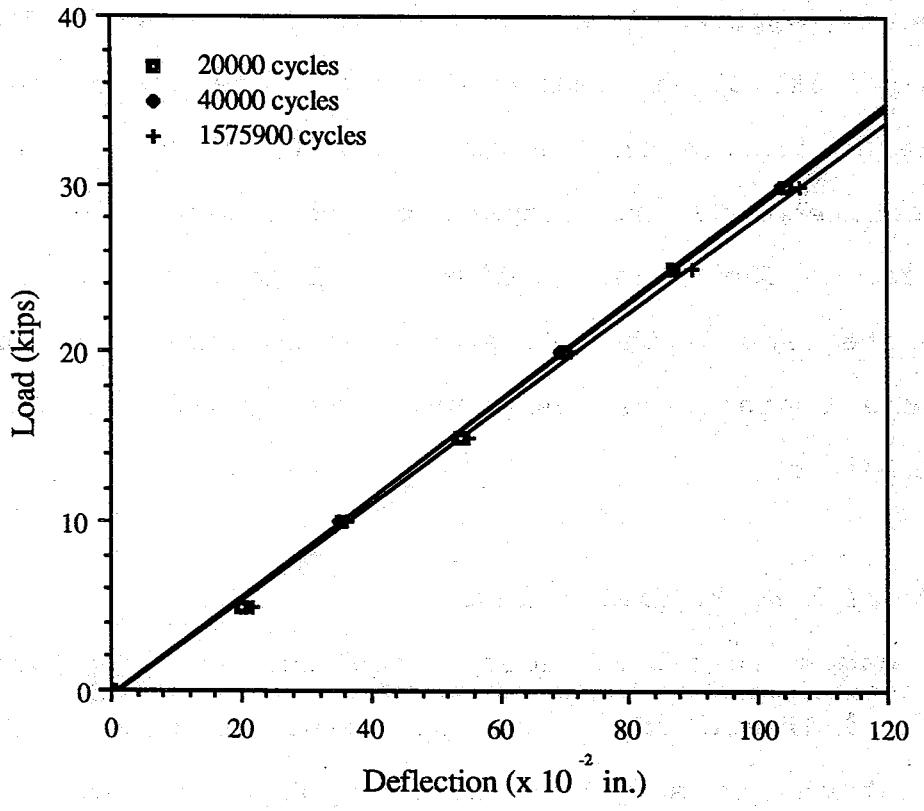

Fig. 5.40 Load vs. deflection for gage A - load position 5

corresponding to the serviceability conditions is relatively low. The loss of stiffness with progressive repeated loading is also seen in Figures 5.41 and 5.42 for load position 3. It can be observed from Table 5.1 that the maximum applied moment is approximately only one third of the estimated cracking moment. This ratio is smaller than that reported by other researchers [27] where no loss of stiffness and subsequent fatigue failure have been reported. The loss of stiffness with progressive repeated loading beyond one million cycles was found to be negligible for both load positions 1 and 3.

The multi-box beam bridge model was analyzed using grillage analogy for a maximum applied load of 30 kips at load position 1. The material properties used in the analysis correspond to the design (f'_c = 5000 psi) and the actual strengths (f'_c = 8200 psi). The experimentally measured deflections along the span are shown in Figure 5.43 together with the computed displacements using the grillage analysis. The measured displacements compare reasonably well with the predicted values corresponding to the higher concrete strength.

Figures 5.44 and 5.45 show the load deflection characteristics and the deflection profile along the span for static load position 2. The load vs. deflection plot for gage 3 and the longitudinal deflection profile for increasing loads in load position 6 are shown in Figs. 5.46 and 5.47. Similar results are presented in Figs. 5.48 and 5.49 for load position 4. The load deformation, behavior of the bridge model under the static

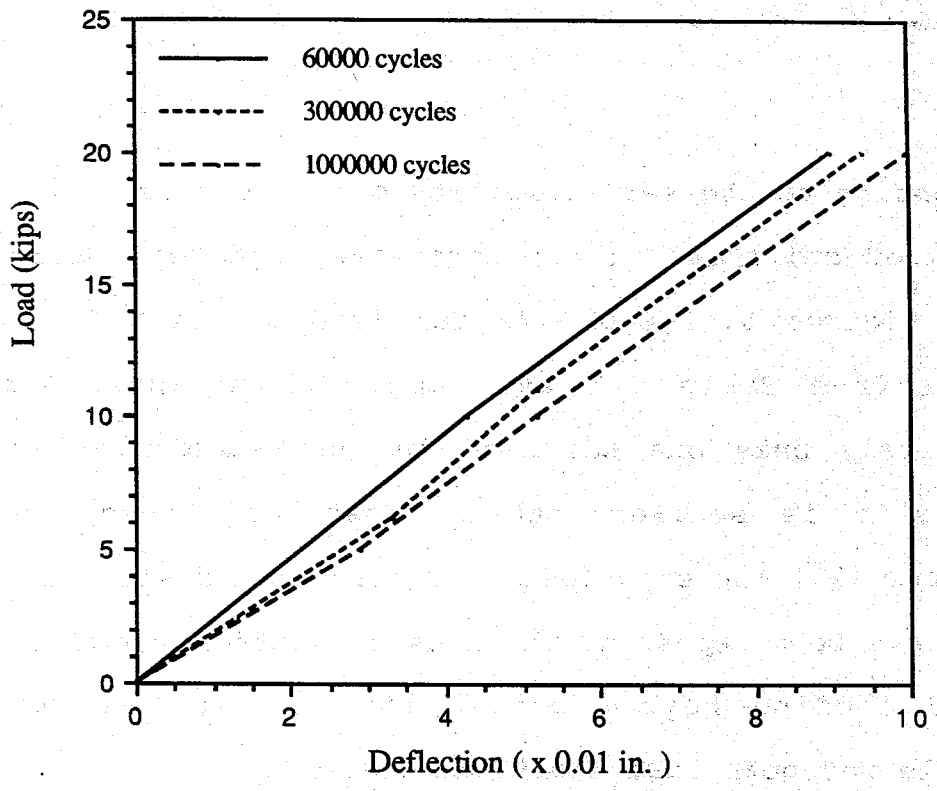

Fig 5.41 Load vs. deflection for gage B - load position 3

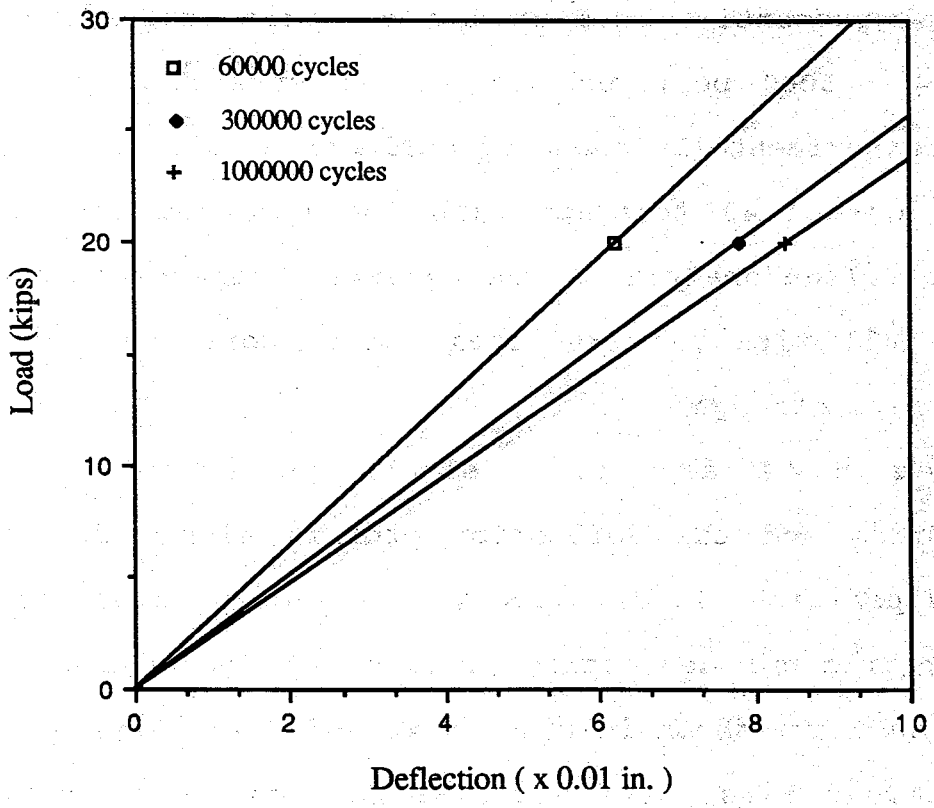

Fig 5.42 Load vs. deflection for gage 3 - load posiiton 3

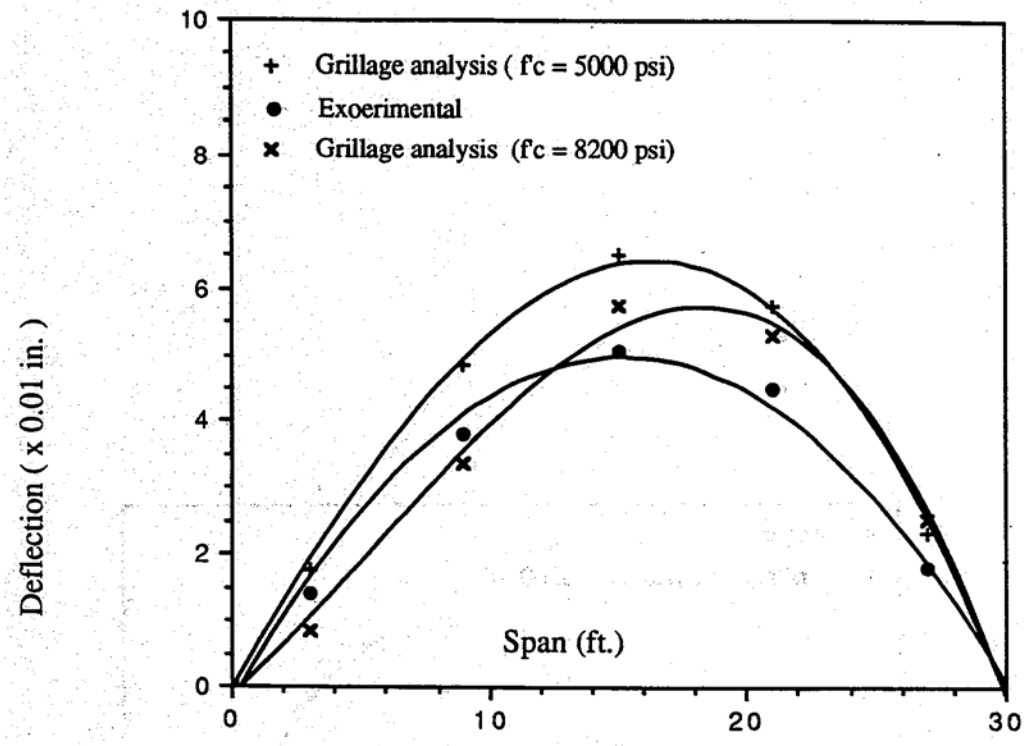

FIG 5.43 Comparison of experimental and analytical results load position 1, load = 30 kips and 0 cycles

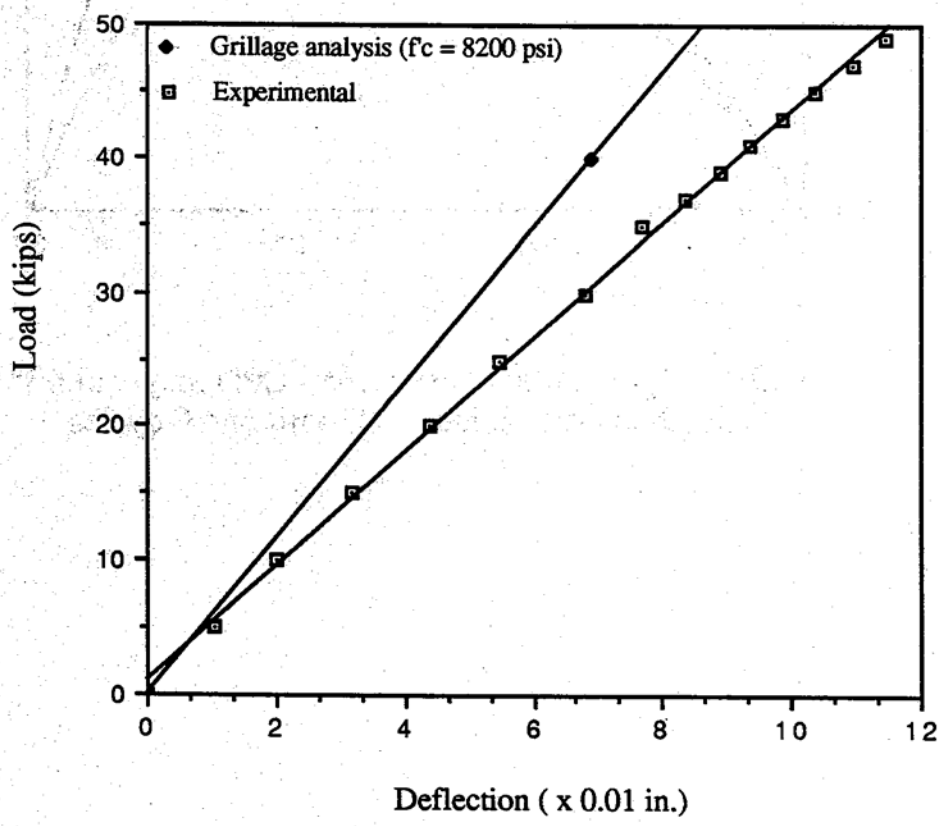

FIG 5.44 Load vs. deflection for gage 3 - load position 2

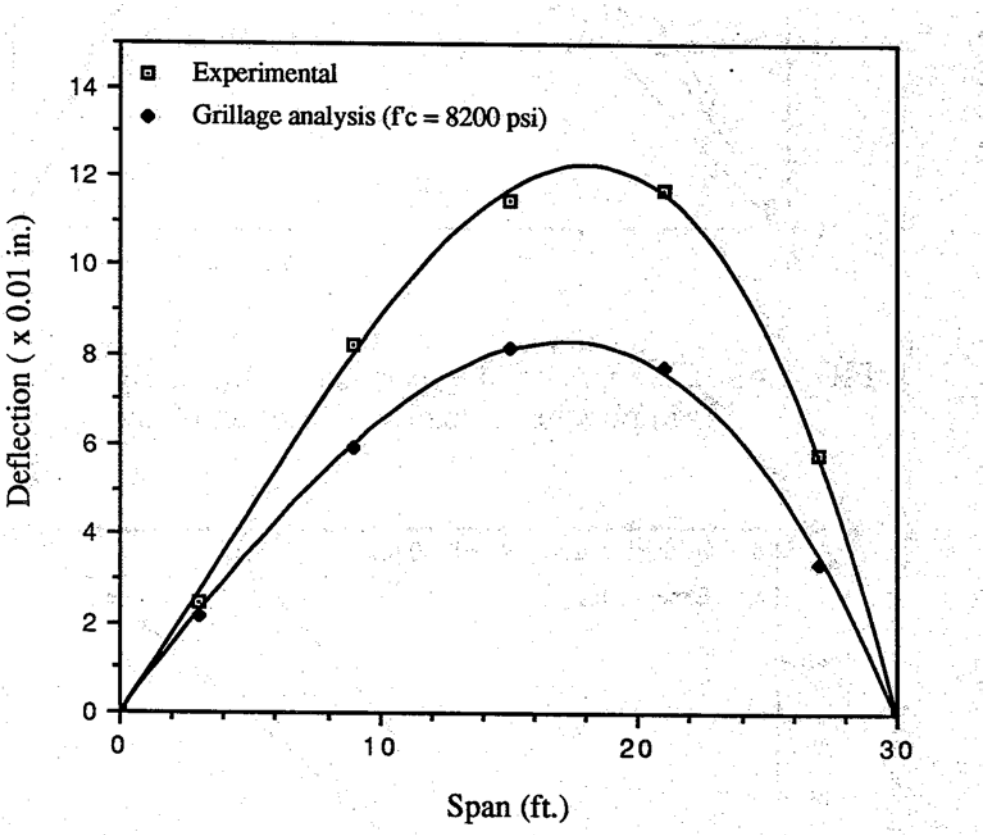

Fig 5.45 Comparison of experimental and analytical results load posiiton 2, load = 47 kips and 0 cycles

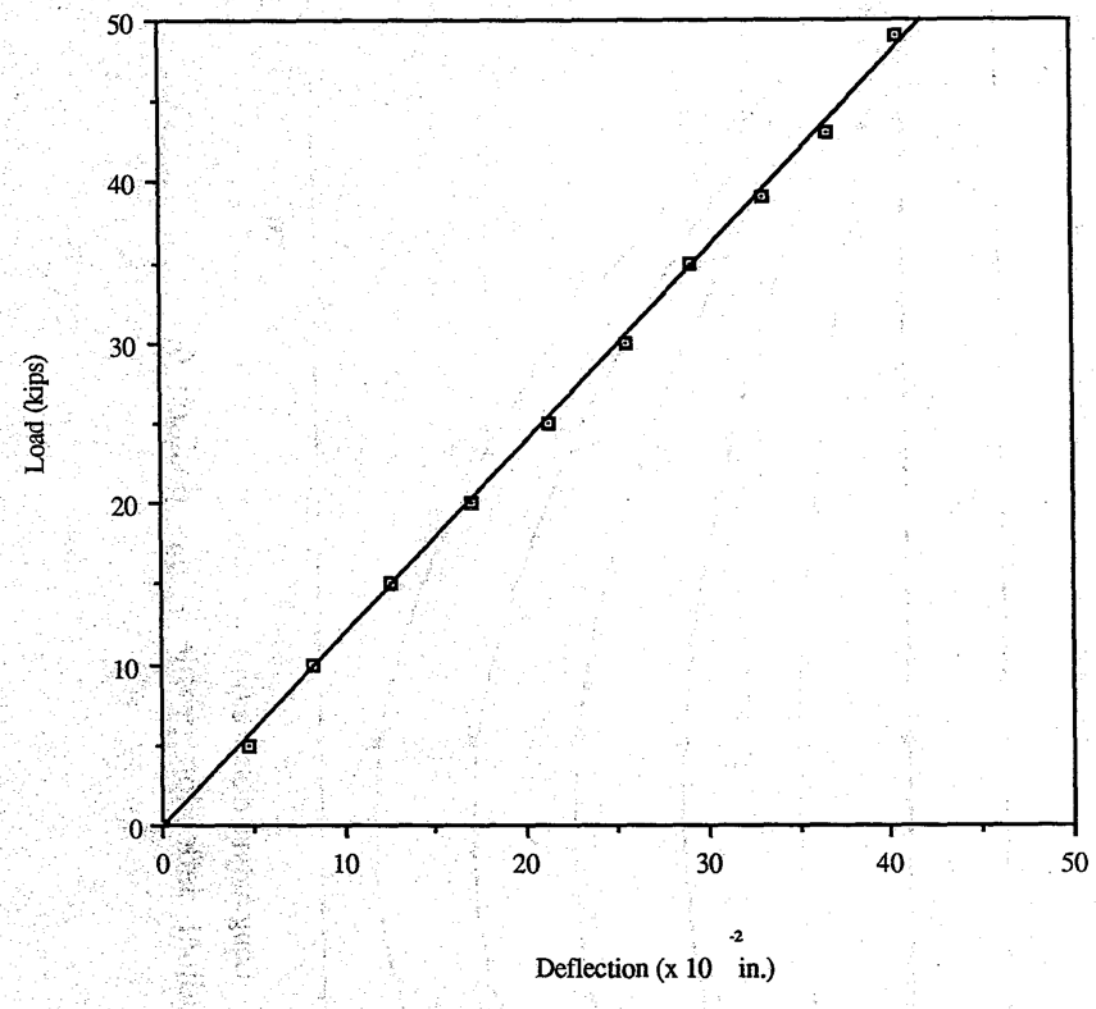

Fig. 5.46 Load vs. deflction for gage 3 - load position 6

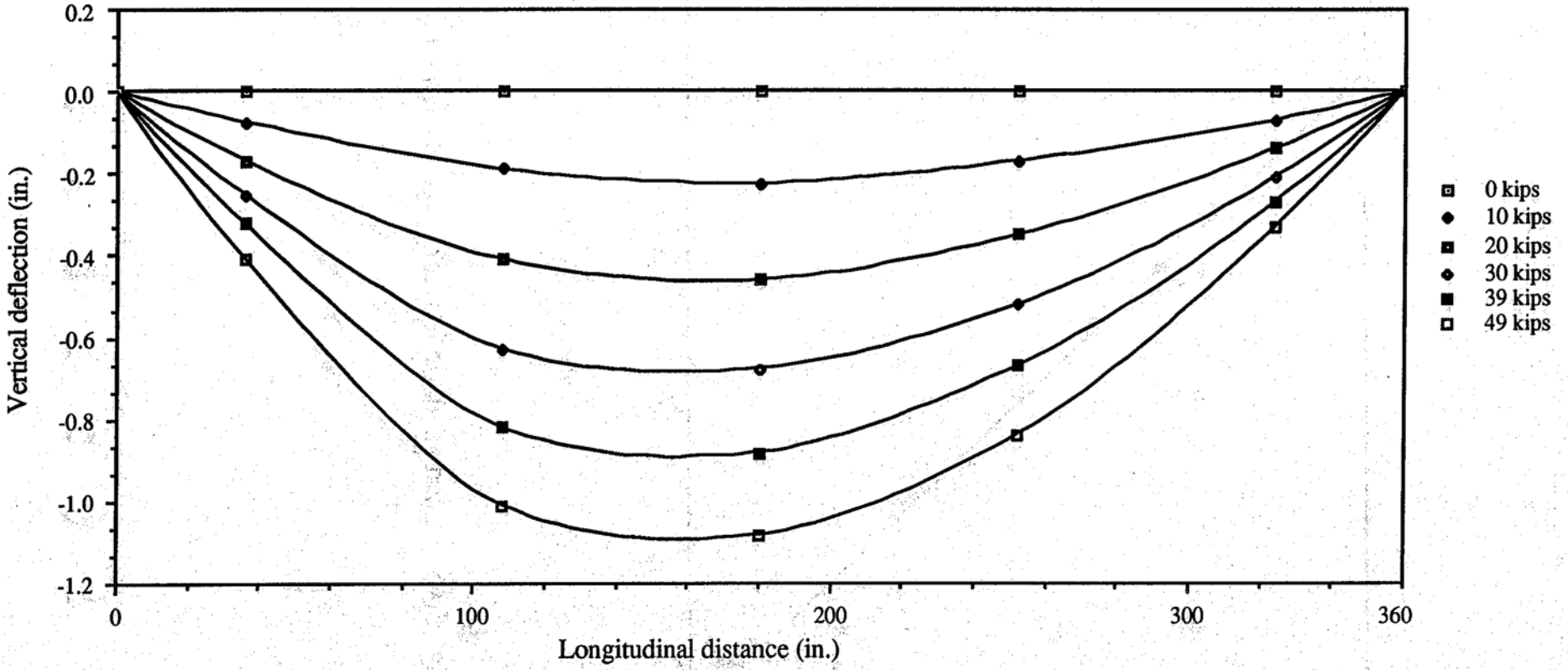

Fig. 5.47 Longitudinal deflection profile - load position 6

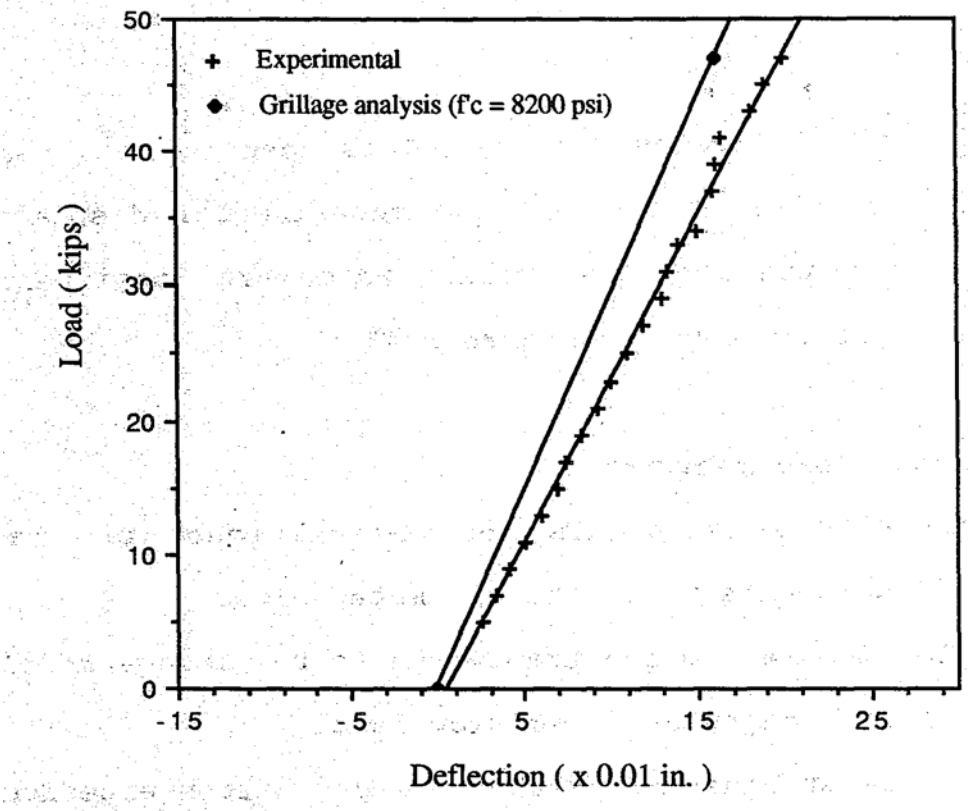

FIG 5.48 Load vs. defletion for gage 3 - load position 4

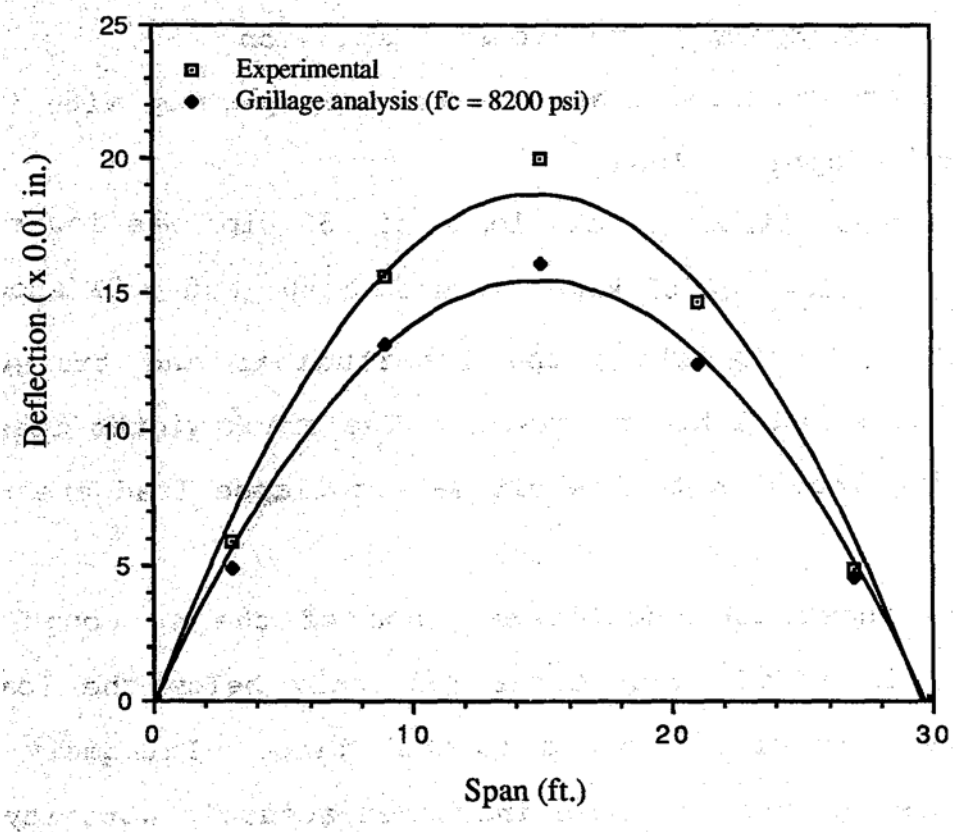

FIG 5.49 Comparison of experimental and analytical results load position 4, load=49 kips and 0 cycles

loading for the load cases 2,4 and 6 is seen to be linear and well within the elastic range. The experimental displacements are greater than the predicted values which are consistent with the earlier trend observed in Figure 5.43.

5.3.6 Ultimate load behavior

The following measurements and observations were made at regular load increments up to the ultimate values:

i) Deflections along and transverse to the bridge model-span using dial gages and precision level

ii) Concrete strains across the beam depth from embedded strain gages and those on the beam surface

iii) Longitudinal crack openings using crack gages

iv) Crack monitoring using acoustic emission

v) Crack propagation, based on visual inspection with increasing applied load

The observed first crack load of 58 kips was lower than the predicted value of 65 kips. Figures 5.50 and 5.5.1 show the measured displacements along the longitudinal and transverse directions of the model bridge system. The rack widths measured with increasing loads up to the ultimate collapse load are shown in Fig. 5.52.

Fig. 5.53 shows the cumulative graph of the AE counts, as picked up by the middle transducer (directly below the loading point) in the form of AE counts against time. Extremely good correlation was observed between increased acoustic activity and

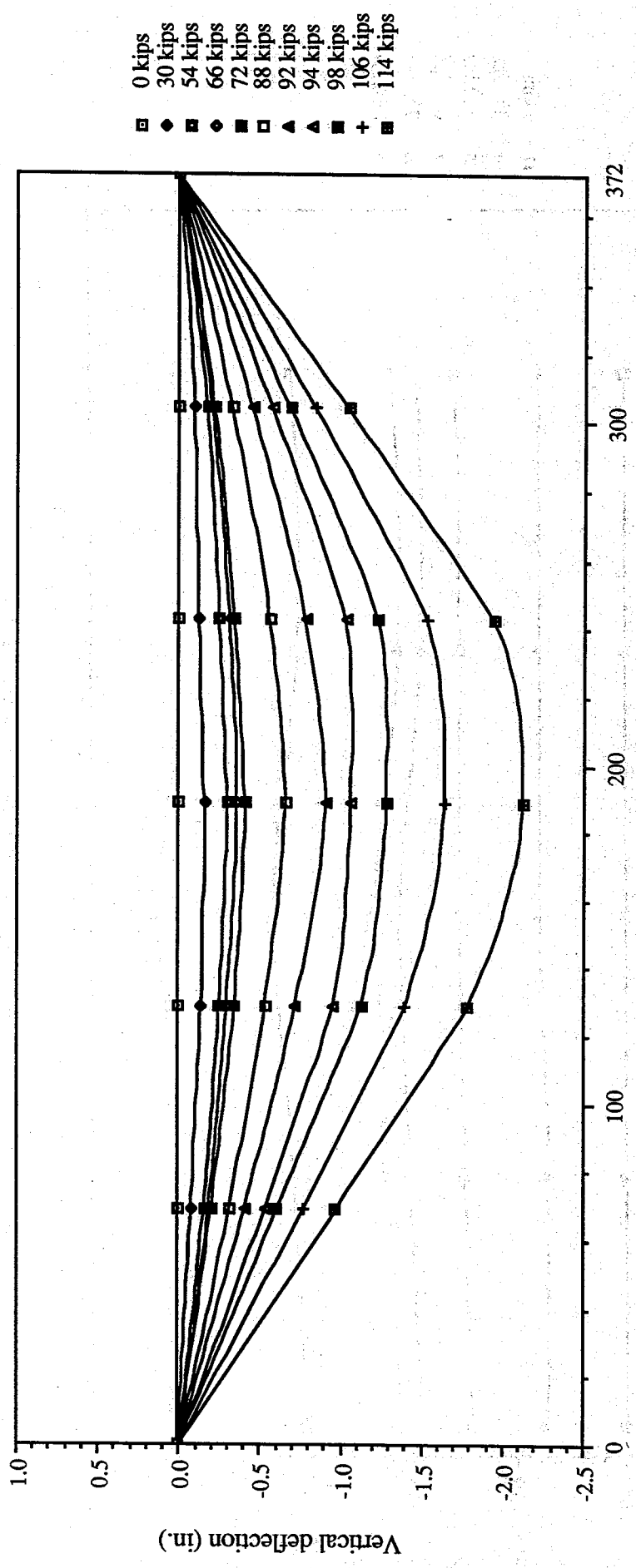

Fig. 5.50 Measured displacements along the longitudinal direction

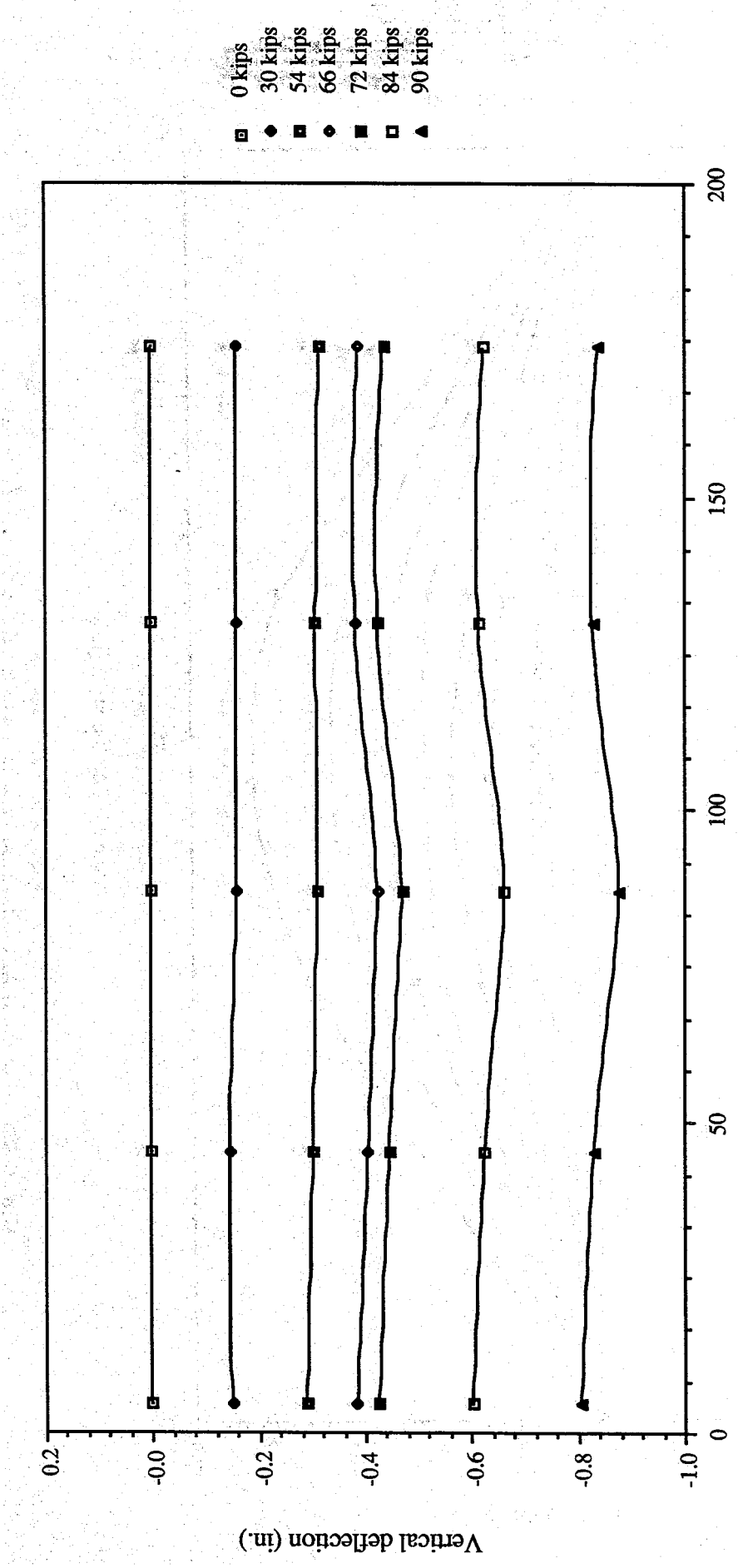

Fig. 5.51 Measured displacements along the transverse direction

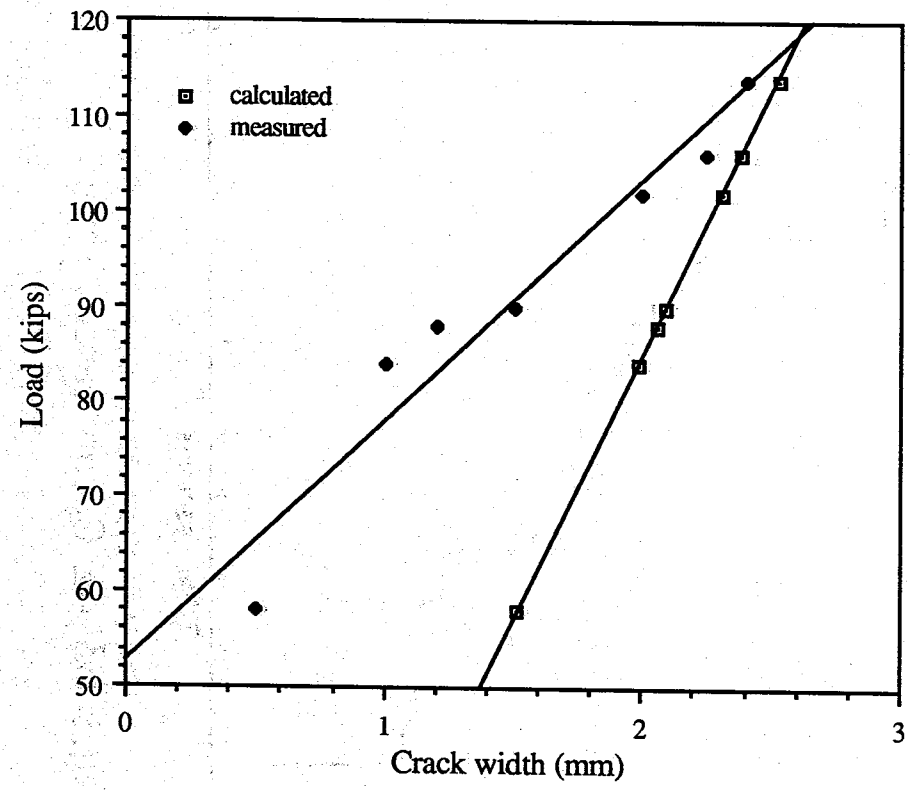

Fig. 5.52 Load vs. crack width

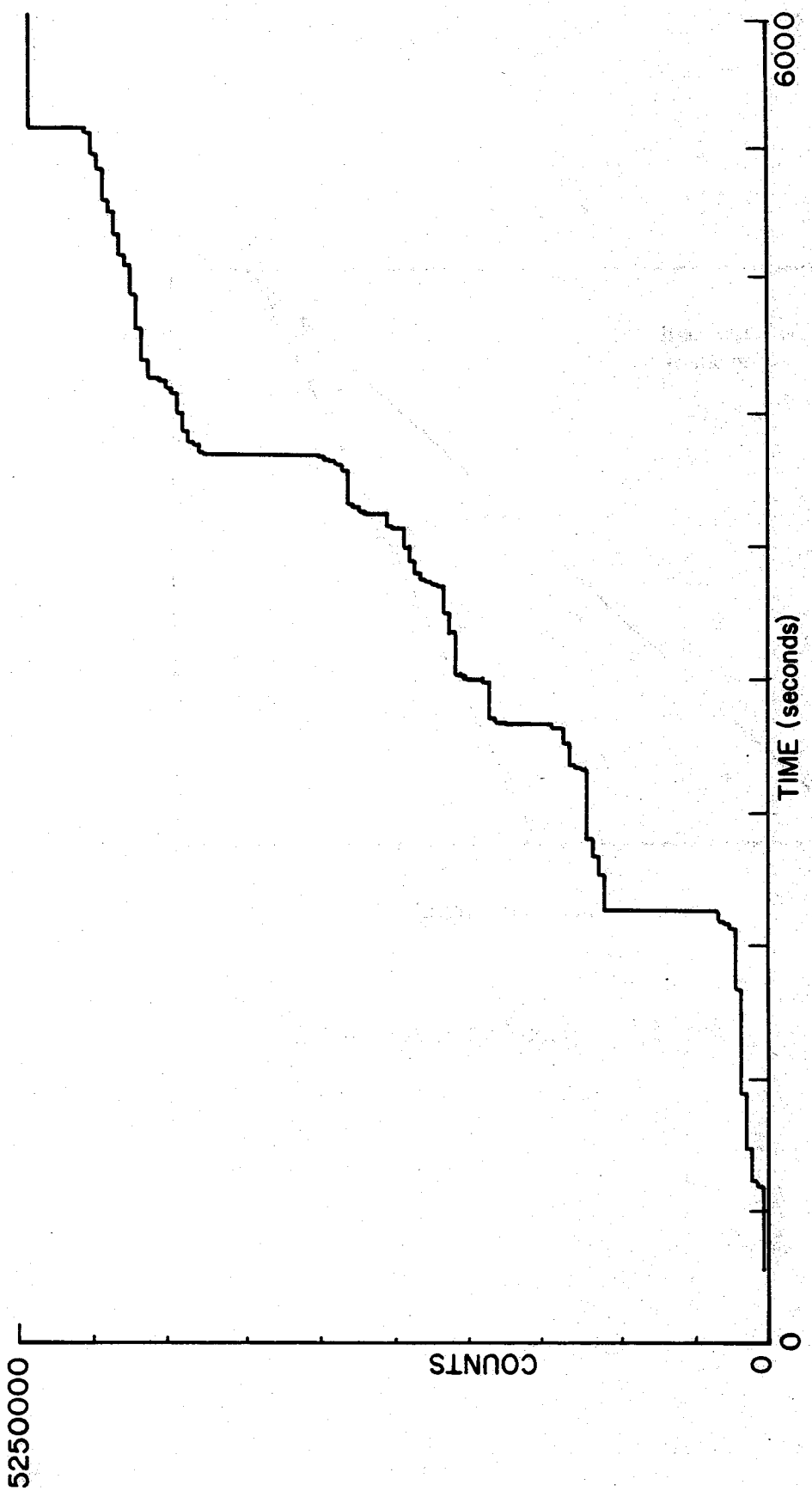

Fig. 5.53 AE Counts versus Time

each incremental loading. The start of the graph around 300 seconds, corresponds to the initiation of microcracks in the bridge model The sharp rise in AE counts at about 1975 seconds shows the merging of the microcracks to form the first macrocrack.

Fig. 5.54 shows the load vs. strain at the top surface of the deck. The load versus central deflection of the bridge is given in Fig. 5.55. It can be observed that the magnitude of deflection increases considerably around 90 kips with a simultaneous surge in AE activity at 4000 seconds. The ultimate load taken up by the model bridge system was 115 kips and this is indicated by a jump in AE counts during the final incremental loading at about 5500 seconds. Figure 5.56 shows the acoustic transducers and the transverse cracks in the direction coinciding with the duct holes housing the transverse post-tensioning strands with increase in the applied loads, the crack widths increased considerably together with the formation and growth of a new crack approximately midway between successive transverse posttensioning tendons Fig. 5.57 and 5.58. The longitudinal joints did not exhibit any sign of visible cracking both at the bottom and top surfaces up to the ultimate collapse load.

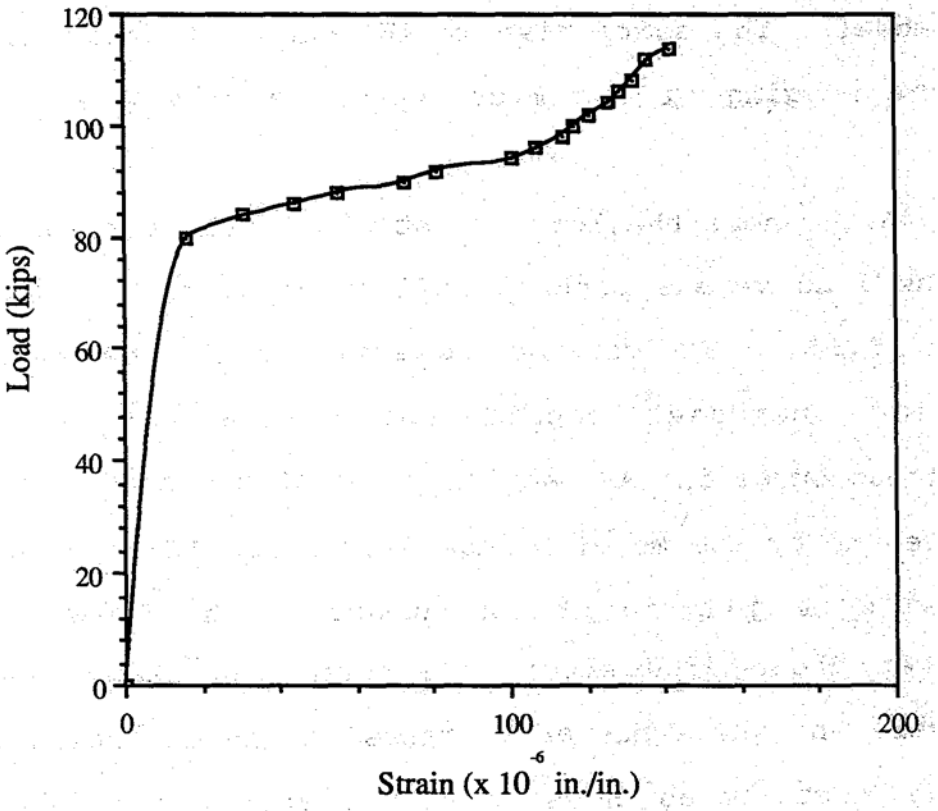

Fig. 5.54 Load vs. strain at the top surface of model bridge deck

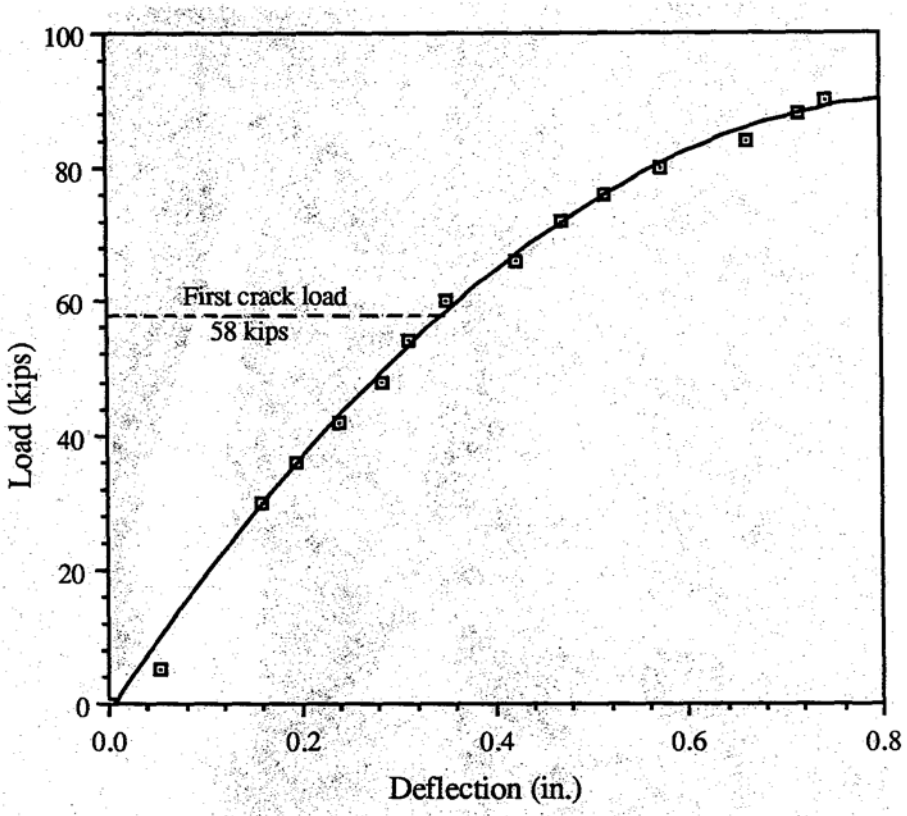

Fig. 5.55 Load vs. central deflection

Fig. 5.56 Photograph showing acoustic transducers and the transverse cracks coinciding with the duct holes

North end

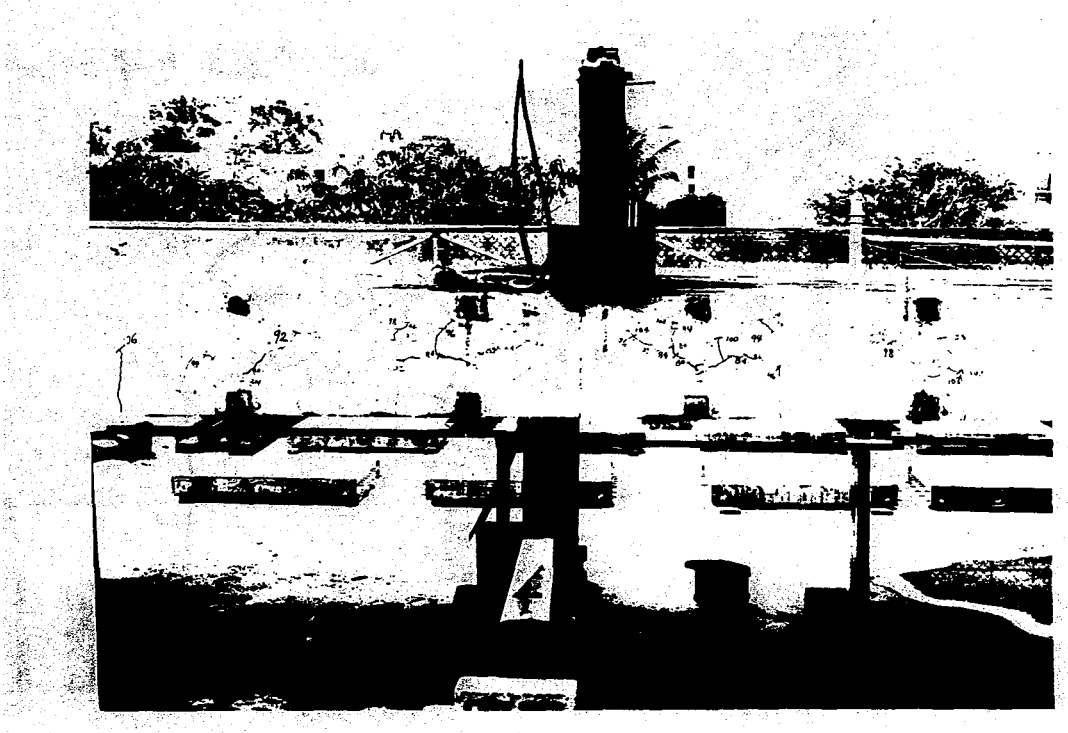

South end

Fig. 5.57 Crack patterns as observed from the south and north sides

North end

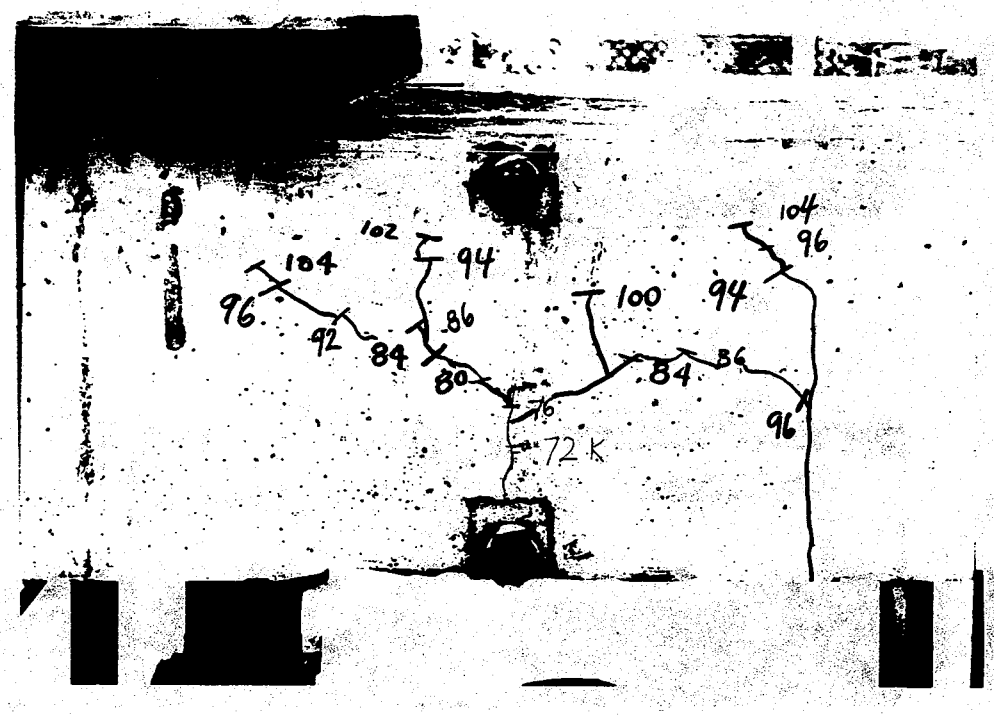

South end

Fig. 5.58 Crack patterns originating from the post - tensioning ducts as observed from the north and south sides

CHAPTER 6

CONCLUSIONS

The analytical and experimental studies on the acrylic and precast prestressed concrete multi-box beam model systems establish the concept feasibility as demonstrated by the improved structural serviceability in terms of` reduced deflections. The use of voided beams with bottom flange reduces considerably the dead load and also provides higher torsional strength. The grouted in-situ joints at the bottom and cast-in-situ slab at the top, which are prestressed by the lateral post-tensioning, contribute significantly to efficient lateral load distribution characteristics.

On the basis of the analytical and experimental investigation the following conclusions are made:

i) The analytical displacements based on the grillage analysis compare reasonably well with the experimental values.

ii) The predicted strains in concrete across the depth of the beam under serviceability conditions agree reasonably with the measured concrete strains. However, the increase in concrete strains with the increase in the number of cycles of fatigue loading is negligible indicating little softening characteristics with fatigue loading.

iii) Longitudinal grouted joints with an initial prestress of 150 psi in the transverse direction exhibit adequate structural integrity even up to 6 million cycles of repeated loading. This can be attributed to the low stress values in the bottom fibers due to the applied fatigue loads, which are much less than the modulus of rupture of concrete. No deterioration was observed in the overall behavior of the bridge system nor were any cracks noticed.

iv) The loss of stiffness of the prestressed multi box beam model bridge system is not significant since the load level corresponding to the serviceability condition is relatively low.

v) The measured deflections indicate no loss of post tension stress even after six million cycles of loading.

vi) The cracking moment computed using the elastic theory, is a fraction of the ultimate flexural strength. The ratio of the ultimate to cracking moments is greater than 1.2, which ensures the adequacy of the total amount of prestressed and nonprestressed reinforcement [36].

vii) The longitudinal joints at the bridge deck and the bottom flange levels of the multi-box bridge system exhibited excellent structural integrity without developing any visible cracks up to six million cycles of fatigueloading.

viii) The agreement between the computed first crack and ultimate collapse load and the measured values was quite reasonable.

REFERENCES

1. Biswas, Mrinmay, "Precast Bridge Deck Design Systems, Prestressed Concrete Institute (PCI) Journal/March-April, 1986 pp. 40-94.

2. "Segmentare Spannbeton-Trager in Bruckenbau", Deutsches Ausschuss fur Stahlbeton, Part 311, 1980.

3. Koseki, K., and Breen, J.E., "Exploratory Study of Shear Strength of Joints for Precast Segmental Bridges", Center for Transportation Research, Rept. 248 - 1, Univ. of Texas at Austin, 1983.

4. Wium, D.J.W., and Buyukozturk, O., "Behavior of Precast Segmental Concrete Bridge", Research Report R 84-06, Massachusetts Institute of Technology, May 1984.

5. Moreton, A. J., "Epoxy Glue Joints in Precast Concrete Segmental Bridge Construction", Proc. Inst. Civil Engrs., Part Feb. 1981, pp. 163-177.

6. Reddy, D. V., and Arockiasamy, M., "Static and Cyclic Behavior of Joints in Precast Prestressed Concrete DoubleTee Bridge Systems", Final Report, Research Project No. 99700-7364, Florida Department of Transportation, March 1987, pp. 68.

7. Arockiasamy, M., Reddy, D. V., Badve, A. P., and Rao, B. V., “Fatigue Strength of Joints in Precast Prestressed Concrete Double-Tee Bridge Systems”, PCI Journal, 1990.

8. Poston, Randall, W., Carrasquillo, Ramon, L., and Breen, J. E., "Durability of Post Tensioned Bridge Decks, American Concrete Institute Materials Journal, July-August 1987, pp. 315-326

9. Poston, Randall W., Phipps, Alan R, Almustafa Riyadh A, Breen, John E. and Carrasquillo, Ramon L., "Effects of Transverse Prestressing in Bridge Decks" ASCE Journal of Structural Engineering 114 (4), (1988) pp. 743-764.

10. Bakht, Baidar, Jaegar, Leslie G, Cheung M. S. and Mufti, Aftab A., "The State of the Art in Analysis of Cellular and Voided Slab Bridges", Canadian Journal of Civil Engineering, Vol. 8 (1981) pp. 376-391.

11. Rowe, R.E., "Concrete Bridge Design" (1962), CR Books Ltd. Publication.

12. National Cooperative Highway, Research Program Report (NCHRP) 287, "Load Distribution and Connection Design for Precast Stemmed Multibeam Bridge Superstructures", (1986) Transportation Research Board, National Research Council.

13. Arendts, J.G. and Sanders, W.W., "Concrete Box Girders as Sandwich Plates", ASCE Journal of the Structures Division 96 (ST11) (1970), pp. 2353-2371.

14. Hendry, A.,W., and Jaeger, L.G., "The Analysis of Grid Frame Work and Related Structures", Chatto and Windus. London, 1958.

15. Lightfoot, E., "A Grid Framework Analogy for Laterally Loaded Plates", J. Institution of Mech. Sci. 6, 1964.

16. Yettram, A L. and Husain, M.H., "A Grid Framework Method for Plates in Flexure", ASCE J. Eng. Mech. Div. 91, EM3, 1965, pp 53-64.

17 Sawko, F., "Recent Developments in the Analysis of Steel Bridges Using Electronic Computers", British Constructional Steelwork Association Conference on Steel Bridges, London, 1968, pp. 1-10.

18. Smyth, W.J.R. and Srinivasan, R., "The Analysis of Gateshead Viaduct", The Structural Engineer, 5 (2), 1973, pp. 51-59.

19. Hambly, E.C. and Pennells, E., "Grillage Analysis Applied to Cellular Bridge Decks", The Structural Engineer, 53 (7), 1975, pp. 267-275.

20. Zienkiewicz, O.C., "The Finite Element Method", McGraw-Hill Book Company, (1977).

21. Davies., J.D., Somerville, I.J., and Zienkiewicz, O.C., "Analysis of Various Types of Bridges, by Finite Element Method", Developments in Bridge Design and Construction, (1971) Crosby Lockwood and Sons, Ltd. publication.

22. Scordelis A C., "Analytical Solutions For Box Girder Bridges", Developments in Bridge Design and Construction, (1971), Crosby Lockwood and Sons, Ltd.

23. Loo Chaye Yew and Cusens Anthony R, "The Finite Strip Method in Bridge Engineering", (1978) Viewpoint publication.

24. Abeles, Brown and Hu, "Fatigue of Concrete", Abeles Symposium ACI SP-41-11 (1974), pp. 237-278.

25. Abeles, Brown and Hu, "Behavior of Under Reinforced Prestressed Concrete, Beams Subject to Different Stress . Ranges", ACI SP-41-12 (1974), pp. 279-300.

26. Naaman, "A.E , "Fatigue in Partially Prestressed Beams", American Concrete Institute Publication SP 75-2, (1982), pp. 25-46.

27. Abeles, Barton and: Brown, "Fatigue Behavior of Prestressed Concrete Beams" ACI SP-23-32, Concrete Bridge Design.

'28. Balaguru, P.N., "Analysis of Prestressed Concrete Beams for Fatigue Loading" PCI Journal May-June 1981, pp. 70-94.

29. Al-Zaid, R. Z. and Naaman, A.E., "Analysis of Partially Prestressed Concrete Beams", Journal of Structural Engineering, ASCE 112 (4), (1986), pp. 709-725.

30. Glucklich, Joseph, "The Effect of Microcracking on Time Dependent Deformations and the Long-term Strength of Concrete" Structure of Concrete and its Behavior Under Load, Cement and Concrete Association, London, 1968, pp. 176-189.

31 Ishai, Ori, "The Time-Dependent Deformational Behavior of Cement Paste, Mortar and Concrete", Structure of Concrete and its Behavior Under Load, Cement and Concrete Association, London, 1968, pp. 345-364.

32. Meyers, Bernard I., Slate, Floyd O., and Winter, George, "Relationship Between Time-Dependent Deformation and Microcracking of Plain Concrete", ACI Journal. Proceedings V. 66. No. l, Jan. 1969 pp. 60-68.

33. Ruetz, Walter "The Two Different Physical Mechanisms of Creep in Concrete," Structure of Concrete and Its Behavior Under Load, Cement and Concrete Association, London, 1968, pp. 146-153.

34. Rusch, H., "Physical Problems in the Testing of Concrete (Physikalische Fragen der Betonprufung)", Zement-Kalk-Lips (Wiesbaden), V. 12, No. 1, 1959, pp. 1-9, Also Library Translation No. 86, Cement and Concrete Association, London, 1959.

35. Ravichandran, T.V., "An Analytical and Experimental Investigation of a Multicellular Box Beam Bridge System Using An Acrylic Model", M.S. Thesis, Florida Atlantic University, Boca Raton, FL, April, 1988.

36. The American Association of State Highway and Transportation Officials, (AASHTO), Standard Specifications for Highway Bridges", Thirteenth Edition, 1983.

37. Oduyemi, T.O.S. and Clark, L.A., "Prediction of Crack Widths in Circular Voided Reinforced Concrete Slabs Subjected to Transverse Bending", Magazine of Concrete Research, Vol. 39, No. 140, Sept. 1987, pp.124-132.

38. Pollock, A.A., "Acoustic Emission Amplitude Distribution", International Advances in Non-Destructive Testing, Brussels, March 1982.

39. Ramkumar, K. P., Analytical and Experimental Studies on the Static and Fatigue behavior of Precast Prestressed Concrete Multi-Box Beam Bridge System", M.S. Thesis, Florida Atlantic University, Boca Raton, Florida, October 1988.